

# *Ultra-high-performance polymer foils*

*Jérôme Lefèvre*





Diss. ETH No. 17603

# Ultra-high-performance polymer foils

A dissertation submitted to

ETH ZURICH

for the degree of  
Doctor of Sciences

presented by

JÉRÔME PATRICE LEFÈVRE

Dipl. Werkstoff-Ing. ETH  
born September 6, 1977  
citizen of Islisberg, AG, Switzerland

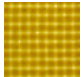
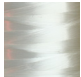
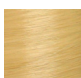

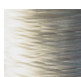

accepted on the recommendation of

Prof. Paul Smith, examiner  
Prof. Han E. H. Meijer, co-examiner  
Prof. A. A. J. M. (Ton) Peijs, co-examiner  
Dr. Theo A. Tervoort, co-examiner

2008



# Contents

Summary		1	
Zusammenfassung		3	
Résumé		7	
I		Introduction	9
II		Ultra-High Molecular Weight Polyethylene	29
III		Thermotropic Liquid-Crystalline Polyester	65
IV		Lyotropic Liquid-Crystalline Aramid	93
V		Bacterial Cellulose	109
VI		Conclusions and Outlook	121
Acknowledgements		133	
Curriculum Vitae		135	



*«I do not propose to say much about the strength of polymers except that they are strong.»*

*Sir F. C. Frank, Proc. R. Soc. London, Ser. A 1970, 319, 127.*





# Summary

High-performance polymer fibers nowadays are used in a broad spectrum of applications. The common feature of these fibers is that they all exhibit a high degree of orientation and extension of their constituent covalently-bonded macromolecular chains. Unfortunately, the response of such highly anisotropic structures is strongly dependent on the direction of applied load or strain, which has major consequences for the design and ultimate characteristics of the products in which they are utilized.

Traditionally, fibers are most often applied in twisted form, such as in yarns and ropes, are woven, as in fabrics and cloth or are used in cut form, e.g. , in non-wovens and in composites.

Attempts have been made to avoid the adversary effects associated with weaving or use of short-fiber-reinforced composites and to manufacture high-performance, biaxially oriented polymer films. Disappointingly, their characteristics are far inferior when compared to those of the corresponding uniaxially oriented fibers.

In order to employ high-performance fibers more efficiently and better exploit their ultimate potential, laminates of multifilament strands and of spread multifilaments have been developed. Unfortunately, there are considerable difficulties in manufacturing such products with high fiber content. In practical applications, that fraction appears to be limited to only about 55-65 %, due to their approximately circular cross sections and incorporated voids. As the stiffness of the matrix materials used generally is low in comparison with that of the high-performance fibers, the mechanical properties of the resulting composite are modest.

The principal objective of the work presented in this thesis is to develop routes for manufacturing high-performance polymer foils that avoid the mechanical losses associated with woven and biaxially deformed structures and are not based on the cumbersome and inefficient spreading and reassembling of multi-filament yarns.

The results presented in this work can be divided into two parts: i) the formation of unidirectionally oriented foils with outstanding mechanical properties, equal or close to those of their fiber counterparts, and ii) the production of high-performance planar balanced foils thereof.

## **Ultra-high-performance unidirectionally oriented polymer foils**

First, ultra-high-performance unidirectionally oriented polymer foils were produced by drawing the flexible, ultra-high molecular weight polyethylene UHMW PE, resulting in transparent foils of thicknesses as low as 2  $\mu\text{m}$  and widths up to 30 cm. It was found that the initial morphology of the as-cast films influenced the drawing behaviour and development of mechanical properties with draw ratio. A model considering the initial macromolecular orientation is presented in this work to account for this phenomenon.

Second, a thermotropic liquid-crystalline copolyester was processed into 3  $\mu\text{m}$  thin foils employing specially designed dies for air-gap extrusion. Post-extrusion heat-treatment yielded films with mechanical properties approaching those of their fiber counterparts. The same concept was adopted to produce oriented foils of a lyotropic aramid, which was dry-jet-wet-extruded from sulphuric acid and coagulated in a water bath. Finally, bacterial cellulose foils were grown and while applying stress, which featured outstanding mechanical characteristics in the stretch direction, while retaining excellent properties perpendicular to it.

In summary, although in the past little success has been reported regarding the production of high-performance polymer foils, in this dissertation it is demonstrated that such products can be produced with mechanical properties that approach those of their fiber counterparts, which opens new possibilities in the design of, for instance, composites.

## **Ultra-high-performance planar polymer foils**

Selected unidirectionally oriented foils were laminated at different angles to yield materials of vastly improved strength and stiffness in the transverse direction.

UHMW PE foils were fused by swelling the surface with a solvent or by incorporating a minor amount of a lower melting polar copolymer, to yield, for instance, planar balanced 4-ply laminated thin foils (ca. 10  $\mu\text{m}$ ) of a Young's modulus of 35 GPa.

In the case of thermotropic polyester, lamination was achieved with as little as 5 wt. % of a hot-melt adhesive, yielding balanced foils with planar mechanical properties approaching their theoretical limits.

# Zusammenfassung

Die Verwendung von Kunststoffen in mechanischen Anwendungen ging von der Entwicklung der hochfesten bzw. Hochmodulfasern in den späten 60er Jahren aus. Heute finden wir sie in einer breiten Palette von Anwendungen, von kugelsicheren Westen über schnittresistente Handschuhe, verstärkte Reifen, bis zu Bauteilen in der Flugzeugindustrie und Raumfahrt. Die Fasern vereinen eine hohe Zugfestigkeit mit einem sehr geringen Gewicht, was sie bei gleicher Gewichtsbasis um einen Faktor 10 stärker als Stahl macht.

Alle Hochleistungsfasern zeichnen sich durch eine hohe Ausrichtung der Polymermoleküle aus, welche nur über spezielle Herstellungsverfahren erreicht werden kann, da Polymere in Abwesenheit von speziellen Kraftfeldern spontan keine solchen Strukturen bilden. Drei mögliche Verarbeitungsmethoden, die zu stark orientierten und gestreckten Polymerketten führen, werden im folgenden Abschnitt kurz erläutert.

Der bekannteste Vertreter von *starr*en Kettenmolekülen ist das aromatische Poly-*p*-phenylenterephthalamid (PPTA), welches unter der Handelsbezeichnung Kevlar<sup>®</sup> oder Twaron<sup>®</sup> erhältlich ist und in Lösung verarbeitet wird, da sein theoretischer Schmelzpunkt oberhalb der Zersetzungstemperatur liegt. Das Spinnen von Polymerfilamenten mit *starr*en Kettenmolekülen erfolgt aus einer lyotropen flüssig-kristallinen Lösung im Trockenstrahl-Nassspinnverfahren. Die Lösung, meist eine hochkonzentrierte Säure, wird nach der Extrusion in einem Koagulationsbad ausgewaschen. Die Faser wird anschliessend bei erhöhter Temperatur leicht gereckt.

Thermotrope Polyester hingegen können dank ihren *halbstarr*en Ketten direkt aus der flüssig kristallinen Schmelze versponnen werden und erfahren bei einer nachträglichen Hitzebehandlung ebenfalls eine Verbesserung der Eigenschaften.

Eine dritte Verarbeitungsmethode ermöglicht das Verspinnen von *flexiblen* Polymerketten, z. B. von ultrahochmolekularem Polyethylen (UHMW PE), aus halbverdünnter Lösung. Durch anschliessendes hochgradiges Verstrecken lässt sich eine der spezifisch stärksten Fasern herstellen.

Der Ursprung der ausserordentlichen Eigenschaften von Hochleistungsfasern liegt in der kovalent gebundener Struktur der Polymerketten in Faserrichtung. Zwischen den

Hauptketten wirken bei den Aramidfasern Wasserstoffbrückenbindungen und bei den Polyethylenfasern nur die relativ schwachen van der Waal'schen Kräfte. Bedauerlicherweise ist das Verhalten einer solch anisotropen Struktur stark von der Richtung der wirkenden Kraft abhängig, was zweifellos starken Einfluss auf die letzten Eigenschaften eines daraus fabrizierten Bauteils hat.

Traditionell werden die Fasern, meist als Garne geliefert, maschinell verwoben. Die resultierenden Gewebe und Stoffe zeichnen sich durch eine reduzierte Festigkeit aus, welche von der Zickzackführung der Garne herrührt. Um solch negative Effekte des Webens zu verhindern, wurden Hochleistungsfolien verschiedenster Kunststoffe durch biaxiales Verstrecken erzeugt. Leider sind deren Eigenschaften weit unter denen der hochorientierten Filamente.

Zusätzlich wurden weitere Techniken entwickelt, um Hochleistungsfasern in effizienter Bauweise, z. B. in Form von Laminaten aus gespreizten Garnen oder Multifasergelegen zu verwirklichen, um näher an die Kenngrößen einzelner Filamente heranzukommen. Die grosse Schwierigkeit in diesen Verfahren besteht darin einen hohen Fasergehalt zu erzeugen. Das obere Limit bei konstruktiven Bauteilen liegt bei ca. 55-65 %, welches einerseits vom runden Querschnitt der Filamente und andererseits von der Verarbeitungsmethode herführt. Aufgrund der unterlegenen mechanischen Charakteristiken einer Matrix im Vergleich zu denen ihrer Fasern, hat folglich der produzierte Verbundwerkstoff selbst weit reduzierte Eigenschaften.

Zusammenfassend lässt sich folgern, dass grosse technische Verbesserungen seit der Einführung von Hochleistungsfasern erzielt worden sind, welche weit entwickelte Produkte ermöglicht haben. Jedoch besitzen diese meist nur Bruchteile der möglichen ausserordentlichen Charakteristiken und lassen demzufolge noch viel Spielraum offen, um die intrinsischen Eigenschaften von orientierten Polymerketten voll zu entfalten.

Das grundsätzliche Ziel dieser These war, verschiedene Möglichkeiten zur Produktion von Hochleistungsfolien zu entwickeln, welche die mechanischen Verluste durch biaxialverstreckte oder gewobene Strukturen umgehen und auch das zeitaufwendige und ineffiziente Spreizen oder Verlegen von Multifilamenten vermeiden.

Die Resultate dieser vorliegenden Arbeit können in zwei Bereiche aufgeteilt werden: i) die Herstellung unidirektionaler Folien mit annähernden oder gleichwertigen mechanischen Eigenschaften wie handelsübliche Fasern und ii) die damit produzierten

planaren Lamine.

## Unidirektionale Hochleistungsfolien

Bis zu 2  $\mu\text{m}$  dünne Polyethylenfolien, mit einer Breite von bis zu 30 cm und herausragenden mechanischen Eigenschaften, wurden durch einen Verstreckungsprozess hergestellt. Obwohl die Folien höchst unidirektionale Eigenschaften aufwiesen, zeigten sie genügend Resistenz gegenüber Fibrillation. Die ursprüngliche Morphologie des gegossenen Materials zeigte einen grossen Einfluss auf das Verhalten der Verstreckung und wirkt sich somit direkt auf die mechanischen Eigenschaften aus. In dieser Arbeit wird ein Modell zur Begründung dieses Phänomens präsentiert, welches die ursprüngliche Mikrostruktur durch Parameter einschliesst, welche wiederum aus Röntgenmessungen bestimmt wurden.

Durch ein speziell Düsendesign und durchoptimierte Prozessbedingungen konnten thermotropische Polyester aus flüssigkristalliner Schmelze zu 5  $\mu\text{m}$  dünnen und 15 mm breiten Folien extrudiert werden. Die erzeugten Folien erreichten nach einer Hitzebehandlung äquivalente mechanische Eigenschaften wie handelsübliche hochfeste Fasern.

Die weit entwickelte Verarbeitungsmethode für thermotrope Polymere wurde auch auf lyotrope, in Schwefelsäure gelöste Aramide mit *starrer* Hauptkette angewendet und in Folien verarbeitet. Auch in diesem Fall konnte die Steifigkeit mit Hilfe einer Hitzebehandlung verbessert werden.

Ein weiteres Kapitel befasst sich mit der *in-situ* Orientierung von bakterieller Cellulose. Es gelang, mit einer kleinen Verminderung der transversalen Eigenschaften, den unidirektionalen Modul und die Festigkeit zu verdoppeln.

Die hergestellten unidirektionalen Folien haben eine kleinere Oberfläche als eine Vielzahl von Filamenten, einfach verbindbare äusserst flache Aussenseiten und reduzieren somit die benötigte Menge des oft schwächeren Matrixmaterials zur Produktion von Verbundwerkstoffen drastisch. Zusätzlich entstehen beim Laminieren durch die backsteinähnliche Struktur weit weniger Fehlstellen im fertigen Verbundwerkstoff und ermöglicht damit den Matrixanteil auf unter 10 % zu verringern.

## Planare Hochleistungsfolien

Wie bereits erwähnt, wurden die unidirektionalen Folien durch Laminierung zu planaren Hochleistungsfolien verarbeitet. Die Verwendung von mehreren Lagen bei verschiedenen Ausrichtungen resultiert in eine Reduktion der Eigenschaften, jedoch wird dadurch die völlige Richtungsunabhängigkeit in der Ebene gewonnen.

Einerseits wurden UHMW PE-Folien mit Hilfe des Aufschwellens der Oberflächen durch ein Lösungsmittel verbunden. Andererseits konnte durch Zumischen von Copolymeren, welche im Gegensatz zum apolaren Polyethylen, polare Eigenschaften aufwiesen, die Adhesion verbessert und somit die Matrix überflüssig gemacht werden. Aufgrund der sehr dünnen Folien, welche keinerlei Matrix benötigten, konnten 4-Lagen Lamine mit hervorragenden mechanischen Eigenschaften und geringerer Dicke als ein kommerzielles Standard-Filament (ca. 15  $\mu\text{m}$ ) gefertigt werden.

Die Folien aus thermotropen Polyester wurden mit sehr wenig (5 %) niedrignschmelzendem Copolyester laminiert. Die resultierenden Eigenschaften des Laminats liegen nahe an den theoretisch möglichen Werten.

Obschon in der Vergangenheit nur wenig Erfolg in der Produktion von hochfesten unidirektionalen Folien erzielt worden ist, zeigt diese Dissertation mögliche Wege auf, Strukturen mit mechanischen hohen Eigenschaften, vergleichbar mit denjenigen von kommerziell erhältlichen Hochleistungsfasern, zu erreichen. Die Verfügbarkeit von solchen Produkten hat das Potential eine Vielzahl neuer Designmöglichkeiten von Verbundwerkstoffen zu eröffnen.

# Résumé

Les fibres de polymères hautes-performances sont aujourd'hui utilisées dans une large gamme d'applications. Ces fibres ont la particularité d'avoir un degré d'orientation élevé, ainsi qu'une extension de leurs chaînes macromoléculaires liées par des liaisons covalentes. Malheureusement, la réponse de ces structures hautement anisotropes est fortement dépendante de la direction du chargement ou de la tension, ce qui a d'importantes conséquences sur les caractéristiques des produits qui en sont composés.

Traditionnellement, les fibres sont le plus souvent tressées (corde), tissées (tissu) ou coupées (non-tissé et matériau composite).

Des tentatives de fabrication de films de polymères hautes-performances, biaxialement orientés ont été entreprises, afin d'éviter les effets néfastes dus au tissage ou à l'utilisation de matériaux composites à fibres courtes. Malheureusement, les propriétés de ces films sont de loin inférieures à celles des fibres uniaxialement orientées.

Afin d'utiliser de manière plus efficace les fibres hautes-performances et d'utiliser au mieux leur potentiel, des laminâtes/couches de fils multi-filaments ont été développés. Malheureusement, des tels produits à pourcentage élevé en fibres sont très difficiles à fabriquer.

Dans des applications pratiques, ce pourcentage apparaît limité à seulement 55-65 %, à cause de leurs sections approximativement circulaires et leurs vides incorporés. Puisque la rigidité de la matrice est en général basse en comparaison avec la rigidité des fibres hautes-performances, les propriétés mécaniques du composite fabriqué sont modestes.

Le principal objectif du travail présenté dans cette thèse est le développement de voies de fabrication de films de polymères hautes-performances, qui évitent les pertes mécaniques associées aux structures tissées et biaxialement déformées et qui ne sont pas basées sur le processus lourd et inefficace de l'étalement et le regroupement de ficelles multi-filaments.

Les résultats obtenus lors de ce travail peuvent être divisés en deux parties: 1) la formation de feuilles unidirectionnelles aux propriétés mécaniques augmentées ou égales à celles des fibres; 2) la production des feuilles à géométrie plane.

## **Feuilles de polymères hautes-performances uniaxialement orientées**

Des transparentes feuilles de polymères d'ultra-haute performance d'une épaisseur de 2  $\mu\text{m}$  et d'une largeur de 30 cm ont été produites par étirement d'un polyéthylène à haut poids moléculaire (UHMW PE).

Dans un 2eme temps, un co-polyester cristal liquide a été extrudé en feuilles de 3  $\mu\text{m}$  par des buses spéciales. Le traitement thermique suite à l'extrusion a permis d'obtenir des feuilles dont les propriétés mécaniques sont proches de celles des fibres commerciales.

Le même procédé a été utilisé pour produire des feuilles orientées d'aramid lyotropic en extrusion d'acide sulfurique et coagulation dans un bain d'eau.

Enfin, des feuilles de cellulose bactérienne ont été cultivées et orientées in-situ. Ces feuilles ont montré d'excellentes propriétés mécaniques en étirement, et conservent de très bonnes propriétés dans la direction perpendiculaire.

En guise de résumé: cette thèse montre que des feuilles de polymères aux propriétés mécaniques aussi élevées que celles des feuilles de fibre peuvent être produites. Ceci ouvre des nouvelles possibilités dans la conception de matériaux composites.

## **Feuilles de polymères hautes-performances à géométrie plane**

Les feuilles unidirectionnelles ont été laminées à différents angles pour produire des matériaux dont la force dans la direction transversale est grandement augmentée.

Les feuilles d'UHMW PE ont été fusionnées en utilisant un solvant ou en incorporant directement un co-polymère avec un point de fusion réduite. De cette manière, un laminât en 4 couches avec une épaisseur de 10  $\mu\text{m}$  et un module de Young de 35 GPa à direction plane a été fabriqué.

La lamination de polyester thermotropic a été accomplie avec seulement 5 % d'adhésif, ce qui a produit des feuilles aux propriétés mécaniques proches des limites théoriques.



# I

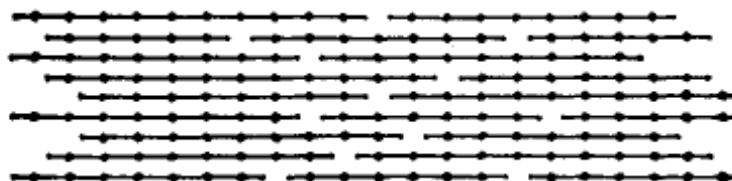
## *Introduction*



# 1 Background

The use of polymers in demanding mechanical applications has surged since the development - starting in the late 1960's - of high-performance fibers, which by now have found a broad spectrum of applications, including bulletproof vests and panels, cut-resistant gloves, reinforced tires, ropes, composites in aviation and aerospace, surgical sutures, etc. Table 1 lists a selected number of such high-performance fibers, together with more traditional versions, which reveals that these materials, on equal weight basis, are up to 10 times stronger than steel.

The common feature of high-performance polymer fibers is that they all exhibit a high degree of orientation and extension of the macromolecular chains that constitute them, which permits sharing of an applied load over a large number of covalent bonds. Remarkably, already in 1932, pondering the question “*what conditions of molecular structure are requisite for the production of a useful fiber?*”, in their pioneering, seminal paper,<sup>1</sup> Carothers and Hill “*picture[d] a perfectly oriented fiber as consisting essentially of a single crystal in which the long molecules are in ordered array parallel with the fiber axis*” (Figure 1; 10 in the original paper) - more than three decades before their actual development.



**FIGURE 1** “Perfectly oriented fiber” as a “lattice from molecules of unequal length” postulated by Carothers and Hill in 1932.<sup>1</sup>

Regrettably, in the absence of external fields such as flow or mechanical stress, polymers normally do not form such uniaxially oriented structures, but, rather, tend to assemble into isotropic solids of modest mechanical performance.

Over the years, numerous of different processing routes towards polymer fibers of the above desired macromolecular arrangement have evolved; the more relevant technologies will be briefly summarized below.

Historically, the first approach is based on simple tensile deformation of melt-spun, conventional, *flexible*, coiled macromolecules such as polyesters and polyamides,<sup>1</sup>

which resulted in the first fully synthetic fiber of commercial success (“Nylon”). Unfortunately, the degree of orientation and chain extension in these fibers is, however, modest, due to the relatively low maximum draw ratios that can be reached (final/original length ~4-5; often erroneously referred to as the “natural draw ratio”). As Carothers and Hill already noted: “(In actual fibers a considerable number of the molecules fail to identify themselves completely with [the] perfectly ordered structure)”,<sup>1</sup> and, consequently, their mechanical properties are far below their theoretical limits (cf. Table 1).<sup>2</sup>

The second route involves *rigid* polymers of a highly extended molecular structure, such as the aromatic polyamide (aramid) poly(*p*-phenylene terephthalamide) (PPTA), first synthesized by Kwolek in 1965.<sup>3,4</sup> Because of their rigidity, these polymers exhibit extremely high melting temperatures, well above the onset of their thermal decomposition, and, hence, are spun into filaments from solutions – most often strong acids such as sulfuric acid. Conveniently, above a certain molecular aspect-ratio-dependent polymer concentration, such rigid macromolecules form ordered (lyotropic) solutions, from which they can readily be oriented by application of an elongational flow field, which is achieved simply by applying a draw-down ratio (i.e. windup/extrusion speed)  $\gg 1$ . Consolidation of that orientation is effectuated in the “dry-jet-wet” or “air-gap” spinning process developed by Blades,<sup>5</sup> to yield high-modulus/high-strength organic polymer fibers. The first of such fibers was commercialized by E. I. du Pont de Nemours & Company, Inc. under the trade name Kevlar<sup>®</sup>, followed by AKZO as Twaron<sup>®</sup> (now sold by Teijin); both are based on PPTA. Subsequently developed rigid chain polymers include, for instance, poly(*p*-phenylene benzobisoxazole) (PBO)<sup>6</sup> and poly({2,6-diimidazole [4,5-b:4',5'-e] pyridinylene-1,4(2,5-dihydroxy)phenylene}) (PIPD),<sup>7</sup> which are also processed from lyotropic solutions in strong acids.

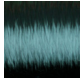
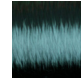
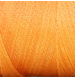
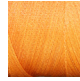








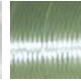
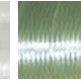
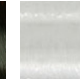
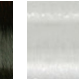
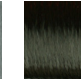
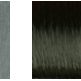
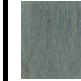

In order to circumvent the above cumbersome and rather unfriendly acid solution-processing scheme, *semi-rigid* (co-)polymers, such as poly(*p*-hydroxybenzoic acid-co-2-hydroxy-6-naphthoic acid), e.g. Vectra<sup>®</sup>, have been developed, which are spun from an ordered (thermotropic) melt, followed by solid-state post-polymerization below their melting point.<sup>8-12</sup> Unfortunately, their processing advantage does compromise the mechanical properties of fibers produced from these materials (cf. Table 1).

A third process for the production of high-performance fibers originated in a careful reexamination of tensile deformation “beyond the ‘natural’ draw ratio” of flexible chain polymers, notably of polyethylene (PE), among others, by Peterlin *et al.*.<sup>13-16</sup> These efforts were motivated by the knowledge that theoretical and experimental estimates of the axial tensile modulus of PE are around 300 GPa.<sup>2</sup> In the early 1970’s Capaccio and Ward succeeded in deforming melt-processed, solid PE to a draw ratio above 20, yielding materials of a Young’s modulus of up to 70 GPa.<sup>17-19</sup> Owing to the relatively low molar mass of the polymers employed, however, their tensile strength was limited. Attempts to draw melt-processed PE grades of higher molar mass to the same ratio - expected to exhibit superior tenacity - failed, and the “classical” natural maximum draw ratio of about 5 was recovered.<sup>20</sup> This limitation was overcome in the late 1970’s due to the recognition that macromolecular entanglements dictate the deformation behavior of weakly-bonded polymer solids such as PE, and that by a reduction of the entanglement density through processing from (semi-)dilute-solution, ultra-high molecular weight polyethylene (UHMW PE) fibers can be drawn to draw ratios in excess of 100, close to their molecular-weight-limited maximum molecular draw ratio.<sup>21-23</sup> With this (erroneously labeled) “gel-spinning” process, high-performance UHMW PE fibers are manufactured with tensile moduli well above 100 GPa, sold by DSM under the trade name of Dyneema<sup>®</sup> and, under license, by Allied-Signal, now Honeywell, as Spectra<sup>®</sup>.

N.B. Not detailed here is the pioneering work of Pennings *et al.* who, in fact, produced the first high-strength fiber of UHMW PE by a solution-based process referred to as “surface growth”,<sup>24</sup> followed by Keller and coworkers;<sup>25</sup> nor of Porter *et al.* who,<sup>26</sup> like Ward and co-workers as well as other authors, adopted a solid-state extrusion technique,<sup>27</sup> as these efforts did not lead to commercially viable products.

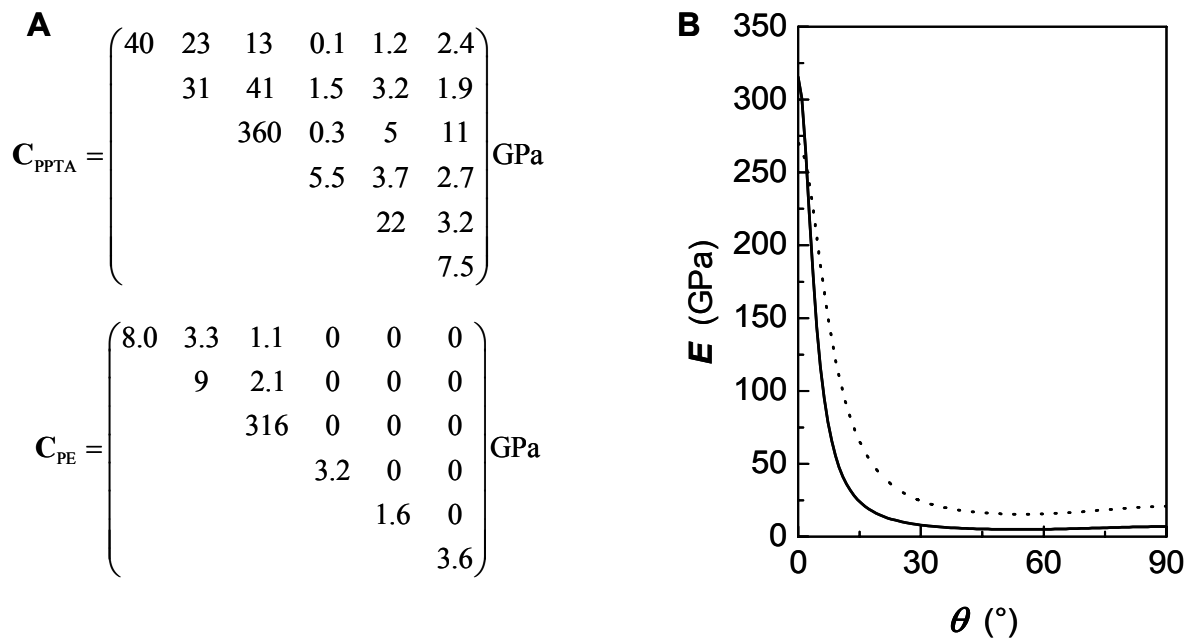
Finally, for the sake of completeness, another class of high-performance fibers should be mentioned, namely carbon fibers. These fibers are produced from a variety of polymer precursor filaments, e.g. polyacrylonitrile (PAN),<sup>28</sup> or directly melt spun from petroleum or coal-tar pitch.<sup>29</sup> The precursor fibers first are oxidized at elevated temperatures (200-400 °C) and in a second step at higher temperatures (2,700-3,000 °C) to a certain extent graphitized.

**TABLE 1** Properties of selected high-performance fibers: Young's modulus  $E$ , tensile strength  $\sigma$ , strain at break  $\epsilon$  and density  $\rho$ . Flex-loss is a measure of strength after 60 bending cycles. UV resistance is expressed as the amount of exposure time it takes for a yarn to lose 50 percent of its initial modulus.  $T_m$ ,  $T_{dec}$  melting or thermal decomposition temperature. Approximate cost from ref. 40 or provided by the supplier. n/a is not affected. # Material starts to decompose before melting.

material	chemical structure	$E$		$\sigma$		$\epsilon$ %	$\rho$ g/cm <sup>3</sup>	flex-loss %	UV months	$T_m$ , $T_{dec}$ °C	cost €/kg	ref.
		GPa	N/tex	GPa	N/tex							
	Poly(1,2,6-dimidazole [4,5- <i>b</i> :4',5'- <i>e</i> ] pyridinyne-1,4(2,5-dihydroxy)phenylene) PPPD M5 <sup>®</sup>											
	<chem>[*]c1ccc(O)c2nc(O)c3nc(O)c(O)c3n2c1</chem>	330	194	5.5	3.2	1.7	1.7	-	-	530 <sup>#</sup>	-	30
	Poly( <i>p</i> -phenylene benzobisoxazole) PBO Zylon <sup>®</sup> HS											
	<chem>[*]c1ccc2oc3ccccc3o2c1</chem>	270	173	5.8	3.7	2.5	1.56	30	2	650 <sup>#</sup>	220	31
	Ultra-high molecular weight polyethylene UHMW PE Dyneema <sup>®</sup> SK76											
	<chem>[*]CC(C)C[*]</chem>	116	120	3.6	3.7	3.8	0.97	0	7	150	30-95	32
	Poly( <i>p</i> -phenylene terephthalamide) PPTA Kevlar <sup>®</sup> 49											
	<chem>[*]c1ccc(cc1)C(=O)Nc2ccc(cc2)C(=O)N[*]</chem>	113	78	3.0	2.1	2.5	1.44	28	2-3	550 <sup>#</sup>	40-65	33
	Poly( <i>p</i> -hydroxybenzoic acid-co-2-hydroxy-6-naphthoic acid) copolymer HBA/HNA Vectran <sup>®</sup> HS 1500/300											
	<chem>[*]c1ccc(cc1)C(=O)O</chem>	72	52	3.2	2.3	3.7	1.40	15	1-2	330	70	34
	Poly( $\beta$ -1,4-D-glucan) Cellulose Cordenka <sup>®</sup> EHM-Rayon											
	<chem>[*]OC(O)[C@H]1O[C@@H](O)[C@H](O)[C@@H](O)[C@H]1O</chem>	38	25	0.9	0.6	4.6	1.50	-	5	200 <sup>#</sup>	-	35
	Poly(ethylene terephthalate) PET											
	<chem>[*]OC(=O)c1ccc(cc1)C(=O)O[*]</chem>	14	10	1.0	0.8	8-11	1.39	0	6	260	5	36
	Poly(6-aminocaproic acid) Nylon 6											
	<chem>[*]NCCCCCCCC(=O)O[*]</chem>	5	4	1.0	0.8	12-17	1.14	0	3-4	220	5	37
	Carbon HexTow <sup>®</sup> IM9											
	<chem>[*]C1=CC=C2C=CC=CC2=C1</chem>	304	167	6.14	3.4	1.8	1.80	100	n/a	3700 <sup>#</sup>	80-270	38
	Stainless Steel Type 304											
	<chem>[*]X[Cr]Ni18[Cr]10[*]</chem>	195	25	0.6	0.1	30	7.90	-	n/a	550	5	39

## 2 From Fiber to Fabric and Film and Foil

As mentioned above, the origin of the outstanding mechanical properties of high-performance polymer fibers is the covalently bonded nature of their constituent macromolecules and their predominantly uniaxial arrangement. Unfortunately, the response of such highly anisotropic structures, not surprisingly, is strongly dependent on the direction of applied load or strain, as is quantitatively reflected in their stiffness matrices, shown in Figure 2A for ideal single crystals of PPTA<sup>41</sup> and PE<sup>42</sup>. Figure 2B displays the extraordinary pronounced dependence of the Young's modulus on the test angle of such structures, calculated according to Bastiaansen *et al.*<sup>43</sup> Most illustratively, at an inclination of only 10°, the modulus of PE reduces to only about *one-tenth* of the axial (macromolecular) stiffness. The somewhat less sensitive “off-axis performance” of PPTA is, of course, due to the stronger hydrogen bonds between the polymer chains in comparison to the weak van der Waals interactions between PE macromolecules.

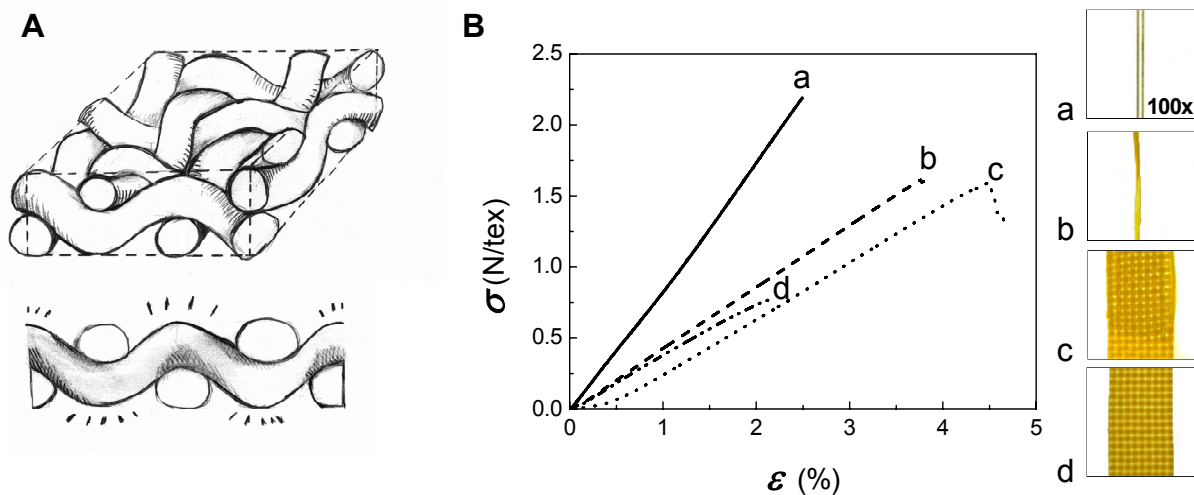


**FIGURE 2** A. Stiffness matrices of PPTA<sup>41</sup> (top) and PE<sup>42</sup> (bottom). B. Theoretical test-angle,  $\theta$ , dependence of the Young's modulus,  $E$ , of an ideal, extended-chain single crystal of PPTA (dashed curve) and PE (solid curve), calculated according to ref. 43.

The above strong test-angle dependence of the mechanical properties of high-performance polymer fibers, naturally, has major consequences for the design and

ultimate characteristics of the products in which they are utilized.

Traditionally, fibers are most often applied in twisted form, such as in yarns and ropes, are woven, as in fabrics and cloth (Figure 3A), or are used in cut form, for instance in non-wovens and in custom composites - i.e. generally not in a fashion in which they experience strictly uniaxial load. In view of the highly anisotropic characteristics of high-performance fibers, it is well known and readily understood that this leads to a more or less severe reduction of the mechanical properties of the final objects in which they are incorporated.<sup>44-46</sup> The latter is illustrated in Figure 3B which displays the stress-strain behavior recorded at room temperature of a PPTA (Kevlar<sup>®</sup> 49) single filament, a twisted yarn of 1,000 filaments, a woven fabric and that of the same fabric embedded in epoxy.



**FIGURE 3** A. Sketch of typical plain-weave fabric and warp cross-section. B. Stress-strain behavior of a PPTA single filament (a), twisted 1,000 filament yarn (b), woven fabric (c) and the same fabric embedded in epoxy (d); all normalized to the quantity of directly load-bearing filaments. The width of the images corresponds to 15 mm; single filament (a) is shown at a 100x magnification. Test procedure described in ref. 47.



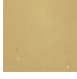
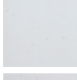

Especially at low strain, the development of stress is markedly influenced by the crimp causing uncontrollable shape distortion, which is reflected in ‘j-shape’ stress-strain behavior.<sup>48</sup> The results clearly demonstrate the significant reduction in the stiffness - when compared to that of the single filament - due to “off-axis” loading of the various fiber assemblies.

Attempts have been made to avoid the adversary effects associated with weaving or use of short-fiber-reinforced composites and to manufacture high-performance,

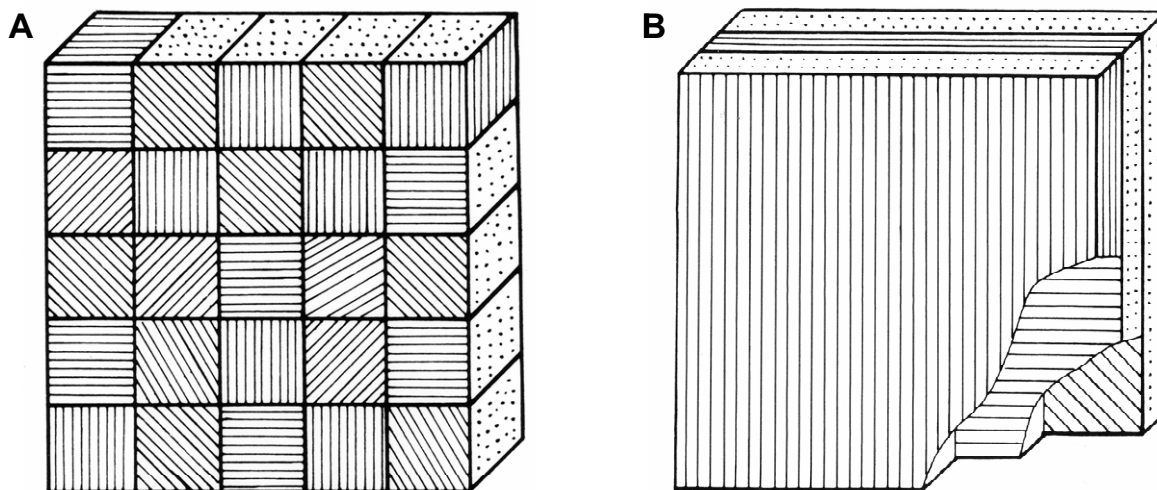


biaxially oriented polymer films. Such films have been produced by biaxial deformation in the solid state or, for instance in the case of PPTA, using a mandrel-guided precipitation process.<sup>49-51</sup> Another technique, specifically designed to process thermotropic liquid-crystalline polymers, such as Vectra<sup>®</sup>, employs a die with three rotating cylinders to form films.<sup>52, 53</sup> An alternative - most elegant - process is the *in-situ* growth of planar oriented bacterial cellulose films.<sup>54</sup> Table 2 displays relevant mechanical properties of a number of such “high-performance” polymer films. Even cursory examination reveals that their characteristics are far inferior when compared to those of the corresponding uniaxially oriented fibers (Table 1).

**TABLE 2** Mechanical properties of selected high-performance polymer films. \*Value provided by the supplier.

	material	Young's modulus $E$ GPa	Strength $\sigma$ MPa	Strain at break $\varepsilon$ %	Density $\rho$ g/cm <sup>3</sup>	ref.
	Bacterial Cellulose	18	230	2	0.99	54
	PPTA Aramica <sup>®</sup>	15	400	20	1.44	55
	HBA/HNA Vectra <sup>®</sup>	10	240	3*	1.40	56
	UHMW PE	6	600	50	0.98	57
	PET Mylar <sup>®</sup>	5	250	120	1.39	58

Calculations of Bastiaansen *et al.*<sup>43</sup> indicate that, owing to their structure, the stiffness of such films, in fact, can be expected to be relatively low. Biaxially oriented films typically resemble a planar aggregate of small crystals and not a sheet-like laminate of extended-chain single crystals (see Figures 4A and 4B). Assuming, for instance, that the constituent entities are ideal single crystals of polyethylene with the stiffness matrix presented in Figure 2A, the maximum Young's modulus of such an aggregate was shown to be only 12 GPa, while that of the hypothetical laminate of ideal single crystals was calculated to be 111 GPa. As the latter structure is of key interest in the present work, their mechanical properties will be elaborated upon in some more detail in the next section.



**FIGURE 4** A. Schematic of a planar oriented aggregate of crystalline entities, as often found in biaxially deformed films. B. Structure of a planar assembly of perfect, extended-chain polymer crystals.<sup>43</sup>

## 2.1 Classical Lamination Theory

Uniaxially oriented polymer foils, such as drawn tapes or even single-crystal layers, can typically be regarded as transversely isotropic materials, characterized by five independent elastic constants, having a high stiffness in the longitudinal direction and a low isotropic modulus in the plane transverse to the longitudinal direction. The off-axis stiffness and strength of laminates from these foils is then described, respectively, by classical lamination theory, and anisotropic failure rules, such as the Tsai-Hill criterion.<sup>59</sup>

In classical lamination theory, it is assumed that a laminate is in a plane stress state, reducing the number of relevant elastic constants for a single foil to four: the longitudinal modulus,  $E_l$ , the transverse modulus,  $E_t$ , the shear modulus,  $G_{lt}$ , and the Poisson's ratio,  $\nu_{lt}$ . It can be shown through an appropriate coordinate transformation of the compliance tensor, that in uniaxial deformation, the off-axis Young's modulus,  $E_\theta$ , of a single foil varies with  $\theta$ , the angle between the loading direction and the longitudinal axis as:

$$\frac{E_\theta}{E_l} = \left( \cos^4 \theta + \left( \frac{E_l}{G_{lt}} - 2\nu_{lt} \right) \cos^2 \theta \sin^2 \theta + \frac{E_l}{E_t} \sin^4 \theta \right)^{-1} \quad (1)$$

When the longitudinal and transverse modulus,  $E_l$  and  $E_t$ , and the Poisson's ratio  $\nu_{lt}$

(often assumed to be equal to that of the isotropic material) are known, the shear modulus,  $G_{lt}$ , can be calculated from  $E_{45}$ , the off-axis stiffness determined in a tensile test at  $\theta = 45^\circ$ , as:

$$\frac{G_{lt}}{E_l} = \left( 4 \frac{E_l}{E_{45}} - (1 - 2\nu_{lt}) - \frac{E_l}{E_t} \right)^{-1} \quad (2)$$

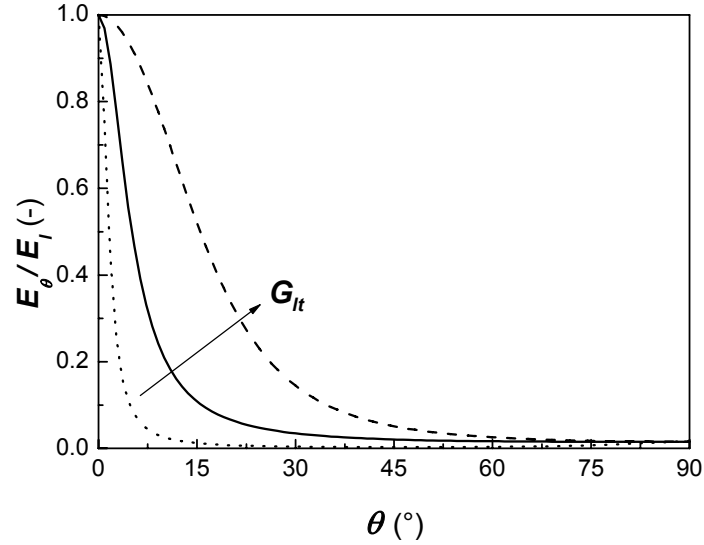
Similarly, the anisotropic failure criterion of Tsai-Hill allows calculation of the off-axis strength,  $\sigma_\theta$ , from the longitudinal, transverse and shear strength (respectively,  $\sigma_l$ ,  $\sigma_t$ , and  $\tau_{lt}$ ) as:

$$\sigma_\theta = \left( \frac{\cos^2 \theta (\cos^2 \theta - \sin^2 \theta)}{\sigma_l^2} + \frac{\cos^4 \theta}{\sigma_t^2} + \frac{\cos^2 \theta \sin^2 \theta}{\tau_{lt}^2} \right)^{-1} \quad (3)$$

Here, the shear strength,  $\tau_{lt}$ , can be determined from the off-axis tensile strength,  $\sigma_{10}$ , measured at an angle  $\theta = 10^\circ$ , as:<sup>60</sup>

$$\tau_{lt} = \sigma_{10} \sin(10^\circ) \cos(10^\circ) \quad (4)$$

The influence of the elastic constants on the anisotropic behavior of a single foil is depicted in Figure 5. Obviously, the longitudinal and transverse modulus determine, respectively, the upper and lower limit of the foil stiffness. However, from Figure 5, it can be seen that the off-axis stiffness of the foil strongly depends on the shear modulus,  $G_{lt}$ .



**FIGURE 5** Normalized off-axis Young's modulus,  $E_\theta/E_l$ , calculated with  $E_l = 130$  GPa (that of a typical foil described in Chapter II),  $E_t = 2$  GPa,  $\nu_{lt} = 0.4$  and values of the shear modulus,  $G_{lt}$ , of, resp. , 0.1, 1, and 10 GPa.

To reduce the anisotropic properties of the foils, it is common practice to stack differently oriented foils, and bind them together to form a laminate. The stiffness of such multi-foil laminates is described by classical lamination theory. Assuming that the in-plane strains in all foils are equal and that all foils have the same thickness, the elastic behavior of the laminate follows from the average value of the stiffness tensor, taking into account for each foil the mismatch between the loading and longitudinal direction. Analogous to the case of a single foil, the Young's modulus of the laminate as a function of loading angle then follows from the average compliance tensor, which is the inverse of the average stiffness tensor, albeit not resulting in a simple relation as Equation 1. In general, not surprisingly, the anisotropy of the laminate is reduced with increasing number of differently oriented foils and may even vanish. This is depicted in Figure 6, which shows the angular dependence of the Young's modulus of a single foil, a  $[0/90]$ ,  $[0/60/120]$  and  $[0/45/90/135]$  laminate. In this figure, it can be observed that the in-plane Young's modulus for the latter two laminates is independent of the loading direction, and such laminates are, therefore, referred to as "quasi-isotropic". The general lay-up that leads to quasi-isotropic laminates is  $\left[0/\frac{180}{m}/\dots/(m-1)\frac{180}{m}\right]$ , where  $m$  is the number of different orientations in the laminate, with  $m \geq 3$ . For all these laminates the in-plane stiffness constants can be

expressed as: <sup>61</sup>

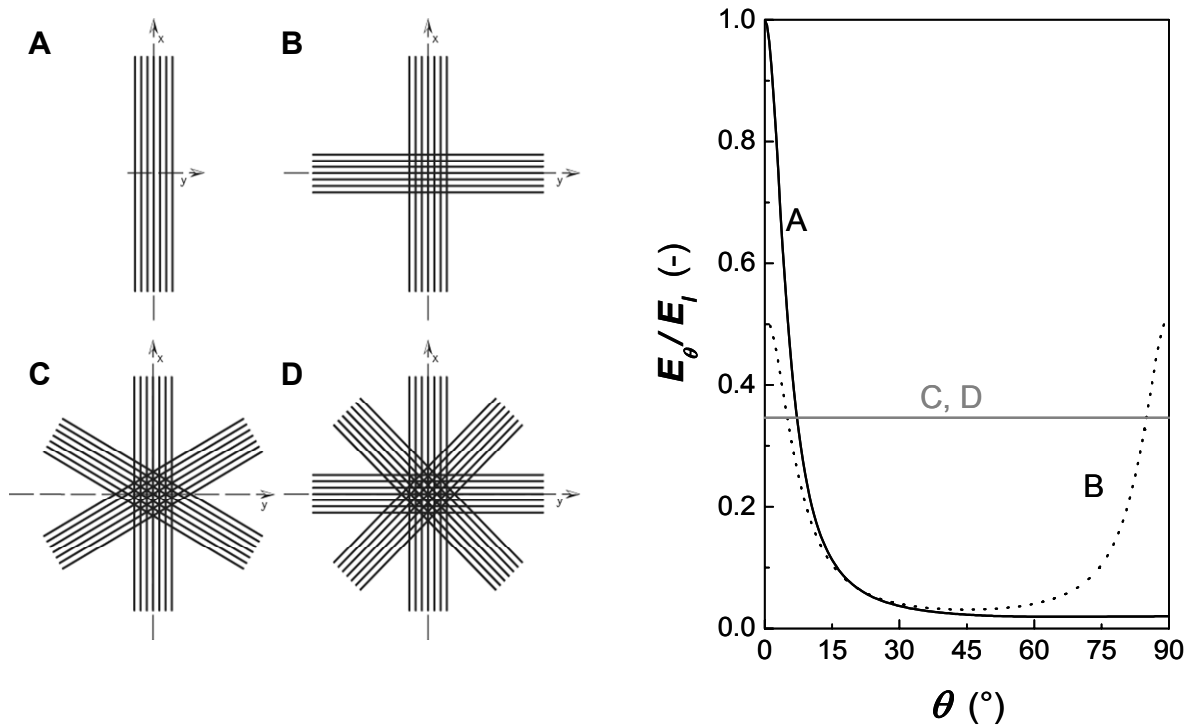
$$G = \frac{1}{2}G_{lt} + \frac{1}{8} \frac{E_l(E_l + E_t - 2\nu_{lt}E_t)}{E_l - \nu_{lt}^2E_t} \quad (5)$$

$$\nu = \frac{-\frac{1}{2}G_{lt} + \frac{1}{8} \frac{E_l(E_l + E_t + 6\nu_{lt}E_t)}{E_l - \nu_{lt}^2E_t}}{\frac{1}{2}G_{lt} + \frac{1}{8} \frac{E_l(3E_l + 3E_t + 2\nu_{lt}E_t)}{E_l - \nu_{lt}^2E_t}} \quad (6)$$

$$E = 2(1 + \nu)G \quad (7)$$

For most oriented polymer foils it holds that  $E_l \gg E_t, G_{lt}$ . Under these conditions, the above in-plane elastic constants approach asymptotically the following limiting values: <sup>61</sup>

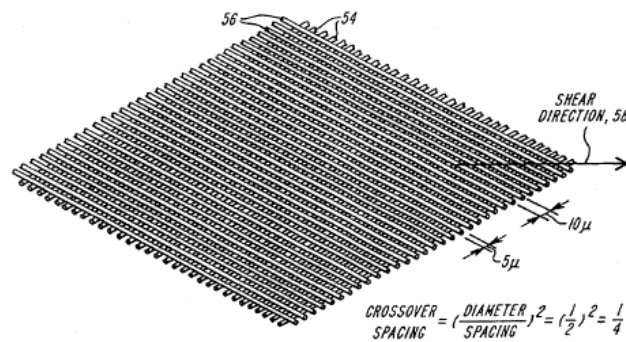
$$E \approx \frac{E_l}{3}, \quad \nu \approx \frac{1}{3}, \quad G \approx \frac{E_l}{8} \quad (8)$$



**FIGURE 6** Various ply geometries of uniaxially oriented layers and their normalized off-axis Young's modulus,  $E_\theta/E_t$ , calculated with  $E_l = 130$  GPa,  $E_t = 2$  GPa,  $G_{lt} = 800$  MPa and  $\nu_{lt} = 0.4$  (see text): **A** Single, unidirectional layer [ $\theta = 0$ ], **B** Cross-ply [ $0/90$ ], **C** [ $0/60/120$ ], and **D** [ $0/45/90/135$ ] laminate.

### 3 Recent Developments

In order to employ high-performance fibers more efficiently and better exploit their ultimate potential, more recently, laminates of multifilament strands and of spread multifilaments have been developed. Striking examples in the arena of high-performance sails are products made with the three-dimensional laminate (3DL<sup>®</sup>) technology by North Sails Group,<sup>62</sup> the Cuben<sup>®</sup> fiber laminates (Figure 7)<sup>63</sup> and Createx Amalgame sheets (Figure 8).<sup>64</sup>



**FIGURE 7** Schematic of a Cuben<sup>®</sup> fiber laminate, comprising untwisted UHMW PE or carbon filaments embedded in an elastomeric polymer matrix; from US Patent 5,470,632.<sup>63</sup>



**FIGURE 8** 2007 America's Cup Defender Team Alinghi testing their new experimental front sail (genoa), constructed with Createx Amalgame spread-fiber technology.<sup>64</sup> The mainsail is a North Sails Group 3DL<sup>®</sup> product.<sup>62</sup> Photograph reprinted with permission.<sup>65</sup>

The properties of such laminated strands and embedded spread filaments are well understood and can readily be calculated with well-known theories.<sup>66</sup> Unfortunately, there are considerable difficulties in manufacturing such products of high fiber content. The theoretical maximum fiber volume fraction for random packing is 82 %.<sup>67</sup> In practice, however, that fraction appears to be limited to about 55-65 % only.<sup>68</sup> As the stiffness of the matrix or encompassing foils, generally, is low in comparison with that of the high-performance fibers, the upper limit of the axial stiffness that is reached - even for composites and laminates comprising perfectly-aligned filaments - is approximately only half of the actual value of the reinforcing elements.

Recent attempts to employ no foreign matrix and produce “single-species” fiber-based composites have been met with some success, notably in the case of PE<sup>69,70</sup> and isotactic polypropylene (i-PP).<sup>71-74</sup> Typically, in the processes developed, uniaxially oriented fibers or tapes are hot compacted in the vicinity of their melting temperature, causing partial melting of the polymer, which leads them to fuse together - invariably, however, with a partial loss of their initial properties.

In summary, since the development of high-performance polymer fibers, considerable progress has been made in constructing advanced products thereof retaining a significant fraction of their outstanding mechanical characteristics. But also, clearly, there is room for improvement and better exploitation of the unique intrinsic mechanical properties of assemblies of oriented extended-chain macromolecules.

## 4 Objectives and Scope of Thesis

The principal objective of the work presented in this thesis was to develop routes for manufacturing ultra-high-performance polymer foils that avoid the mechanical losses associated with, for instance, woven and biaxially deformed structures, and that are not based on the cumbersome and inefficient spreading, reassembling and consolidation of high-performance multi-filament yarns.

In Chapter II (relatively large-scale) processing and properties of *unidirectionally* oriented foils of solution(“gel”)-cast/drawn ultra-high molecular weight polyethylene (UHMW PE) are described and the dependence of their characteristics on various processing and structural variables (including macromolecular pre-orientation) is addressed. In addition, the formation and mechanical characteristics of *planar balanced* multi-layer foils produced with these uniaxially oriented UHMW PE foils (as in Figure 4B) are presented. Special attention is paid to adhesion between the constituent layers, which is enhanced by the addition of partially polar copolymers.

In Chapter III, a novel process is advanced for manufacturing of oriented foils from a *thermotropic* liquid-crystalline polyester, the semi-rigid poly(*p*-hydroxybenzoic acid-co-2-hydroxy-6-naphthoic acid) (HBA/HNA), which is based in part on the use of specially designed multi-filament-fusion spinnerets. In addition, a detailed comparison is made between the mechanical characteristics of the foils produced and those of melt-spun monofilaments of the same polymer. Furthermore, in analogy to Chapter II for UHMW PE, balanced foils of this material are presented.

Chapter IV describes the use of one of the multi-filament-fusion spinnerets disclosed in Chapter III for production of oriented foils of the *lyotropic* liquid-crystalline rigid polymer poly(*p*-phenylene terephthalamide) (PPTA) by “air-gap extrusion”. The efficacy of the novel die is evaluated and the angular dependence of the stiffness of the uniaxially oriented foils produced is presented.

Chapter V is concerned with the formation of high-performance, oriented bacterial cellulose foils. Major improvements in stiffness and tenacity are demonstrated for foils grown while under strain.

Finally, in Chapter VI, general conclusions and an outlook are presented.



## 5 References and Notes

1. Carothers, W. H. ; Hill, J. W. *J. Am. Chem. Soc.* **1932**, 54, 1579.
2. Kausch, H. H. *Polymer Fracture*, 2nd ed. ; *Springer*, Berlin **1987**.
3. Kwolek, S. L. *FR Patent* 1,526,745 **1968**; *US Patent* 3,600,350 **1971**.
4. Kwolek, S. L. ; Morgan, P. W. ; Schaeffgen, J. R. ; Gulrich, L. W. *Macromolecules* **1977**, 10, 1390.
5. Blades, H. *US Patents* 3,767,756 **1973**; 3,869,429 **1975**.
6. Sweeny, W. ; Kwolek, S. L. *US Patent* 4,608,427 **1986**.
7. Sikkema, D. J. *Polymer* **1998**, 39, 5981.
8. Jackson, W. J. ; Kuhfuss, H. F. *US Patent* 3,778,410 **1973**.
9. Roviello, A. ; Sirigu, A. *J. Polym. Sci. Polym. Lett.* **1975**, 13, 455.
10. Jackson, W. J. ; Kuhfuss, H. F. *J. Polym. Sci. Polym. Chem.* **1976**, 14, 2043.
11. Kleinschuster, J. J. ; Pletcher, T. C. *US Patent* 4,006,620 **1978**.
12. Calundann, G. W. *US Patents* 4,161,470 **1979**; 4,184,996 **1980**; 4,256,624 **1981**.
13. Meinel, G. ; Morosoff, N. ; Peterlin, A. *J. Polym. Sci. Polym. Phys.* **1970**, 8, 1723.
14. Meinel, G. ; Peterlin, A. *J. Polym. Sci. Polym. Phys.* **1971**, 9, 67.
15. Peterlin, A. *J. Mater. Sci.* **1971**, 6, 490.
16. Peterlin, A. *J. Macromol. Sci.-Phys.* **1981**, B19, 401.
17. Capaccio, G. ; Ward, I. M. *Nature (Phys. Sci.)* **1973**, 243, 130.
18. Capaccio, G. ; Ward, I. M. *Polymer* **1974**, 15, 233.
19. Ward, I. M. ; Capaccio, G. *US Patent* 3,962,205 **1976**.
20. Capaccio, G. ; Ward, I. M. *Polymer* **1975**, 16, 239.
21. Smith, P. ; Lemstra, P. J. *US Patents* 4,344,908 **1982**; 4,422,993, **1983**; 4,430,383 **1984**; 4,436,689 **1984**.
22. Smith, P. ; Lemstra, P. J. *J. Mater. Sci.* **1980**, 15, 505.
23. Smith, P. ; Lemstra, P. J. ; Booij, H. C. *J. Polym. Sci. Polym. Phys.* **1981**, 19, 877.
24. Zwijsenburg, A. ; Pennings, A. J. *J. Polym. Sci. Polym. Lett.* **1976**, 14, 339.
25. Barham, P. J. ; Hill, M. J. ; Keller, A. *Colloid Polym. Sci.* **1980**, 258, 899.
26. Kojima, S. ; Porter, R. S. *J. Polym. Sci. Polym. Phys.* **1978**, 16, 1729.
27. Ciferri, A. ; Ward, I. M. *Ultra-High Modulus Polymers*; *Applied Science Publishers LTD*, London **1979**.
28. Donnet, J. B. ; Bansal, R. C. *Carbon fibers*, 2nd Edn; *Marcel Dekker, Inc.*, New York **1990**.
29. Singer, L. S. *US Patent* 4,005,183 **1977**.
30. Product information; [www.m5fiber.com](http://www.m5fiber.com) **2005**.
31. Product information; Zylon Toyobo Co. Ltd. **2005**.
32. Product information brochure; DSM Dyneema BV **2004**.
33. Northolt, M. G. ; Sikkema, D. J. *Adv. Polym. Sci.* **1991**, 98, 115.
34. Product information; [www.vectranfiber.com](http://www.vectranfiber.com) **2006**.
35. Northolt, M. G. ; Boerstoel, H. ; Maatman, H. ; Huisman, R. ; Veurink, J. ; Elzerman, H. *Polymer* **2001**, 42, 8249.
36. *Encyclopedia of Polymer Science and Engineering* Volume 12; p. 125; *John Wiley & Sons, Inc.* **1988**.

37. Encyclopedia of Polymer Science and Engineering Volume 11; p. 426,429; *John Wiley & Sons, Inc.* **1988**.
38. Product information; [www.hexcel.com](http://www.hexcel.com) **2007**.
39. ASM Metals Reference Book, 2nd ed. ; *American Society for Metals*, Metals Park **1983**.
40. Yang, H. H. Kevlar Aramid Fiber; *John Wiley & Sons Ltd.*, UK **1993**.
41. Rutledge, G. C. ; Suter, U. W. *Polymer* **1991**, 32, 2179.
42. Wunderlich, B. Macromolecular Physics, Vol. 1; *Academic Press*, New York **1983**.
43. Bastiaansen, C. W. M. ; Leblans, P. J. R. ; Smith, P. *Macromolecules* **1990**, 23, 2365.
44. Andrews, M. C. ; Day, R. J. ; Hu, X. ; Young, R. J. *J. Mater. Sci. Lett.* **1992**, 11, 1344.
45. Jortner, J. *Carbon* **1992**, 30, 153.
46. Yurgartis, S. W. ; Morey, K. ; Jortner, J. *Compos. Sci. Technol.* **1993**, 46, 39.
47. Tests were performed at room temperature, at a constant cross-head speed of 5 and 1 mm/min using a Zwick tensile tester Z020. The gauge length was 300 mm for the monofilament and 30 mm for the other samples. The cross-sectional areas of the monofilament were calculated from the weight. Load on the fabric was normalized by the cross-sectional area of the fibers to the test direction only; i.e. the presence of perpendicular threads, as well of the epoxy matrix was disregarded.
48. Hearle, J. W. S. ; Gosberg, P. ; Backer, S. Structural Mechanics of Fibers, Yarns and Fabrics, Volume 1; *John Wiley & Sons, Inc.*, US **1969**.
49. Fellers, J. F. ; White, J. L. ; Onogi, Y. ; Flood, J. ; Aoki, H. ; Hancock, T. A. ; Spruiell, J. E. *Abstr. Pap. Am. Chem. Soc.* **1980**, 179, 46.
50. Flood, J. E. ; White, J. L. ; Fellers, J. F. *J. Appl. Polym. Sci.* **1982**, 27, 2965.
51. Bodaghi, H. ; Kitao, T. ; Flood, J. E. ; Fellers, J. F. ; White, J. L. *Polym. Eng. Sci.* **1984**, 24, 242.
52. Harvey, A. C. ; Lusignea, R. W. ; Rubin, L. S. *US Patent* 5,288,529 **1994**.
53. Lusignea, R. W. *Polym. Eng. Sci.* **1999**, 39, 2326.
54. Yamanaka, S. ; Watanabe, K. ; Kitamura, N. ; Iguchi, M. ; Mitsuhashi, S. ; Nishi, Y. ; Uryu, M. *J. Mater. Sci.* **1989**, 24, 3141.
55. Product information; Aramica<sup>®</sup> PPTA Film, [www.teijin.co.jp](http://www.teijin.co.jp) **2006**.
56. Product information; [www.ticona.com](http://www.ticona.com) **2006**.
57. Gerrits, N. ; Young, R. J. ; Lemstra, P. J. *Polymer* **1990**, 31, 231.
58. Product information; Du Pont Teijin Films **2003**.
59. Hull, D. An introduction to composite materials; *Cambridge University Press*, Cambridge (UK), **1981**.
60. Chamis, C. C. ; Sinclair, J. H. *Exp. Mech.* **1977**, 17, 339.
61. Akkerman, R. *Composites Part B* **2002**, 33, 133.
62. Baudet, J. P. *US Patent* 5,097,784 **1992**.
63. Meldner, H. ; Downs, R. J. *US Patent* 5,470,632 **1995**.
64. Gautier, G. ; Kessi, E. *US Patent Application* 0157189 A1 **2006**.
65. Reprinted with permission from Ivo Rovira/Alinghi; [www.alinghi.com](http://www.alinghi.com) **2007**.
66. Voigt, W. Lehrbuch der Kristallphysik; *B.G. Teubner*, Leipzig **1945**.
67. Kausch, H. H. ; Fesko, D. G. ; Tschoegl, N. W. *J. Colloid Interface Sci.* **1971**, 37, 603.

68. The Composite Materials Handbook-MIL17, Volume 2; *Technomic Publishing Company Inc.*, Lancaster US **1999**.
69. Hine, P. J. ; Ward, I. M. ; Olley, R. H. ; Bassett, D. C. *J. Mater. Sci.* **1993**, 28, 316.
70. Ward, I. M. ; Hine, P. J. *Polym. Eng. Sci.* **1997**, 37, 1809.
71. El-Maaty, M. I. A. ; Bassett, D. C. ; Olley, R. H. ; Hine, P. J. ; Ward, I. M. *J. Mater. Sci.* **1996**, 31, 1157.
72. Loos, J. ; Schimanski, T. ; Hofman, J. ; Peijs, T. ; Lemstra, P. J. *Polymer* **2001**, 42, 3827.
73. Jacobs, J. A. J. ; Peijs, A. A. J. M. ; Schimanski, T. *Patent Application EP 127573 A1* **2003**.
74. Commercial available products: [www.pure-composites.com](http://www.pure-composites.com); [www.curvonline.com](http://www.curvonline.com) **2006**.



# II

*Ultra-High Molecular Weight Polyethylene*



# 1 Introduction

It has long been recognized that polyethylene (PE) is a prime candidate for producing high-performance fibers and films. First of all, this polymer has a relatively high theoretical axial modulus of approximately 300 GPa,<sup>1,2</sup> owing to a favorable crystal unit cell structure that features a high density of chain molecules per unit area, allowing optimal sharing of an applied load. In addition, polyethylene is among a limited number of polymers that have been polymerized to ultra-high molecular weights - a prerequisite for high strength for a polymer in which the transverse interactions are dominated by weak van der Waals forces. Finally, polyethylene is chemically inert and has a low density, as a matter of fact less than water, offering the opportunity to develop structures with superior stiffness and strength to weight ratios. This potential has been realized to a large extent, and nowadays, high-performance polyethylene fibers with a strength up to 4 GPa and a Young's modulus of about 150 GPa are produced commercially by spinning ultra-high molecular weight polyethylene (UHMW PE) from semi-dilute solution, followed by jumbo-drawing in the solid state at elevated temperatures - the so-called "gel-spinning process".<sup>3</sup> These fibers have found widespread applications ranging from anchor lines for oil platforms to bullet-proof vests.<sup>4</sup>

Limiting the use of ultra-drawn polyethylene products are their relatively poor resistance to creep and low melting temperature; both characteristics are due to the weak interactions between the oriented chains.<sup>5,6</sup> Attachment of methyl side groups to the polyethylene main chain was found to limit the mobility of the macromolecules through the crystal lattice, resulting in improved creep resistance, but, unfortunately, at the expense of the maximum attainable draw ratio and therewith, the mechanical properties of the fibers produced.<sup>7-9</sup> Other efforts to reduce creep include cross-linking oriented UHMW PE by irradiation<sup>10,11</sup> or photo inducement, however, with limited success.<sup>12</sup>

As noted in Chapter I, surprisingly little efforts have been directed towards the production of high-performance polyethylene films. Porous films of moderate draw ratio produced of melt-crystallized polyethylene were investigated by Tordella<sup>13,14</sup> and Peterlin *et al.*<sup>15</sup> After the development of the "gel-spinning process", foils were produced by biaxial stretching of solution-processed UHMW PE.<sup>16-19</sup> The films

obtained were also porous and featured disappointing mechanical properties for the reasons already detailed in Chapter I. Nonetheless, taking advantage of their structure, microporous UHMW PE films are produced nowadays principally for use in membrane applications, especially in batteries.<sup>20</sup> (It should be noted, that in 1986 a patent application was filed, that disclosed unidirectionally oriented films with maximum modulus of 85 GPa but this appears not to have been pursued further, neither scientifically nor commercially.)<sup>21</sup>

Hence, the principal objective of the work presented in this chapter is to develop high-performance foils of UHMW PE following the “lamine concept” outlined in Chapter I. There are a number of concerns that need to be addressed. First, of course, is the production of highly oriented foils of sufficient size and in sufficient quantity. Second is the notorious issue of fibrillation of such foils<sup>22,23</sup> and finally, in order to manufacture useful, balanced laminates, adhesion between the foils needs to be sufficient.

Regarding the latter issue, it is noteworthy that numerous attempts have been made to improve the poor adhesion characteristics of polyethylene structures, but most were found not to be very effective. Increasing bond strength by oxidizing surface treatments, such as chemical etching,<sup>24-27</sup> plasma-<sup>28,29</sup> and flame treatment,<sup>30,31</sup> have been attempted. Also, grafting the surface of drawn polyethylene tapes with acrylic acid by photo initiation or corona treatment has been investigated.<sup>32,33</sup> Unfortunately, these methods increased the interlaminar shear strength only by a factor of about 2 to 3, reaching values that are low compared with other advanced composite systems.<sup>34,35</sup>

In the work described here, the concept is explored of incorporating functional polymer additives directly into the foil, instead of applying surface treatments or coextrude a copolymer layer on the foil surface, as is commercially conducted for polypropylene foils (PURE<sup>®</sup>).<sup>36</sup> For this purpose polyethylenes, onto which polar side groups are grafted, are employed. Especially, maleic anhydride grafted PE appears to be an interesting candidate as it is known to improve the wettability of PE<sup>37</sup> and, in addition, has also been demonstrated to be able to clarify this polymer.<sup>38</sup>

In order to reduce fibrillation and improve the transverse properties of oriented UHMW PE foils, addition of branched PE as “transverse connectors” will also be explored. This approach follows concepts described in the literature, which, however,



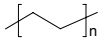
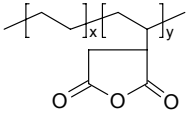
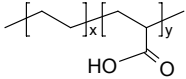
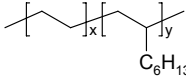
- unlike the present work - focused on the influence of low molecular weight PE on the maximum draw ratio that can be reached.<sup>39-46</sup>

Finally, data will be presented of the formation and properties of balanced, laminated foils of UHMW PE, which were produced by a technique generally referred to as “hot compaction” previously employed for polyolefins.<sup>47, 48</sup>

## 2 Experimental

**Materials.** Ultra-high molecular weight polyethylene (UHMW PE) Stamydan UH 610 (DSM, The Netherlands) with a molecular weight of approximately  $8.7 \times 10^6$  g/mol was used in this work.<sup>49</sup> The solvent was decahydronaphtalene (decalin) from Fluka, which was used as received. The concentration of UHMW PE in the various solutions was kept constant at a weight fraction of 0.01 w/w in all experiments. An amount of 0.1 wt. % (based on UHMW PE content) Irganox<sup>®</sup> B215 FF (Ciba Specialty Chemicals, Switzerland) was added as stabilizer. In selected cases, the polymers listed in Table 1 were added to form blends at a weight fraction of 0.17 w/w (with respect to UHMW PE). In addition, for polyethylene-graft-maleic anhydride (PEgMA) blends of different weight fractions from 0 to 1 w/w were produced.

**TABLE 1** Polymers used; average molecular weight,  $M_w$ , provided by the supplier. Melting points,  $T_m$ , were determined by different scanning calorimetry.

Designation	Description	Chemical structure	$M_w$ g/mol	$T_m$ °C
UHMW PE	Ultra-high molecular weight polyethylene Stamydan <sup>®</sup> UH 610; DSM		$8.7 \times 10^6$	135
PEgMA	Polyethylene-graft-maleic anhydride 3 wt %; Aldrich 456632		-	99
PEAA	Poly(ethylene-co-acrylic acid); 5 wt %; Aldrich 426717		-	103
ULDPE	Poly(ethylene-co-1-octene) Affinity <sup>®</sup> EG 8100; Dow Chemicals		$8 \times 10^4$	55
CoPES	Co-polyester Griltex <sup>®</sup> 1616E; Ems-Grivory	not supplied	-	92

**Foil preparation.** Prior to heating, polymer/solvent mixtures were degassed at room temperature under vacuum for one hour. The suspensions were then stirred at 135 °C, but as soon as (co-)dissolution started, stirring was arrested and the mixtures were kept at that temperature for 2 hours, after which homogenous solutions were obtained. In the case of blends with CoPES, the copolyester was first dissolved in dichloromethane and continuously added to heated UHMW PE/decalin solutions. The hot solutions were subsequently quenched by pouring them into aluminum trays. The solvent was

allowed to evaporate under air flow at ambient, resulting in translucent foils with a typical thickness of  $\sim 150 \mu\text{m}$ . Residual solvent was removed by extraction with dichloromethane at room temperature.

In a first set of experiments, rectangular-shaped specimens were cut from the foils (50 x 20 mm) and elongated with an Instron tensile tester 5864, equipped with a temperature-controlled chamber, at a crosshead speed of 20 mm/min and at a temperature of 130 °C. The draw ratios,  $\lambda$ , were determined from the displacement of marks printed onto the specimen at intervals of 1 mm. Foils drawn to draw ratios exceeding 15 were produced by applying a second drawing step at 135 °C.

In a second set of (larger-scale) experiments, drawing was conducted in a 7 m long horizontal oven (courtesy of NSA SA, now North Sails Research SA). In this case drawing was not effectuated by subjecting the foils to a constant rate of elongation, as above, but by applying a constant load of 10 kg, controlled with a breaking system. The average oven temperature was 125 °C, the width of the as cast foils 250 mm, their typical final width 200 mm, thickness 2  $\mu\text{m}$  and length about 6 m.

In addition, films were prepared by melt-compression molding UHMW PE (Hostalen<sup>®</sup> GUR 7255 P,  $M_w \approx 4 \times 10^5 \text{ g/mol}$ ) at 180 °C for 40 min, followed by quenching to room temperature, yielding 0.3 mm thick samples used for X-ray analysis in this work.

**Laminate preparation.** The unidirectionally oriented UHMW PE foils produced as described above were first cleaned with acetone and in their non-dried state stacked in a four layer arrangement [0/ 45/ 90/ 135], as described in Chapter I, between two polyimide (Kapton<sup>®</sup>) foils. Excess of acetone was removed by rolling a steel bar over the sandwich thus created. Subsequently, the samples were hot-pressed under vacuum (40 mbar) for 30 min between two rubber sheets at 135 °C, i.e. above the melting temperature of all copolymers used in this study, but below the melting point of UHMW PE, and then cooled while constrained.

**Mechanical properties.** The unidirectionally oriented and laminated foils were tested in tension at a cross-head speed of 5 mm/min, using the above-mentioned Instron tensile tester. The specimen width was 2 mm and the gauge length 50 mm in the case of single, unidirectionally oriented foils and 5 mm and 25 mm for laminated samples, respectively. In all cases, the thickness was calculated from the weight of each sample,

taking the density to be 0.98 g/cm<sup>3</sup>.

**Interlayer adhesion.** Adhesion between individual foils in the laminates was examined in simple T-peel-tests. After cleaning with acetone, solution-cast drawn films were “hot-compacted” in a press, using a polyimide strip as a separator at one edge. Selected samples were rapidly dipped in decalin prior to pressing, where indicated. The thickness of the polyimide strip was compensated for by placing another polyimide foil on top of the remaining parts of the samples. The specimens were then pressed between two rubber sheets, during 15 or 30 min at a pressure of 850 Pa, at different temperatures. The resulting samples were quenched to room temperature in a cold press and cut into 10 mm wide T-peel test specimens. T-peel tests were performed at room temperature according to ISO 11339 with an Instron 4411 tensile tester at constant cross-head speed of 20 mm/min.

**X-ray analysis.** Wide-angle X-ray diffraction (WAXD) studies were conducted with an Oxford Diffraction Xcalibur XP (Abingdon, UK) instrument, using a Mo-K $\alpha$  source ( $\lambda=0.7093$  Å) at -50 kV / 40 mA. Patterns were recorded with an Onyx CCD detector at a distance of 65 mm. The  $\langle 200 \rangle$  and  $\langle 020 \rangle$  reflections were used to determine the Hermans' orientation factor,  $f_h$ , and average orientation angles were derived from the half-width at half-maximum intensity of the diffraction peaks.

Small-angle X-ray scattering (SAXS) data were collected at the Dutch-Belgian beam line (DUBBLE)<sup>50</sup> of the European Synchrotron Radiation Facility (ESRF in Grenoble, France) and the UNICAT facility in Argonne (USA).<sup>51</sup> Profiles were recorded with an area detector, positioned at a distance of 4 m from the samples. Dry rat tail collagen was used for calibration of the detectors.

**Thermal analysis.** Melting temperatures were determined with a Mettler DSC822e (Greifensee, Switzerland) differential scanning calorimeter (DSC), calibrated with indium. Samples of about 10 mg were heated from 25 to 160 °C at a scanning rate of 10 °C/min under nitrogen. Melting temperatures refer to the maximum in the endotherms; degrees of crystallinity were calculated adopting a melting enthalpy of 293.6 J/g for 100 % crystalline polyethylene.<sup>52</sup>

Dynamical mechanical thermal analysis (DMTA) was performed with a Mettler DMA861e instrument (Greifensee, Switzerland) at 10 Hz in the range from room temperature to 160 °C.

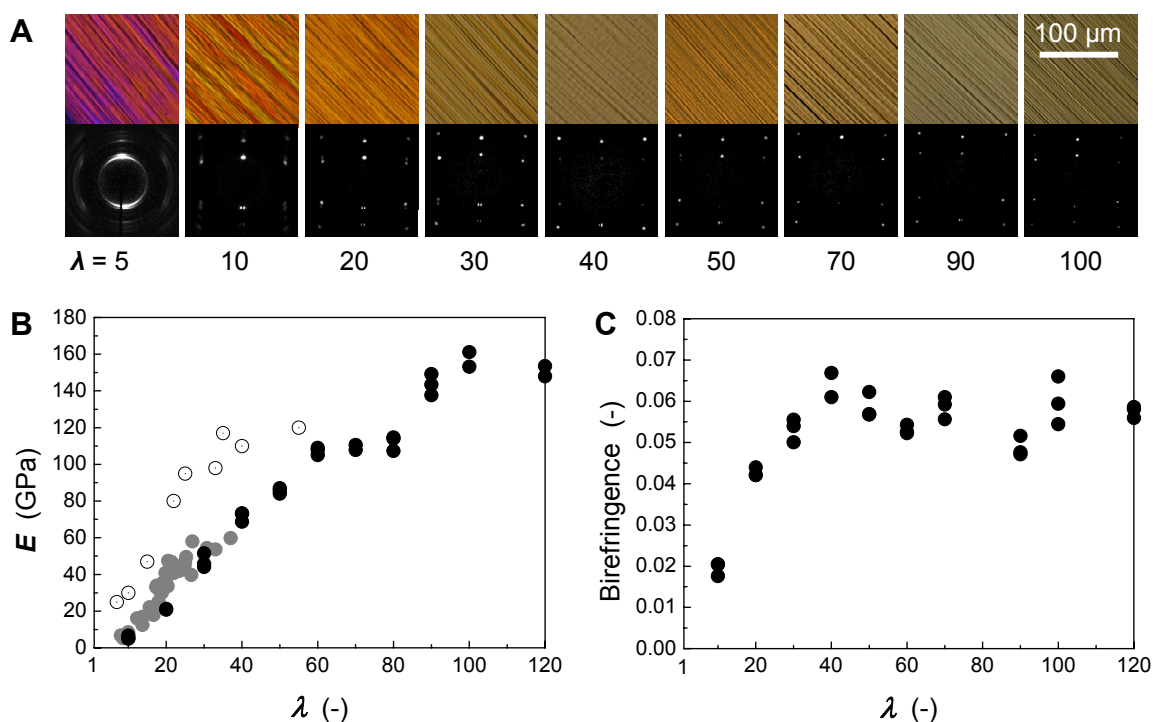
***Infra-red spectroscopy.*** Infra-red (IR) spectra were collected in transmittance mode employing a Bruker Vertex 70 spectrometer (Ettlingen, Germany).

***Microscopy.*** Scanning electron microscopy (SEM) micrographs were taken with a Zeiss/LEO 1530 Gemini instrument (Oberkochen, Germany) of platinum-coated samples. Polarized-light microscopy was performed with a Leica DMRX (Wetzlar, Germany) microscope.

## 3 Results and Discussion

### 3.1 UHMW PE

In a first set of experiments, uniaxially oriented foils of UHMW PE were produced by solution-casting, drying and tensile drawing according to standard procedures.<sup>53</sup> In Figure 1 are presented as function of the draw ratio,  $\lambda$ , the optical appearance (at 45 ° between crossed polarizers) of the samples, as well as their wide-angle X-ray diffraction (WAXD) patterns, Young's modulus,  $E$ , and birefringence. Also included in the latter graphs are results taken from the literature for drawn *melt*-crystallized PE<sup>54</sup> and *solid-state* compressed films of virgin UHMW PE.<sup>55</sup>

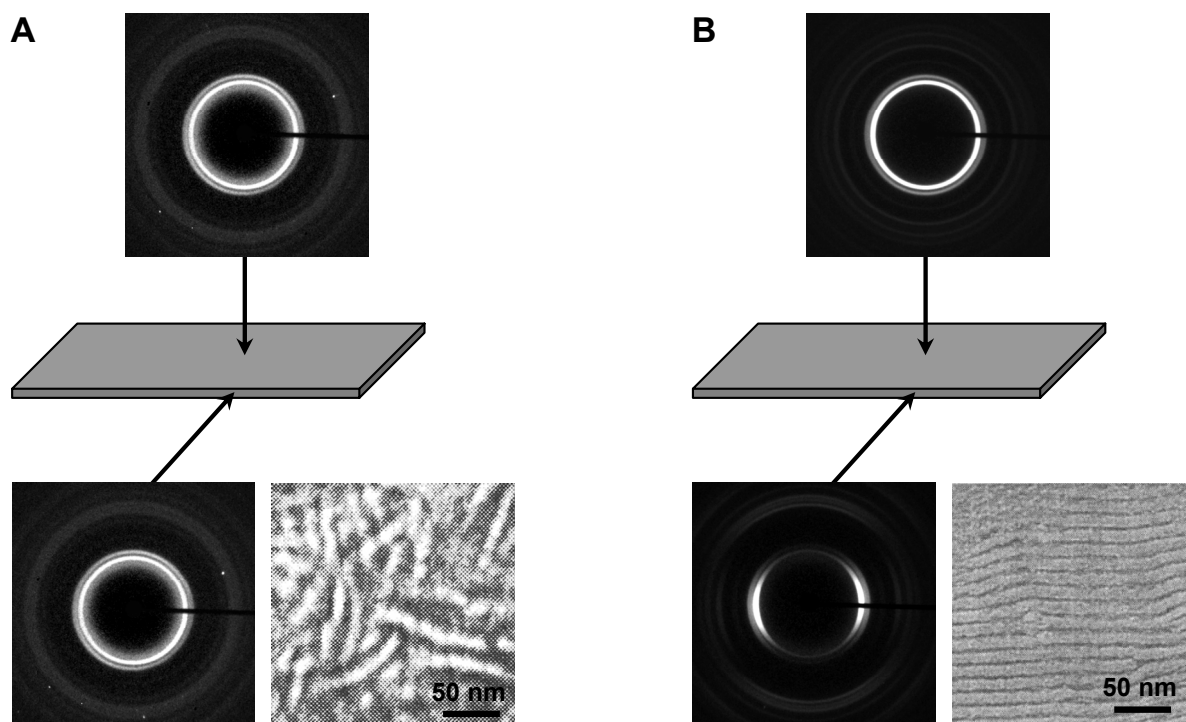


**FIGURE 1** A. Optical micrographs of drawn, solution-cast UHMW PE foils, taken between crossed polarizers and corresponding WAXD patterns; draw ratios,  $\lambda$ , indicated below. B. Development of Young's modulus,  $E$ , with draw ratio,  $\lambda$ , of solution-cast films (●), melt-crystallized samples (●, ref. 54) and solid-state compression-molded films of virgin UHMW PE (○, ref. 55). C. Plot of birefringence vs. draw ratio of the solution-cast films.

From the data presented in this figure, it is evident that the development of the Young's modulus with draw ratio in the present case of foils cast from relatively dilute solutions, lags behind that of melt-crystallized material, as well as solution-spun fibers (ref. 56; data not shown), and even more so when compared to that observed for the

solid-state compressed films of virgin UHMW PE.<sup>55</sup>

These differences can readily be understood, and, as will be shown, quantitatively described when taking into account the subtle, but distinct differences in the macromolecular structure of the initial, undrawn material (cf. Figure 2; Table 2).<sup>23, 57, 58</sup>



**FIGURE 2** Wide-angle X-ray diffraction (WAXD) patterns taken perpendicular and parallel to the plane of melt-crystallized PE (A) and solution-cast UHMW PE (B) films, indicative of random orientation in the former and preferred orientation of the macromolecules perpendicular to the plane of the films in the latter. Transmission electron microscopy (TEM) images were reprinted with permission from ref. 59 (A) and 60 (B), respectively.

WAXD patterns and transmission electron microscopy (TEM) images<sup>59, 60</sup> illustrate that the melt-crystallized samples featured a *random* orientation of the constituent polymer molecules, while the present solution-cast films displayed a preferred arrangement of the polymer chains *perpendicular* and, remarkably, in the solid-state compressed virgin UHMW PE samples *parallel* to the plane of the films (Figure 2, Table 2). This “preorientation” naturally affected the development in chain orientation and, therewith, Young’s modulus with draw ratio, which will be quantified in the following section.

## 3.2 Extended Irvine-Smith Model

It is well known that under optimum drawing conditions, the axial Young's modulus,  $E$ , of cold-drawn polymers is only dependent on the absolute draw ratio,  $\lambda$ . This experimental finding indicates that the axial Young's modulus of drawn fibers and tapes is determined by the overall molecular extension and orientation rather than morphological details.<sup>61, 62</sup>

Furthermore, it is well established that the development of overall molecular orientation proceeds according to the pseudo-affine deformation scheme, although the orientation of both, the crystalline and amorphous phases, is known to change in a non-affine manner during drawing.<sup>63, 64</sup>

Examples of models - based on the above concepts - to describe the development of the Young's modulus during cold-drawing are the so called "aggregate model" by Ward<sup>65</sup> and the closely related Irvine-Smith approach.<sup>66</sup> The latter has proven to be successful in describing  $E$ - $\lambda$  dependence for several polymers,<sup>67</sup> and will be extended here to include the above experimental observations.

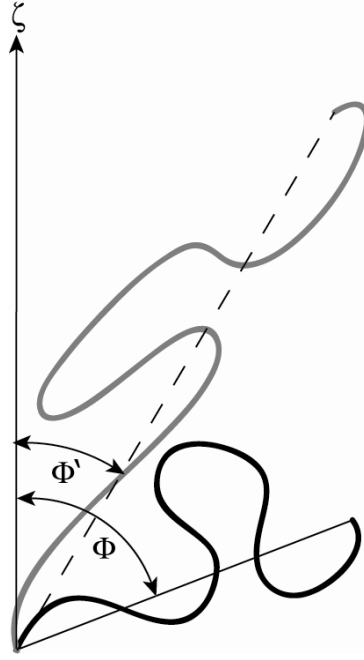
Normally, in these models it is assumed that initially the chain segments are randomly distributed and become anisotropically arranged upon drawing. Considering that only the orientation of the chain segments determines the modulus of the drawn material, it is to be expected that deviation from an initial random arrangement will influence the development of  $E$  with  $\lambda$ . For example, in fiber spinning, there is normally a certain pre-orientation before the cold-drawing step due to extrusion and/or fiber draw down. This effect of *deformation*-induced pre-orientation was studied by Ward.<sup>68</sup> In the following the influence of *structure*-induced pre-orientation on the development of Young's modulus with draw-ratio will be addressed.

The orientation of a chain segment is defined by the angle,  $\phi$ , between the segment and the drawing axis. The distribution function  $P(\phi)$  describing the probability that a chain segment will have an orientation between  $\phi$  and  $\phi+d\phi$  for an isotropic distribution of chain segments is:

$$P(\phi)d\phi = \frac{1}{2} \sin(\phi) d\phi \quad (1)$$



Following pseudo-affine orientation by tensile drawing to a draw ratio,  $\lambda$ , the orientation angle,  $\phi$ , of each segment is transformed to (cf. Figure 3):<sup>69</sup>



**FIGURE 3** Transformation of a polymer chain of a certain orientation  $\phi$  towards the draw axis  $\zeta$  resulting in a changed orientation  $\phi'$ .

$$\phi' = \arctan(\lambda^{\frac{3}{2}} \tan(\phi)) \quad (2)$$

Using this transformation rule (2), the new anisotropic distribution function can be written as:

$$P(\phi', \lambda) = \frac{1}{2} \frac{\lambda^3}{(\lambda^3 - (\lambda^3 - 1) \cos^2(\phi'))^{\frac{3}{2}}} \quad (3)$$

This distribution function can be used to calculate the Hermans' orientation factor,  $f_h$ , as a function of draw ratio  $\lambda$ :

$$f_h(\lambda) = \frac{3 \langle \cos^2(\phi') \rangle - 1}{2} \quad \text{where} \quad \langle \cos^2(\phi') \rangle = \int_0^\pi \cos^2(\phi') P(\phi', \lambda) \sin(\phi') d\phi' \quad (4)$$

which can be solved analytically:

$$\langle \cos^2(\phi') \rangle = \frac{\lambda^3}{\lambda^3 - 1} - \frac{\lambda^3}{(\lambda^3 - 1)^{\frac{3}{2}}} \arctan(\sqrt{\lambda^3 - 1}) \quad (5)$$

Using this equation for the Hermans' orientation factor, the axial Young's modulus,  $E$ , is calculated according to the Irvine-Smith model as:

$$\frac{1}{E} = \frac{f_h}{E_h} + \frac{(1-f_h)}{E_u} \quad (6)$$

Here,  $E_h$  and  $E_u$  are the tensile moduli of perfectly oriented and unoriented polymer, respectively.

We now consider that instead of a random chain segment orientation, a certain pre-orientation characterized by an initial Hermans' orientation factor,  $f_h^o$ , is present in the material that will be subjected to drawing. If the degree of initial orientation is not too pronounced ( $f_h^o \leq 0.5$ ), the initial distribution function can be approximated by the two first terms of its Legendre expansion: <sup>70</sup>

$$P(\phi, f_h^o) = \frac{1}{2} + \frac{5}{2} f_h^o \left[ \frac{3 \cos^2(\phi) - 1}{2} \right] \quad (7)$$

Applying again the transformation rule (2), upon drawing this non-isotropic initial distribution function becomes:

$$P(\phi', \lambda, f_h^o) = \left[ \frac{\lambda^3}{(\lambda^3 - (\lambda^3 - 1) \cos^2(\phi'))^{\frac{3}{2}}} \right] \cdot \left[ \frac{5}{4} f_h^o \left[ \frac{3}{1 + \lambda^3 \tan^2(\phi')} - 1 \right] + \frac{1}{2} \right] \quad (8)$$

From this distribution function the Hermans' orientation function can be calculated, now as function of draw ratio and pre-orientation. The analytical solution for  $\langle \cos^2 \phi' \rangle$  reads:

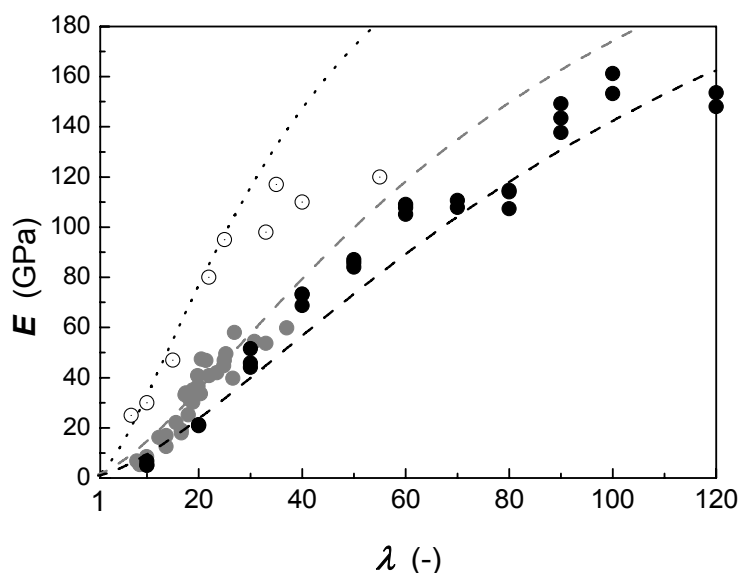
$$\langle \cos^2(\phi') \rangle = \lambda^3 \left[ \left( \frac{1}{\alpha^2} - \frac{\arctan(\alpha)}{\alpha^3} \right) + \frac{5}{4} f_h^o \left( \frac{2 \arctan(\alpha)}{\alpha^3} + \frac{6 \arctan(\alpha)}{\alpha^5} - \frac{6}{\alpha^4} \right) \right] \quad (9)$$

with  $\alpha = \sqrt{\lambda^3 - 1}$

Using expressions (4) and (9) it is then possible to calculate the  $E$ - $\lambda$  relation according to the Irvine-Smith model as function of the initial orientation  $f_h^o$ .

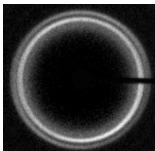
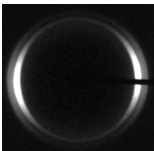
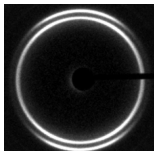
Calculations that take into account different degrees of pre-orientation show that already a small deviation from random starting distribution ( $f_h^o = 0$ ) significantly affects the development of the Young's modulus with draw ratio. In Figure 4 are

shown  $E$ - $\lambda$  plots for foils with different degrees of pre-orientation, calculated with the above model using the values for  $E_h$  (300 GPa),  $E_u$  (1 GPa) and the initial Hermans' factors,  $f_h^\circ$ , determined from the  $\langle 200 \rangle$  and  $\langle 020 \rangle$  reflections of the respective WAXD patterns recorded parallel to the foil planes (Table 2). Clearly, it follows that for both “negative” and “positive” pre-orientation, as well as for isotropic samples, the  $E$ - $\lambda$  data are in good agreement with the calculated curves from the extended Irvine-Smith model. As a note of caution, the Hermans' orientation factor derived from WAXD accounts only for the crystalline orientation and that the overall Hermans' orientation factor, which features in the Irvine-Smith model, will be lower due to segments that reside in the less oriented amorphous phase.



**FIGURE 4** Development of the Young's modulus with draw ratio calculated from the extended Irvine-Smith model, which takes into account the pre-orientation of the initial, undrawn films (cf. Table 2). Solution-cast (●), melt-compression molded (●, ref. 54) and solid-state compression molded (○, ref. 55) UHMW PE films, revealing the influence of preorientation. Data from Figure 1B.

**TABLE 2** Initial Hermans' orientation factors,  $f_h^\circ$ , of UHMW PE films prior to tensile drawing determined from the  $\langle 200 \rangle$  and  $\langle 020 \rangle$  reflections of the respective WAXD patterns taken parallel to the plane of the film.

	melt-processed	solution-cast	solid-state compressed, virgin
$f_h^\circ / -$	0	-0.25	+0.25
WAXD patterns			

To conclude this section, the relatively slow development of the Young's modulus with draw ratio observed for the present solution-crystallized films compared to melt-crystallized films can be accounted for by structure-induced pre-orientation, and is not due to inefficient drawing of the foils.

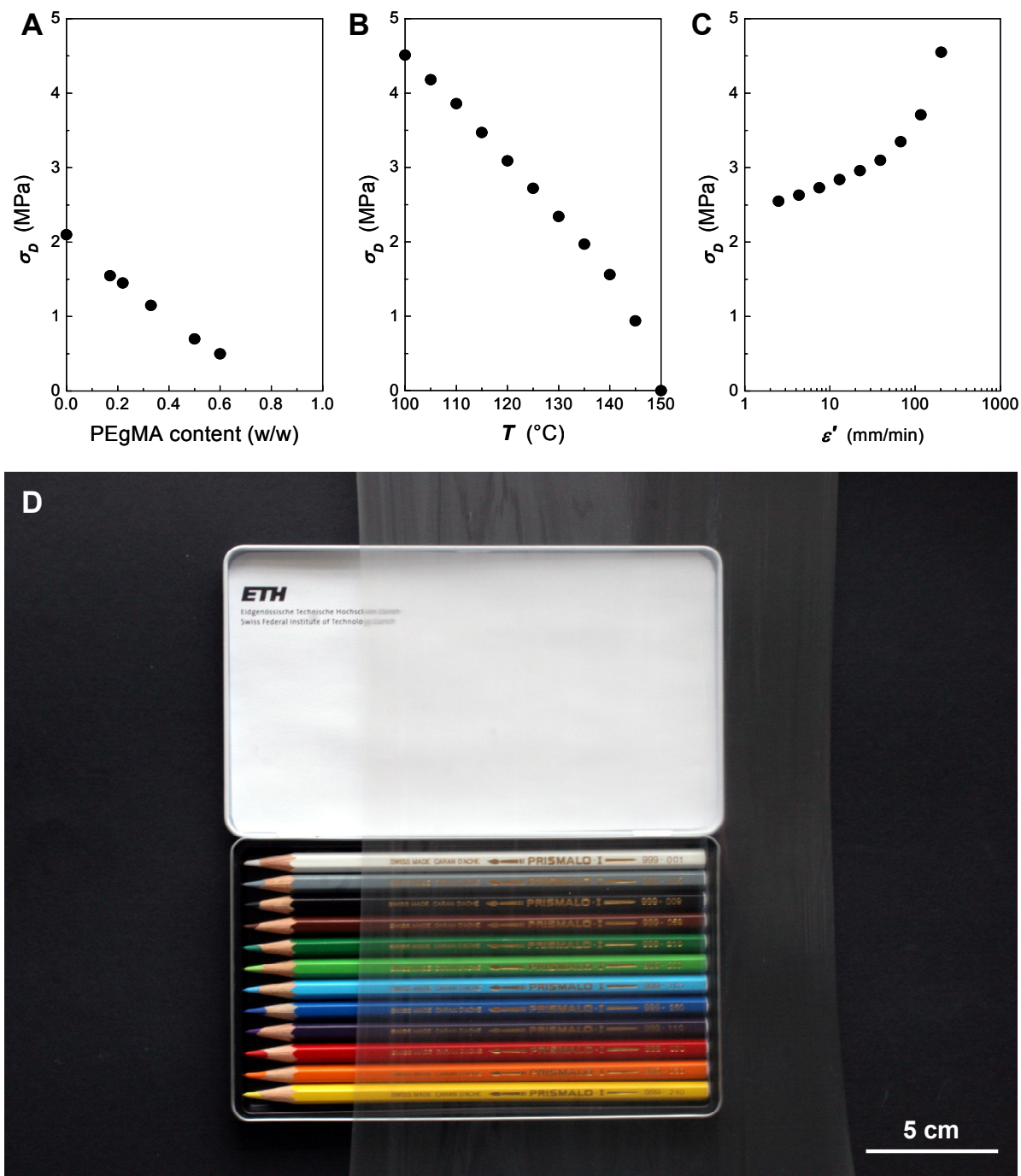
### 3.3 Functional Polymer Additives: Preliminary Experiments

As noted in the introduction, oriented PE films feature notoriously poor mechanical properties when subjected to load in directions not parallel to that of the orientation. In order to improve those characteristics, selected polymer additives were added at a weight fraction of 0.17 w/w (based on polyethylene) to the solutions from which the UHMW PE films were cast. The latter were dried and drawn as described in the experimental section. In the following, general observations will be presented regarding the influence of their presence on the drawing behavior and mechanical properties of the resulting oriented foils.

#### Tensile deformation

Deformation of UHMW PE films that comprised the (lower-molecular weight) polymer additives required lower stresses depending on copolymer content, drawing temperature,  $T_D$ , and drawing rate,  $\dot{\epsilon}$ ' (see Figure 5A-C). Furthermore, the drawn foils containing these additives appeared more transparent (cf. Figure 5D), except for CoPES-containing samples, in which large-scale phase separation was detected.

A common feature of all UHMW PE blend films was that fibrillation rarely occurred upon drawing up to draw ratios as high as 100. Up to 6 m long and ~20 cm wide non-fibrillated foils of a thickness as low as 2  $\mu\text{m}$  were produced by ultra-drawing selected UHMW PE mixtures. This is in contrast to foils produced with neat UHMW PE for which spontaneous splitting occurred already at lower draw ratios, as previously described,<sup>23</sup> and is also observed during uniaxial deformation of polypropylene.<sup>71</sup>



**FIGURE 5** A. Drawing stress,  $\sigma_D$ , vs. PEGMA content of blend films with UHMW PE at 130 °C and 20 mm/min; B. vs. drawing temperature of neat UHMW PE film at 20 mm/min; and C. vs. drawing rate,  $\dot{\epsilon}'$ , at 130 °C (C). D. Image of a section of an 1 m long ultra-drawn foil of a solution-cast UHMW PE/ PEGMA (0.17 w/w) blend film of a draw ratio  $\sim 50$ , revealing its transparency.

## Parallel and transverse properties

The favorable absence of fibrillation of the drawn UHMW PE blend films allowed evaluation of their mechanical properties both parallel and perpendicular to the direction of orientation. In most cases, values of the Young's modulus and strength were similar to those of the neat PE. However, the nature of the polymer additive was found to have a profound influence on the elongation at break,  $\epsilon$ , especially in the transverse direction (Table 3). Remarkably, oriented foils of  $\lambda = 20$  containing PEgMA could be deformed in the direction perpendicular their orientation to an elongation at break as high as 40 %.

**TABLE 3** Mechanical properties of uniaxially oriented foils, drawn to the draw ratios,  $\lambda$ , indicated, of UHMW PE and its blends comprising a weight fraction of 0.17 w/w of the polymers listed, determined parallel and perpendicular to the drawing direction.

material	$\lambda$ -	parallel			perpendicular		
		$E$ GPa	$\sigma$ GPa	$\epsilon$ %	$E$ GPa	$\sigma$ MPa	$\epsilon$ %
UHMW PE	20	21.2	0.8	23	2.6	39	12
	50	87.0	2.4	4	2.1	25	14
PEAA	25	20.1	0.8	8	2.0	38	25
	50	65.6	2.1	8	2.0	20	4
PEgMA	<b>20</b>	<b>22.2</b>	<b>0.7</b>	<b>16</b>	<b>1.8</b>	<b>22</b>	<b>40</b>
	<b>50</b>	<b>90.2</b>	<b>2.5</b>	<b>3</b>	<b>2.1</b>	<b>23</b>	<b>24</b>
CoPES	25	23.8	0.7	7	2.7	23	30
	50	68.7	0.8	2	2.2	23	5
ULDPE	20	18.1	1.1	11	2.1	50	20
	45	78.9	2.4	4	0.8	17	13

Because of its superior transverse properties, the system UHMW PE/PEgMA was selected for more detailed evaluation.

## 3.4 UHMW PE/PEgMA

### Phase behavior and structure of blends

Blends of UHMW PE with PEgMA covering the entire composition range were prepared as described in the Experimental section. These samples were heated in a differential scanning calorimeter to 160 °C, i.e. above the melting temperature of both components, then cooled to room temperature, followed by a second heating scan. The

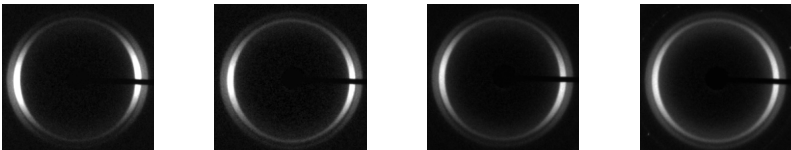
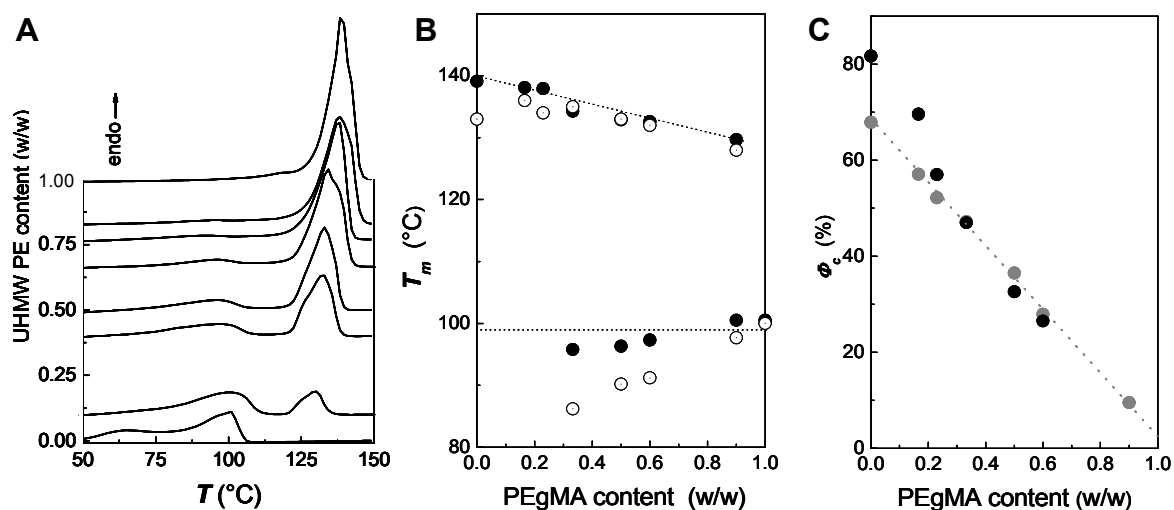
resulting thermograms are presented in Figure 6. A small, but notable melting point depression of UHMW PE was observed, indicative of miscibility with PEgMA in the liquid phase. Phase separation thus occurred only upon crystallization of the polymers, which typically resulted in a fine distribution of PEgMA in UHMW PE.

The structure of the solution-cast UHMW PE/PEgMA films was examined with wide-angle X-ray diffraction. Similar to foils of neat UHMW PE, the as-cast blends featured a preferred orientation perpendicular to the plane of the films (see Table 4).

**TABLE 4** Initial Hermans' factors,  $f_h^\circ$ , calculated from the  $\langle 020 \rangle$  and  $\langle 200 \rangle$  WAXD reflections of solution-cast blends of UHMW PE and PEgMA (weight fractions indicated) and crystallinity,  $\Phi_C$ , of UHMW PE.

PEgMA / w/w	0	0.17	0.5	0.6
$f_h^\circ / -$	-0.25	-0.25	-0.18	-0.12
$\Phi_C / \%$	67.9	57.1	36.5	9.5

WAXD patterns parallel to film plane

**FIGURE 6** A. Differential scanning calorimetry (DSC) thermograms of UHMW PE/PEgMA blends shifted vertically according to their UHMW PE content. B. Melting temperature/composition diagram of drawn UHMW PE/PEgMA foils from first (●) and second DSC heating runs (○). C. Corresponding degree of crystallinity,  $\Phi_C$ , as function of PEgMA content of UHMW PE/PEgMA blends, calculated from PE melting endotherms in the DSC thermograms - not corrected for composition: solution-cast foils (●) and foils drawn to a draw ratio of 50 (○).

Interestingly, at increasing PEgMA content, the chain orientation appeared to become more isotropic, which is advantageous for the development of the Young's modulus with draw ratio, as discussed in Section 3.2. Finally, infra-red spectra of the solution-cast UHMW PE/PEgMA foils did not feature the characteristic peak of the anhydride moiety at  $1790\text{ cm}^{-1}$ , but, instead, at  $1713\text{ cm}^{-1}$ , indicating that the anhydride groups were converted into diacids due to moisture.<sup>72</sup>

## **Mechanical properties**

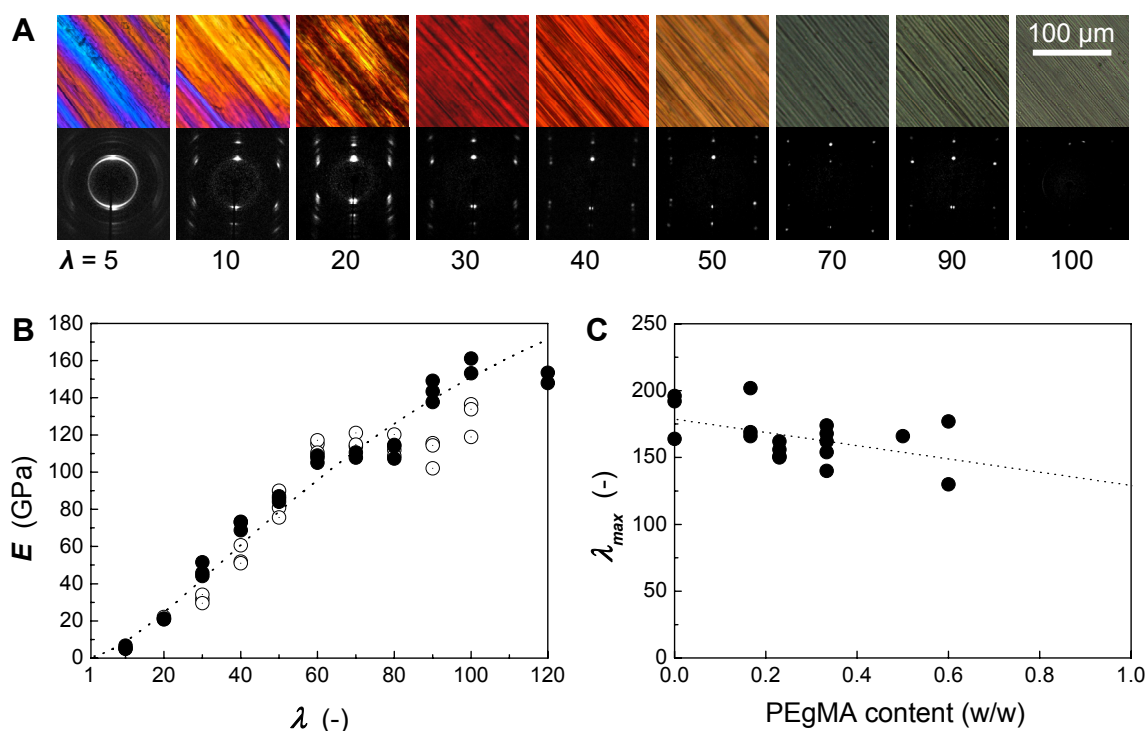
The development of the structure with draw ratio, as observed in polarized optical micrographs and WAXD, and the Young's modulus of a blend containing 0.17 w/w of PEgMA are displayed in Figure 7.

It was found that the drawing behavior of the foils was rather sensitive to the PEgMA content. With increasing PEgMA concentration, less necking was observed and deformation was beneficially homogeneous along the full gauge length of the samples.

Evaluation of the maximum draw ratio,  $\lambda_{max}$ , in tensile experiments at  $130\text{ }^{\circ}\text{C}$  at a cross-head speed of  $20\text{ mm/min}$  showed a modest decrease with increasing PEgMA content (Figure 7C). (N.B. neat PEgMA did not form a uniform film by solution casting from a  $0.02\text{ w/w}$  solution, and, therefore, it was not possible to determine  $\lambda_{max}$  for this copolymer.)

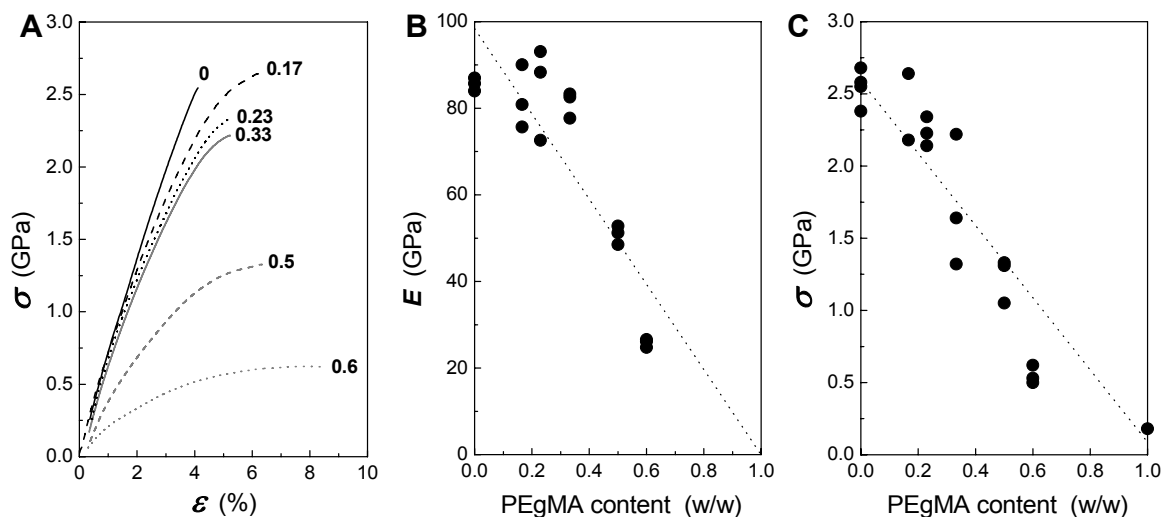
Not surprisingly, it was found that the presence of the low molecular weight PEgMA copolymer reduced the mechanical performance of drawn foils, especially at higher PEgMA copolymer content.





**FIGURE 7** A. Optical micrographs (crossed polarizers; top) and corresponding WAXD patterns (bottom) revealing the development of microstructure with increasing draw ratio,  $\lambda$ , of a solution-cast UHMW PE/PEgMA blend containing 0.17 w/w of PEGMA. B. Young's modulus  $E$  vs.  $\lambda$  ( $\odot$ ). Curve calculated with the extended Irvine-Smith model. For comparison,  $E$  vs.  $\lambda$  of neat UHMW PE is also reprinted ( $\bullet$ ) (cf. Figure 1). C. Influence of PEGMA content in blends with UHMW PE on the maximum draw ratio draw ratio of solution-cast films.

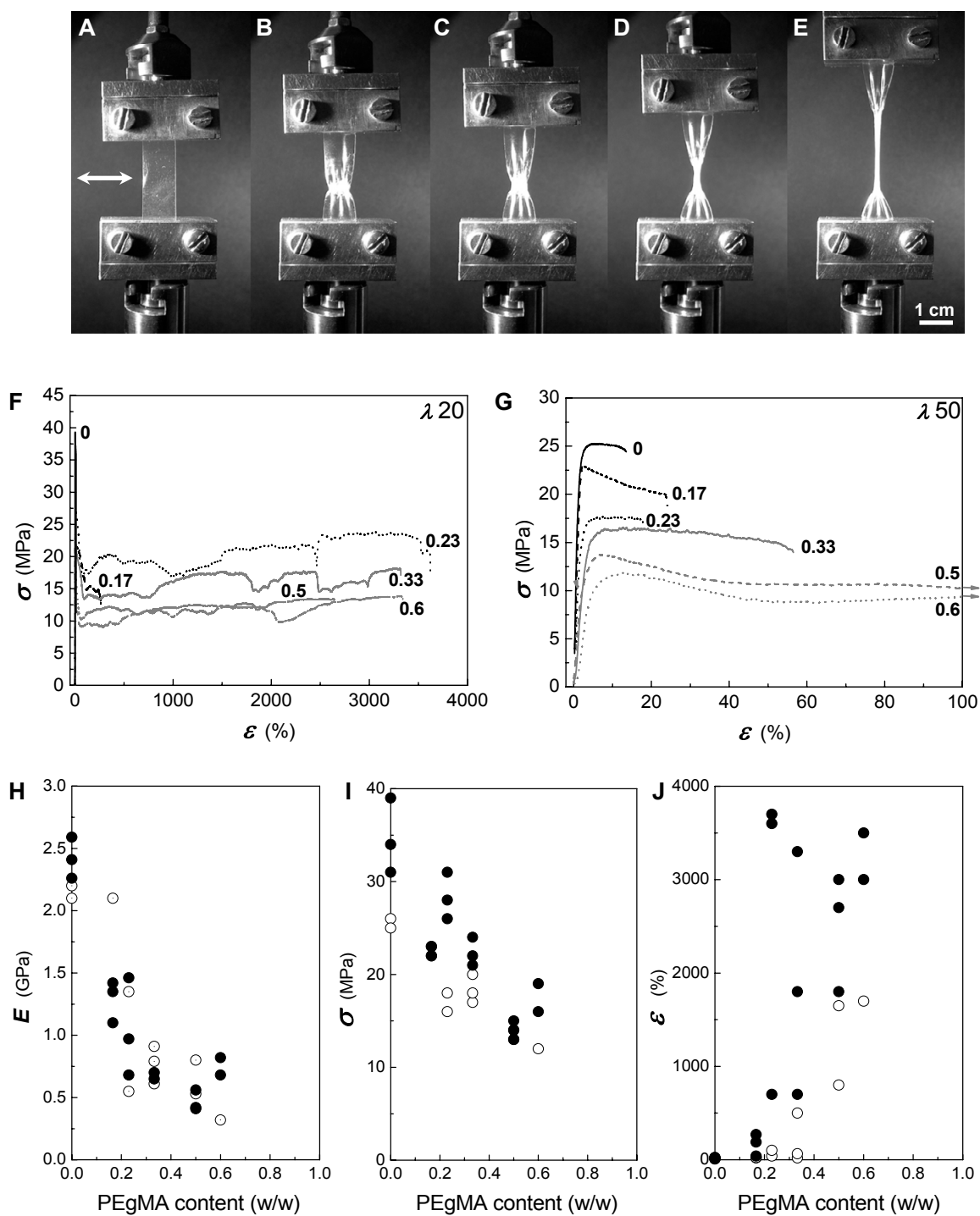
The effect of PEGMA content on stress-strain curves, Young's modulus and tensile strength of foils drawn to a draw ratio of 50 are shown in Figure 8A, B and C, respectively. It can be seen that the stiffness and strength (at constant draw ratio) decreased approximately linear with increasing PEGMA content, but that the strain at break of the oriented foils advantageously increased. At PEGMA contents up to  $\sim 0.2$  w/w the reduction in stiffness and strength of the drawn foils was found to be not very pronounced when compared to similar foils of neat UHMW PE. It might be that at low PEGMA content reduction of the mechanical properties of the foils due to the presence of this copolymer is compensated by a more rapid development of tensile modulus and strength with draw ratio of foils due to a more favorable initial structure, although this was not detected in WAXD (see Table 4).



**FIGURE 8** Influence of PEgMA content on mechanical properties of solution-cast UHMW PE/PEgMA blend foils drawn to  $\lambda = 50$  (compositions indicated). **A.** Typical stress-strain curves. The Young's modulus  $E$  (**B**) and tensile strength  $\sigma$  (**C**) decreased with increasing PEgMA content, whereas the elongation at break increased from 4 to 8 %.

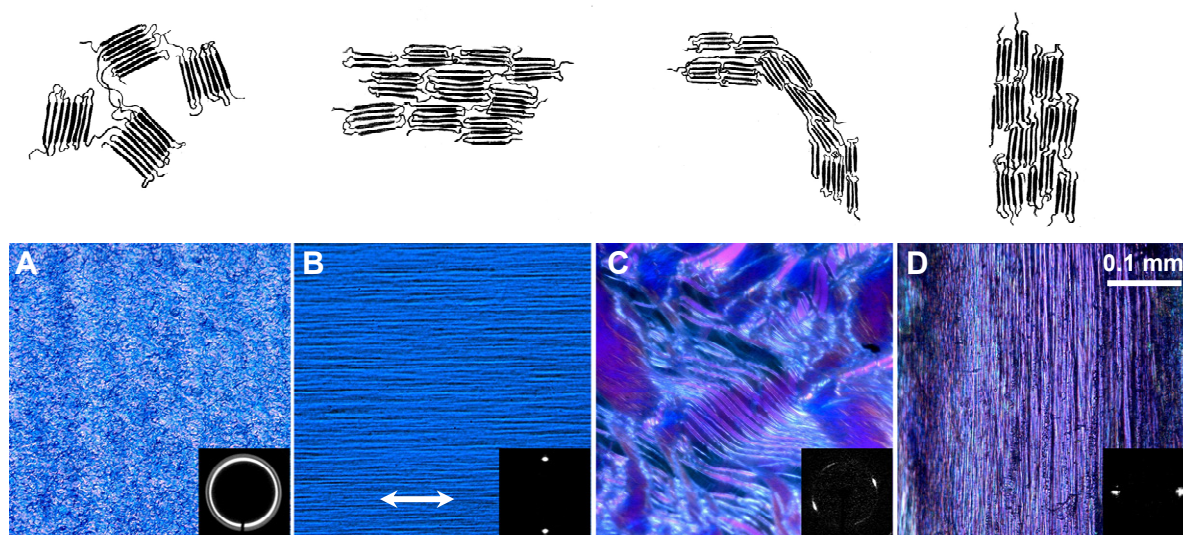
### Transverse deformation

In this section striking effects of incorporation of PEgMA copolymer into uniaxially oriented UHMW PE blend foils on deformation perpendicular to the drawing direction is presented. Most illustrative is the series of photographs in Figure 9A-E, which reveal no fracture, however, severe necking upon drawing the uniaxially oriented foils containing 0.17 w/w PEgMA perpendicular to their orientation direction is observed. Despite extremely inhomogeneous deformation behavior, oriented foils of draw ratios  $\lambda = 20$  and  $\lambda = 50$ , containing various amounts of PEgMA copolymer, could be extended without fibrillation and fracture, as illustrated by the stress-strain curves in Figures 9F and 9G. By contrast, oriented foils of neat UHMW PE rapidly fractured in a brittle fashion upon deformation in the direction transverse to the orientation axis.



**FIGURE 9** A.-E. Photographs taken during tensile deformation at room temperature of a drawn ( $\lambda = 20$ ) solution-cast, UHMW PE/PEgMA blend containing 0.17 w/w of PEgMA *perpendicular* to the direction of orientation (indicated), revealing extraordinary transverse properties of the uniaxially oriented foils. F. Stress-strain curves recorded perpendicular to the direction of draw of oriented UHMW PE/PEgMA blend foils ( $\lambda = 20$ ); weight fractions PEgMA are indicated. G. As in F, but  $\lambda = 50$ . H. Young's modulus  $E$ ; I. tensile strength  $\sigma$ ; and J. elongation at break  $\epsilon$  vs. PEgMA content, derived from the stress-strain curves recorded perpendicular to the orientation direction of drawn UHMW PE/PEgMA blend foils ( $\lambda = 20$  (●), 50 (○)).

The Young's modulus and tensile strength of oriented foils of  $\lambda = 20$  and  $\lambda = 50$ , determined perpendicular to the orientation direction, were found to be almost identical, and decreased with increasing PEgMA content as shown in Figures 9H and I, respectively. By contrast, the transverse elongation at break was strongly depending on the draw ratio and increased with increasing copolymer content to almost 4000 %. A transition from brittle fracture to ductile necking in the transverse direction was found to occur at a draw-ratio dependent minimum PEgMA copolymer content (0.3 w/w for  $\lambda = 20$  and 0.5 w/w for  $\lambda = 50$ ) (cf. Figure 9J). Optical microscopy and WAXD revealed that in the case of ductile necking, during transverse deformation, the macromolecular chains rearranged and ultimately rotated by  $90^\circ$  with respect to their initial orientation direction (see Figure 10), as previously reported, for instance, for polypropylene films.<sup>73</sup>

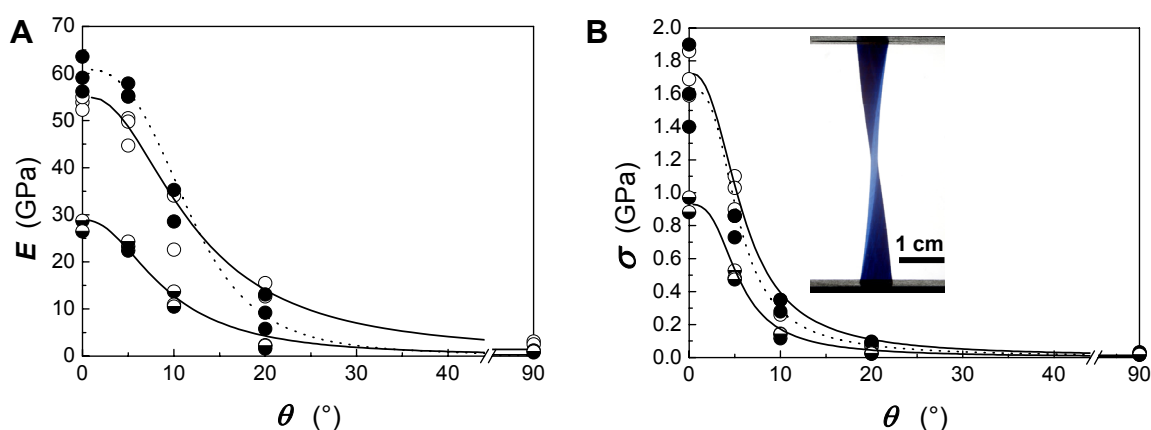


**FIGURE 10** Schematics (top), optical micrographs taken with crossed polarizers and WAXD patterns of (A) solution-cast UHMW PE/PEgMA blend containing 0.17 w/w of PEgMA; (B) foil drawn to  $\lambda = 20$ ; draw direction indicated; (C) foil in B deformed perpendicular to the drawing direction (corresponds to Figure 9B); (D) corresponds to Figure 9E.

### Off-axis mechanical properties

For a selected set of oriented blend films the off-axis mechanical properties were determined as a function of the test-angle  $\theta$ . In Figure 11 data are presented of the Young's modulus and tensile strength of a reference, neat UHMW PE foil and blend films comprising a weight fraction of 0.17 w/w and 0.6 w/w of PEgMA, all drawn to  $\lambda = 50$ . It was discussed in Chapter I that the off-axis deformation behavior of oriented

polymer foils is determined principally by the transverse- and shear modulus,  $E_t$  and  $G_{tb}$ , respectively. Increasing interactions by incorporation of modest quantities of the more polar PEgMA would be expected to increase both  $E_t$  and  $G_{tb}$ , and, consequently lead to a broadening of the  $E$ - $\theta$  correlation (mainly determined by  $G_{tb}$ ) and increased stiffness perpendicular to the orientation axis (dominated by  $E_t$ ). However, upon addition of larger amounts of PEgMA, it is expected that the limited maximum draw ratio of the low molecular weight polymer additive will dominate the properties of the oriented foils, leading to reduced axial and off-axis stiffness and strength. The data shown in Figure 11A gratifyingly demonstrate that incorporation of relatively small amount of PEgMA leads to a (small) increase of the Young's modulus at  $90^\circ$ , as well as a reduced dependence of  $E$  on  $\theta$ . Increasing the PEgMA content of 0.6 w/w resulted in the expected decrease in stiffness. The dependence of the tensile strength on the test angle is shown in Figure 11B. These results indicate that the tenacity of oriented foils comprising 0.17 w/w of PEgMA was virtually identical to that of neat UHMW PE at all angles. Similar to the Young's modulus, the strength of the foils was only reduced at higher PEgMA content. Finally, it was found that the  $E$ - $\theta$  and the  $\sigma$ - $\theta$  dependencies followed, respectively, transverse isotropic elastic behavior and the Tsai-Hill failure criterion discussed in Chapter I.

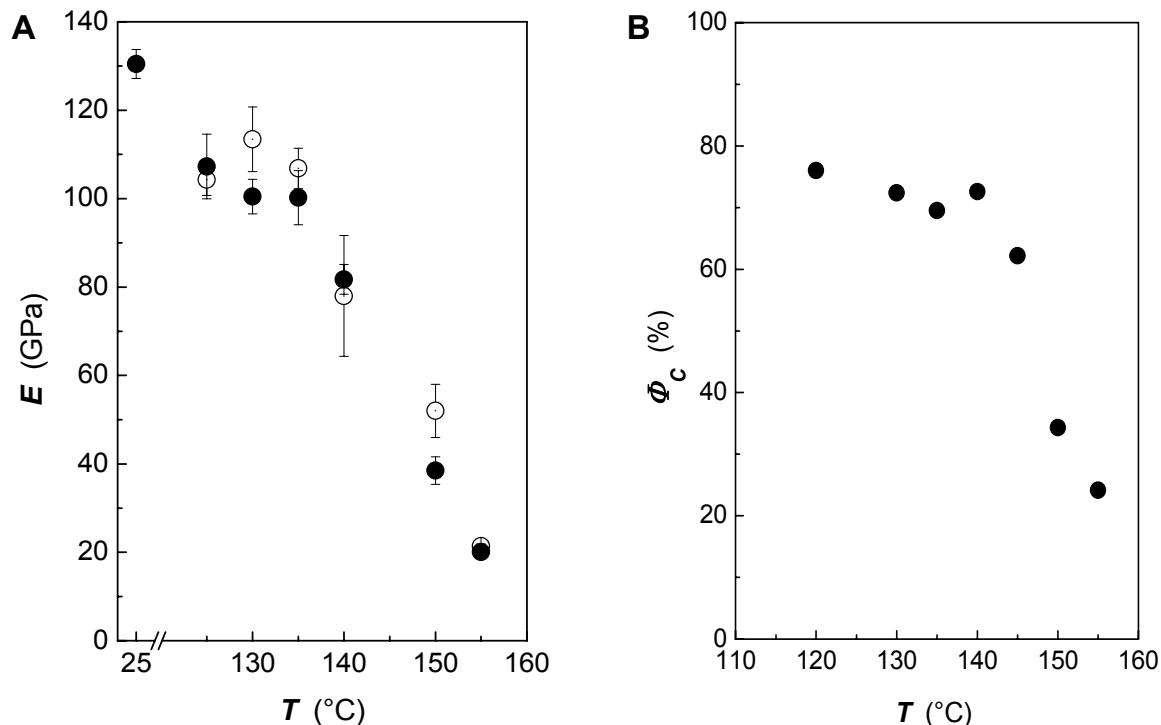


**FIGURE 11** A. Young's modulus,  $E$ , vs. test-angle,  $\theta$ , of oriented ( $\lambda = 50$ ) UHMW PE/PEgMA blend foil containing 0.17 w/w ( $\odot$ ) and 0.6 w/w ( $\bullet$ ) of PEgMA and reference, neat UHMW PE ( $\bullet$ ). B. Tensile strength,  $\sigma$ , vs. test angle,  $\theta$ . Inset: image taken with crossed polarizers of a specimen deformed at a test-angle of  $20^\circ$ . The curves were calculated employing the Tsai-Hill equation using values obtained in tensile tests conducted parallel, perpendicular and at  $45^\circ$  with respect to their orientation direction, employing a Poisson's ratio of 0.4.

In summary, it was found that incorporation of a functional, low molecular weight polar-grafted polyethylene in oriented UHMW PE foils did not lead to a substantial decrease in axial characteristics, but instead to an - albeit modest - increase in off-axis elastic and failure properties, and, most importantly, elimination of the fibrillation issues encountered with neat foils.

### 3.5 Laminates

In this section the formation of quasi-isotropic laminates with a selection of the above described UHMW PE foils will be presented. In order to promote adhesion between the individual foils, the aforementioned “hot compaction” was employed. Therefore, first, the effect of a 15 and 30 min thermal treatment, while constraining the foils, on their stiffness and degree of crystallinity was determined as function of temperature. Typical results, shown in Figure 12 for oriented UHMW PE blend foils comprising 0.17 w/w PEgMA, revealed that up to 140 °C both, the crystallinity and Young’s modulus, were little affected by this treatment, and, therefore, that temperature was selected as the maximum one for subsequent lamination experiments.

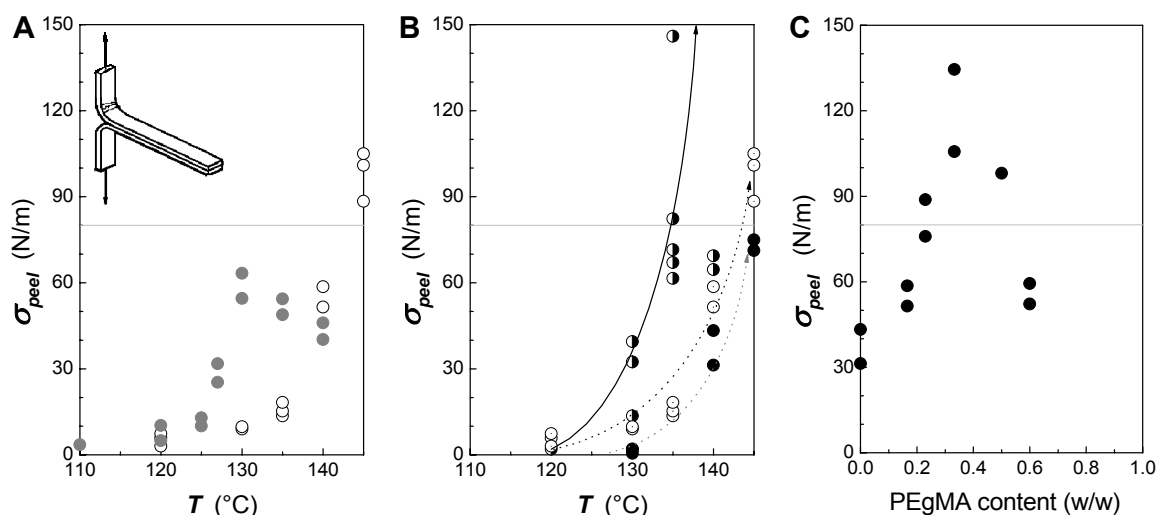


**FIGURE 12** A. Dependence of the Young’s modulus,  $E$ , on heat-treatment temperature and time (15 min (○) and 30 min (●)) of oriented UHMW PE/PEgMA foils comprising 0.17 w/w PEgMA (draw ratio  $\lambda = 50$ ). B. Degree of crystallinity,  $\Phi_c$ , vs. heat-treatment temperature,  $T$ , of foils annealed for 30 min.

## Adhesion

In order to promote adhesion between the ultra-drawn polyethylene foils, two routes were explored. First, the contact surfaces were exposed to the solvent decalin with the intent to reduce the melting temperature of the foil surface material, therewith attempting to increase the lamination temperature window.<sup>74, 75</sup> A second approach was to adhere the foils directly at elevated temperatures - i.e. without solvent-induced surface melting - relying solely on the polarity of the selected polymer additives. Three oriented foils were employed, i.e. neat UHMW PE, UHMW PE/PEgMA and UHMW PE/CoPES.

In an illustrative experiment, UHMW PE/PEgMA foils were assembled parallel to the direction of orientation and pressed according to both lamination methods for 30 min at a pressure of 850 Pa at various temperatures, and then subjected to the peel-strength test (see Figure 13A and Table 5).



**FIGURE 13** Results of peel-tests of laminates of various oriented UHMW PE foils parallel to their direction of orientation, “hot-compacted” for 30 min at 850 Pa. **A.** Dipping blend foils comprising 0.17 w/w PEGMA prior to pressing in decalin (●) allowed a larger processing window than without (○). **B.** Blend foils comprising 0.17 w/w of the copolymers CoPES (●) and PEGMA (○) and neat UHMW PE (●). **C.** Peel strength vs. PEGMA content of blend foils pressed at 140 °C. For reference purposes, the gray horizontal lines correspond to the peel strength of two Scotch<sup>®</sup> tapes.

It can be seen that the solvent-induced surface melting, indeed, allowed for increased adhesion at lower temperatures when compared to direct lamination, which permits more favorable retention of the mechanical properties of the uniaxially oriented foils employed. However, this advantage is offset to a certain degree by a reduction in peel-

strength at higher lamination temperatures, possibly because of enhanced relaxation of the macromolecules due to residual solvent.

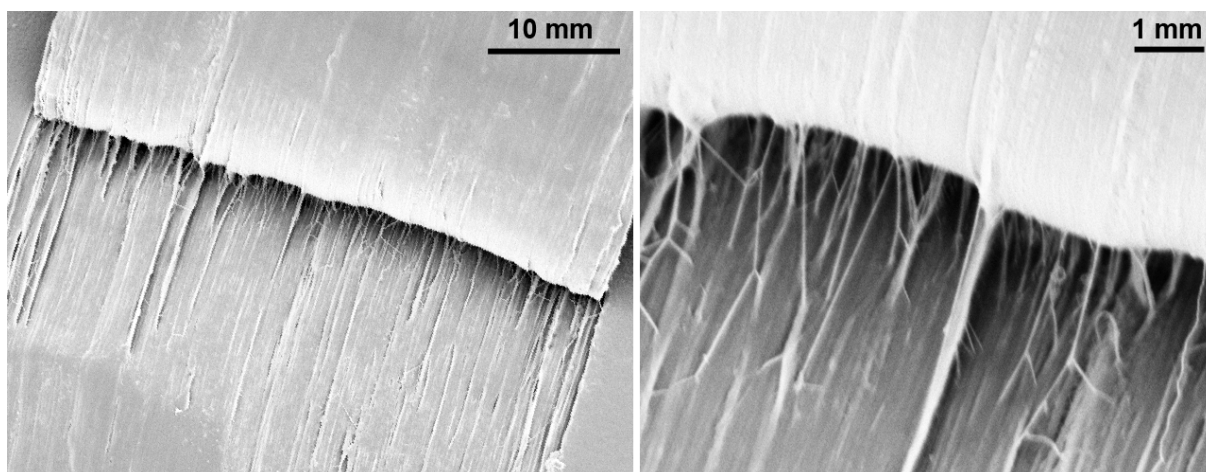
Optimal results were obtained with the system UHMW PE/CoPES by direct compaction at 140 °C. Unfortunately, the CoPES additive is incompatible with UHMW PE, leading to phase separation in solution in decalin (cf. Figure 13B). As a result, the UHMW PE/CoPES foils were inhomogeneous and featured a low strain to break in the transverse direction (see Table 5), rendering them less suitable for off-axis loading as it occurs in quasi-isotropic laminates.

**TABLE 5** Peel strength (N/m) for different oriented blend foils (draw ratio 50), laminated for 30 min at, respectively, 135 and 140 °C.

	content w/w	$\sigma_{peels}$ pressed at 135 °C	$\sigma_{peel}$ pressed at 140 °C
		N/m	N/m
UHMW PE	-	15	43
UHMW PE/PEgMA	0.17	18	59
UHMW PE/PEgMA	0.33	23	<b>134</b>
UHMW PE/PEgMA	0.50	44	98
UHMW PE/PEAA	0.17	14	69
UHMW PE/ULDPE	0.17	15	59
UHMW PE/CoPES	0.17	<b>146</b>	65

The effect of PEgMA content on the peel-strength of oriented blend foils produced by direct lamination at 140 °C for 30 min, is presented in Figure 13C. In this figure, a maximum in the peel-strength can be observed around a weight fraction of 0.3 w/w PEgMA. However, in the previous section it was shown that oriented UHMW PE foils containing more than 0.2 w/w PEgMA are of reduced uniaxial stiffness and strength (see Figures 9H, I). Therefore, finally, direct lamination of UHMW PE oriented foils containing 0.17 w/w PEgMA was selected for the preparation of quasi-isotropic laminates. Direct lamination of the latter at 140 °C resulted in a peel strength of 59 N/m, which is not particularly elevated, but sufficient to cause enhanced filament pull-out, indicative of sufficient adhesion (Figure 14).

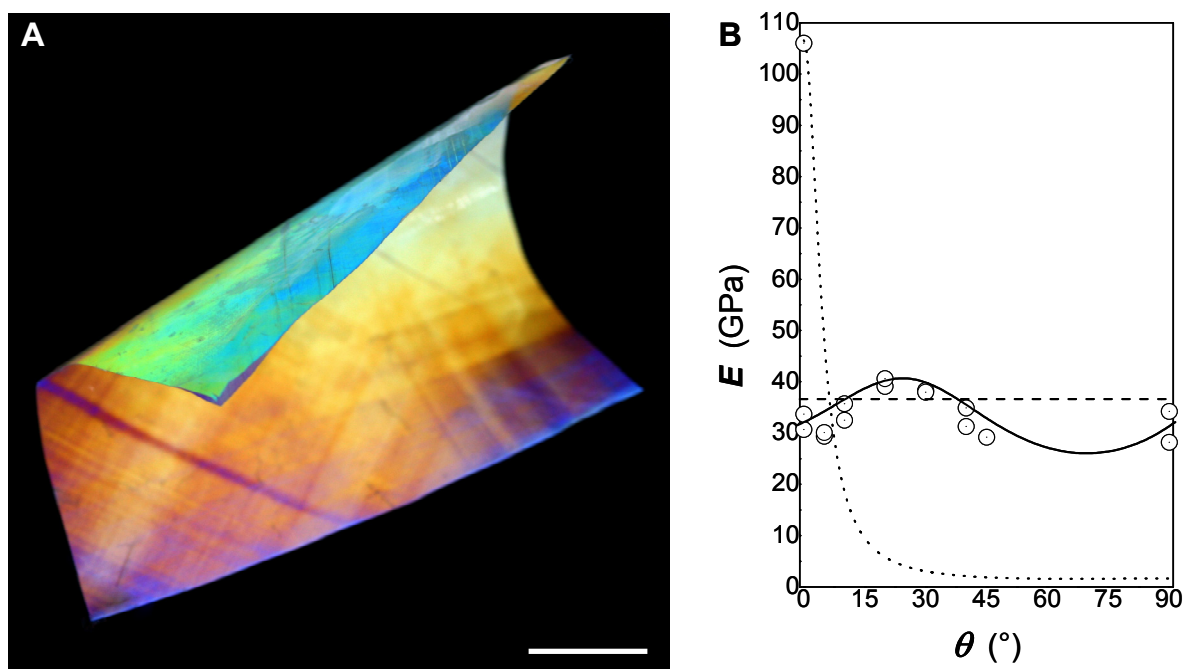




**FIGURE 14** Scanning electron micrographs taken at different magnifications showing a peeled interface between two foils of UHMW PE/PEgMA 0.17 w/w pressed at 140 °C and 850 Pa for 30 min.

### High-performance, quasi-isotropic UHMW PE-based laminated foils

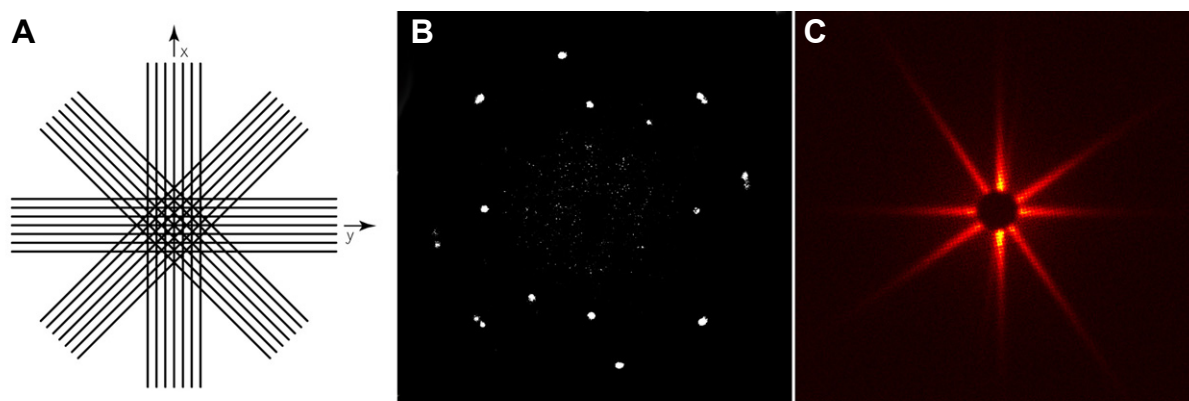
Unidirectional UHMW PE foils comprising 0.17 w/w PEgMA of a uniaxial Young's modulus of 130 GPa were directly laminated at 140 °C for 30 min to produce 4-ply [0/ 45/ 90/ 135] quasi-isotropic foils (cf. Figure 15A).



**FIGURE 15** A. Photograph taken between crossed polarizers of a typical planar, 4-ply foil; thickness 15  $\mu$ m, scale bar corresponds to 2 cm. B. Dependence of the Young's modulus,  $E$ , on test-angle,  $\theta$ , of a 4-ply foil of UHMW PE/PEgMA 0.17 w/w and, for comparison, of the constituent uniaxially heat-treated oriented film shown as dotted curve (see text).

The test-angle dependence of the stiffness of these laminated foils is presented in Figure 15B. Nearly isotropic high-performance foils were obtained, with a maximum Young's modulus of 40 GPa at a test angle of 20 °. Taking into account the favorable low density of polyethylene (0.98 g/cm<sup>3</sup>), these high-performance 4-ply UHMW PE-based laminated foils featured a specific in-plane *average* Young's modulus of ~35 GPa, which is superior compared to most other materials in terms of specific stiffness (see Table 2 in Chapter I).

According to classical lamination theory (see Chapter I), the in-plane isotropic stiffness of quasi-isotropic laminates should be angle-independent and approximately 1/3 of the uniaxial stiffness of the single foil. The in-plane stiffness of the present laminate was found to be slightly angle dependent, and a slightly below one third of the uniaxial stiffness of the single foil employed (130/3 = 43 GPa). The observed (minor) discrepancy is attributed to two factors: misalignment of the individual foils and reduction of the uniaxial modulus due to the heat treatment in the lamination process. From the WAXD and SAXS patterns of the 4-ply foil (Figure 16), the exact ply orientations were determined to be [0/ 35/ 90/ 124].

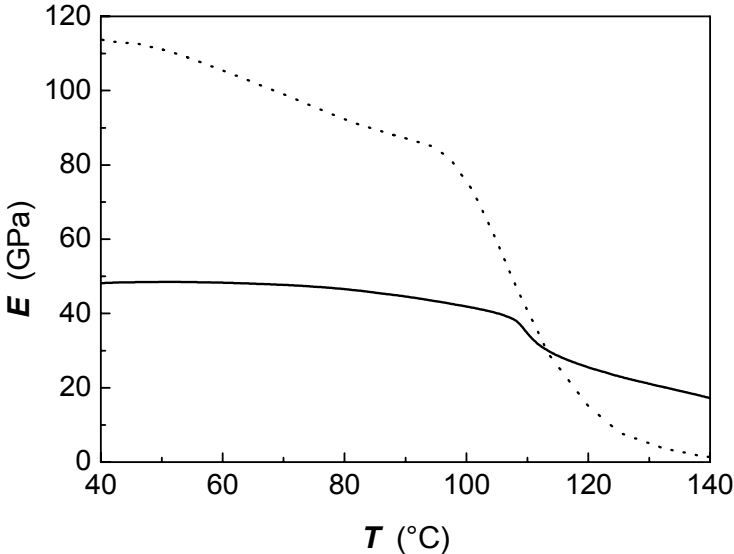


**FIGURE 16** A. Schematic of a 4-ply balanced foil. B. WAXD pattern and C. SAXS pattern of actual 4-ply UHMW PE/PEgMA 0.17 w/w foil.

Using these values, the angle-dependent stiffness was calculated using classical lamination theory with an uniaxial modulus of a single foil of 106 GPa; i.e. the value measured for a single foil after 30 min heating in a press at 140 °C (see Figure 12B), which corresponds to the heat treatment during lamination. Comparison between the experimental and theoretical angle-dependent in-plane stiffness of the 4-ply laminated

foil is shown in Figure 15B, and found to be in excellent agreement.

Finally, dynamic mechanical thermal analysis (DMTA), most interestingly, revealed that the temperature dependence of the stiffness of the hot-compacted 4-ply laminate was considerably less pronounced than that observed for the uniaxially oriented foils (Figure 17), which, of course, significantly expands the application range of these interesting materials.



**FIGURE 17** Dynamic mechanical thermal analysis of a uniaxially oriented UHMW PE/PEgMA 0.17 w/w ( $\lambda \sim 90$ ; dotted line) and 4-ply laminate made thereof (solid line).

## 4 Conclusions

In this chapter the development of high-performance, quasi-isotropic foils, based on UHMW PE were presented. As demonstrated by previous reports such foils can not be produced by biaxial drawing of solution-cast UHMW PE films, here, unidirectionally oriented foils were produced by ultra-drawing which, subsequently, were assembled to form quasi-isotropic, stacked laminated foils. In order to achieve this, two main problems had to be addressed: ultra-drawing of solution-cast UHMW PE foils typically results in fibrillating foils with poor transversal mechanical properties. Furthermore, PE is an apolar, relatively inert material that is not readily adhered even to itself. As both these problems originate in the weak van der Waals interactions between the polyethylene chains, it was attempted to increase these interactions by incorporating polymer additives with increased polarity, prior to stretching the solution-cast UHMW PE foils.

Initial screening of different polymer additives of varying polarity showed, as expected, that increasing polarity results in better adhesion between the unidirectionally oriented foils. Unfortunately, polymer additives with high polarity are incompatible with the apolar UHMW PE, leading to phase separation during solution-casting of the films. The resulting inhomogeneous structure of the foils caused a poor transverse strain-to-break of such blend systems.

A polymer additive of intermediate polarity, i.e. polyethylene-graft-maleic anhydride (PEgMA), was found to feature an optimum balance of adhesion and an advantageous homogeneous microstructure. Foils containing 0.17 w/w PEgMA drawn to a draw ratio of  $\lambda = 50$  exhibited a Young's modulus of 90 GPa and a transverse strain-to-break of 24 %. Remarkably, foils of higher PEgMA content ( $\geq 0.23$  w/w) and  $\lambda = 20$ , could be extended in the transverse direction to draw ratios approaching  $\lambda = 40$ , whereas similar foils of neat UHMW PE readily split in a brittle manner upon transverse loading, and, hence, are difficult to handle.

Unidirectionally drawn foils of UHMW PE containing 0.17 w/w PEgMA and of a Young's modulus of 130 GPa were laminated by direct compaction in a hot press for 30 min at 140 °C to yield [0/ 45/ 90/ 135] quasi-isotropic foils. The resulting 10  $\mu$ m-thin high-performance foils featured an isotropic in-plane modulus of about 35 GPa.

Small deviations from quasi-isotropy and the average in-plane modulus were in excellent agreement with classical lamination theory, taking into account a residual uniaxial modulus of 106 GPa of the constituent uniaxially oriented films after treatment for 30 min at 140 °C, and the discrepancy between the optimum [0/ 45/ 90/ 135] and experimental ply orientations [0/ 45/ 90/ 124] determined by WAXD/SAXS.

## 5 References

1. Kausch, H. H. *Polymer Fracture*, 2nd ed. ; Springer, Berlin **1987**.
2. Frank, F. C. *Proc. R. Soc. London, Ser. A* **1970**, 319, 127.
3. Smith, P. ; Lemstra, P. J. *US Patents* 4,344,908 **1982**; 4,422,993, **1983**; 4,430,383 **1984**; 4,436,689 **1984**.
4. Hearle, J. W. S. *High Performance Fibres*; p. 85; Woodhead Publishing Ltd. **2001**.
5. Govaert, L. E. ; Lemstra, P. J. *Colloid Polym. Sci.* **1992**, 270, 455.
6. Govaert, L. E. ; Bastiaansen, C. W. M. ; Leblans, P. J. R. *Polymer* **1993**, 34, 534.
7. Yagi, K. ; Toyota, A. *US Patent* 5,115,067 **1992**.
8. Motamedi, F. ; Bastiaansen, C. W. M. ; Smith, P. *Macromolecules* **1992**, 25, 1006.
9. Ohta, Y. ; Sugiyama, H. ; Yasuda, H. *J. Polym. Sci. Polym. Phys.* **1994**, 32, 261.
10. Klein, P. G. ; Woods, D. W. ; Ward, I. M. **1987**, 25, 1359.
11. Penning, J. P. ; Pras, H. E. ; Pennings, A. J. **1994**, 272, 664.
12. Jacobs, M. J. N. *Creep of Gel-Spun Polyethylene Fibres*; TU Eindhoven, NL **1999**.
13. Tordella, J. P. *US Patent* 3,502,764 **1970**.
14. Tordella, J. P. ; Dunion, P. F. *J. Polym. Sci. Polym. Phys.* **1970**, 8, 81.
15. Peterlin, A. ; Williams, J. L. ; Olf, H. G. *US Patent* 3,839,516 **1974**.
16. Burlet, R. J. H. ; Lemstra, P. J. *European Patent* 0,181,016 **1985**.
17. Fujii, T. ; Handa, K. ; Watanabe, K. *US Patent* 5,683,634 **1997**.
18. Fujii, T. ; Mochizuki, T. *US Patent* 5,759,678 **1998**.
19. Motooka, M. ; Mantoku, H. ; Ohno, T. *US Patents* 4,545,950 **1985**; 4,612,148 **1986**.
20. Product information; www.dsm.com/solutech **2007**.
21. Lemstra, P. J. *UK Patent Application* 2,164,897 A **1986**.
22. Krässig, H. *Macromol. Rev. Pt. D-J. Polym. Phys.* **1977**, 12, 321.
23. Smith, P. ; Lemstra, P. J. ; Pijpers, J. P. L. ; Kiel, A. M. *Colloid Polym. Sci.* **1981**, 259, 1070.
24. Olsen, D. A. ; Osteraas, A. J. *J. Polym. Sci. Polym. Chem.* **1969**, 7, 1921.
25. Blais, P. ; Carlsson, D. J. ; Csullog, G. W. ; Wiles, D. M. *J. Colloid Interface Sci.* **1974**, 47, 636.
26. Mercx, F. P. M. ; Benzina, A. ; Vanlangeveld, A. D. ; Lemstra, P. J. *J. Mater. Sci.* **1993**, 28, 753.

27. Silverstein, M. S. ; Sadovsky, J. ; Alon, D. ; Wahad, V. *J. Appl. Polym. Sci.* **1999**, 72, 405.
28. Ladizesky, N. H. ; Ward, I. M. *J. Mater. Sci.* **1983**, 18, 533.
29. Mercx, F. P. M. *Polymer* **1994**, 35, 2098.
30. Piiraja, E. K. ; Lippmaa, H. V. *Acta Polym.* **1984**, 35, 669.
31. Sheng, E. ; Sutherland, I. ; Brewis, D. M. ; Heath, R. J. ; Bradley, R. H. *J. Mater. Chem.* **1994**, 4, 487.
32. Feng, Z. G. ; Ranby, B. *Angew. Makromol. Chem.* **1992**, 195, 17.
33. Mercx, F. P. M. *Polymer* **1993**, 34, 1981.
34. Peijs, A. ; Catsman, P. ; Govaert, L. E. ; Lemstra, P. J. *Composites* **1990**, 21, 513.
35. Peijs, T. ; Rijdsdijk, H. A. ; Dekok, J. M. M. ; Lemstra, P. J. *Compos. Sci. Technol.* **1994**, 52, 449.
36. Alcock, B. ; Cabrera, N. O. ; Barkoula, N. M. ; Spoelstra, A. B. ; Loos, J. ; Peijs, T. *Composites Part A* **2007**, 38, 147.
37. Sanchez-Valdes, S. ; Picazo-Rada, C. J. ; Lopez-Quintanilla, M. L. *J. Appl. Polym. Sci.* **2001**, 79, 1802.
38. Lustiger, A. *WO Patent Application* 00/04,088 **2000**.
39. Yeh, J. ; Lin, Y. L. ; Fan-Chiang, C. C. *Macromol. Chem. Phys.* **1996**, 197, 3531.
40. Yeh, J. T. ; Chang, S. S. ; Yen, M. S. *J. Appl. Polym. Sci.* **1998**, 70, 149.
41. Yeh, J. T. ; Wu, H. C. *Polym. J.* **1998**, 30, 1.
42. Yeh, J. T. ; Chang, S. S. *J. Mater. Sci.* **2000**, 35, 3227.
43. Bin, Y. Z. ; Ma, L. ; Adachi, R. ; Kurosu, H. ; Matsuo, M. *Polymer* **2001**, 42, 8125.
44. Yeh, J. T. ; Lin, Y. T. ; Chen, K. N. *J. Appl. Polym. Sci.* **2003**, 89, 3728.
45. Yeh, J. T. ; Lin, Y. T. ; Chen, K. N. *J. Polym. Res.-Taiwan* **2003**, 10, 55.
46. Azuma, M. ; Ma, L. ; He, C. Q. ; Suzuki, T. ; Bin, Y. ; Kurosu, H. ; Matsuo, M. *Polymer* **2004**, 45, 409.
47. Hine, P. J. ; Ward, I. M. ; Olley, R. H. ; Bassett, D. C. *J. Mater. Sci.* **1993**, 28, 316.
48. Hine, P. J. ; Ward, I. M. ; Jordan, N. D. ; Olley, R. H. ; Bassett, D. C. *J. Macromol. Sci.-Phys.* **2001**, B40, 959.
49. Product information; [www.stamylanuh.com](http://www.stamylanuh.com) **2004**.
50. Borsboom, M. ; Bras, W. ; Cerjak, I. ; Detollenaere, D. ; van Loon, D. G. ; Goettkindt, P. ; Konijnenburg, M. ; Lassing, P. ; Levine, Y. K. ; Munneke, B. ; Oversluizen, M. ; van Tol, R. ; Vlieg, E. *J. Synchr. Rad.* **1998**, 5, 518.
51. The UNICAT facility at the Advanced Photon Source (APS) is supported by the U.S. DOE under Award No. DEFG02-91ER45439, through the Frederick Seitz Materials Research Laboratory at the University of Illinois at Urbana-Champaign, the Oak Ridge National Laboratory (U.S. DOE contract DE-AC05-00OR22725 with UT-Battelle LLC), the National Institute of Standards and Technology (U.S. Department of Commerce) and UOP LLC. The APS is supported by the U.S. DOE, Basic Energy Sciences, Office of Science under contract No. W-31-109-ENG-38.
52. Flory, P. J. ; Vrij, A. *J. Am. Chem. Soc.* **1963**, 85, 3548.
53. Smith, P. ; Lemstra, P. J. *Colloid. Polym. Sci.* **1980**, 258, 891.
54. Capaccio, G. ; Crompton, T. A. ; Ward, I. M. *J. Polym. Sci. Polym. Phys.* **1976**, 14, 1641.
55. Smith, P. ; Chanzy, H. D. ; Rotzinger, B. P. *J. Mater. Sci.* **1987**, 22, 523.

56. Smith, P. ; Lemstra, P. J. *J. Mater. Sci.* **1980**, 15, 505.
57. Kunz, M. ; Drechsler, M. ; Möller, M. *Polymer* **1995**, 36, 1331.
58. Luo, C. P. ; Atvars, T. D. Z. ; Meakin, P. ; Hill, A. J. ; Weiss, R. G. *J. Am. Chem. Soc.* **2003**, 125, 11879.
59. Voigt-Martin, I. G. ; Mandelkern, L. *J. Polym. Sci. Polym. Phys.* **1984**, 22, 1901.
60. Xue, Y. Q. ; Tervoort, T. A. ; Rastogi, S. ; Lemstra, P. J. *Macromolecules* **2000**, 33, 7084.
61. Capaccio, G. ; Ward, I. M. *Nature (Phys. Sci.)* **1973**, 243, 130.
62. Capaccio, G. ; Crompton, T. A. ; Ward, I. M. *Polymer* **1976**, 17, 644.
63. Sadler, D. M. ; Barham, P. J. *Polymer* **1990**, 31, 36.
64. Sadler, D. M. ; Barham, P. J. *Polymer* **1990**, 31, 46.
65. Ward, I. M. *Proc. Physical Soc.* **1962**, 80, 1176.
66. Irvine, P. A. ; Smith, P. *Macromolecules* **1986**, 19, 240.
67. Postema, A. R. ; Smith, P. *Macromolecules* **1990**, 23, 3296.
68. Allison, S. W. ; Ward, I. M. *Brit. J. Appl. Phys.* **1967**, 18, 1151.
69. Kuhn, W. ; Grün, F. *F. Kolloid. Z.* **1942**, 101, 248.
70. Nomura, S. ; Kawai, H. ; Kimura, I. ; Kagiya, M. *J. Polym. Sci. Polym. Phys.* **1970**, 8, 383.
71. Schimanski, T. ; Loos, J. ; Peijs, T. ; Alcock, B. ; Lemstra, P. J. *J. Appl. Polym. Sci.* **2007**, 103, 2920.
72. Colbeaux, A. ; Fenouillot, F. ; Gerard, J. F. ; Taha, M. ; Wautier, H. *Polym. Int.* **2005**, 54, 692.
73. Hinrichsen, G. ; Eberhardt, A. ; Lippe, U. ; Springer, H. *Colloid Polym. Sci.* **1981**, 259, 73.
74. Takagi, K. ; Fujimatsu, H. ; Usami, H. ; Ogasawara, S. *J. Adhes. Sci. Technol.* **1996**, 10, 869.
75. Cohen, Y. ; Rein, D. M. ; Vaykhansky, L. *Compos. Sci. Technol.* **1997**, 57, 1149.





# III

*Thermotropic Liquid-Crystalline Polyester*



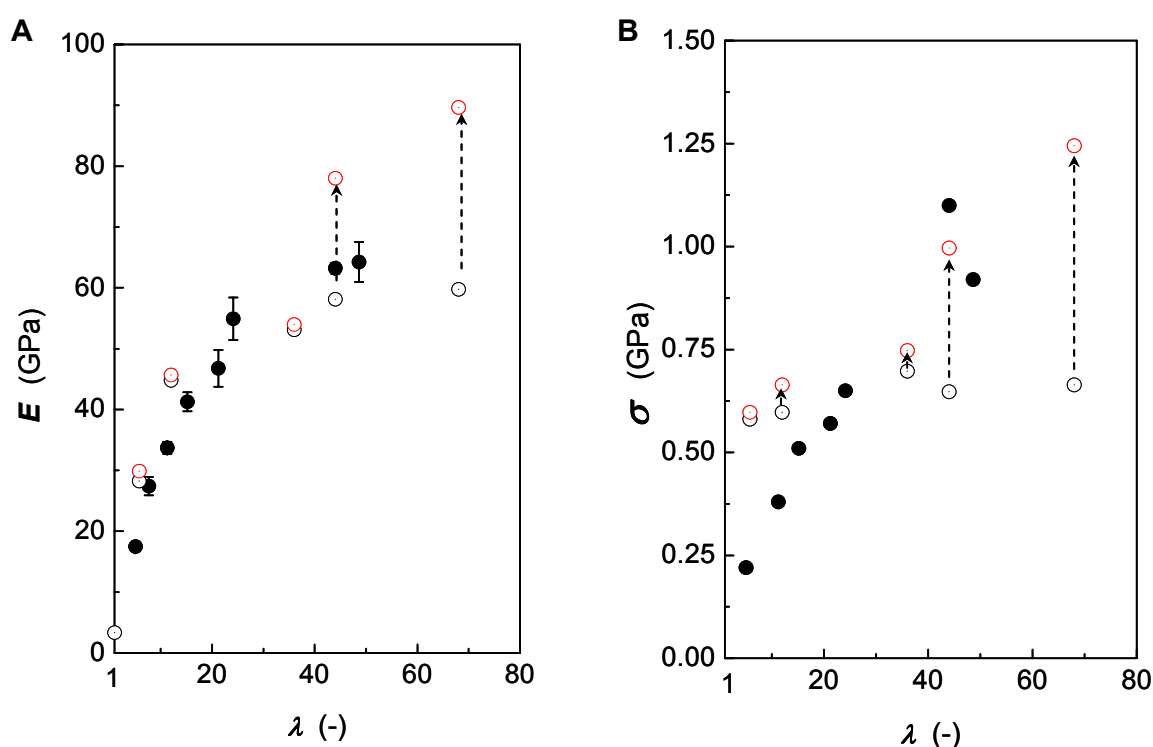
# 1 Introduction

In this chapter, efforts are described that were directed to the formation of ultra-high-performance foils, not from flexible-chain polymers through solid-state tensile deformation as shown in the previous chapter for ultra-high molecular weight polyethylene, but by direct orientation in the liquid-crystalline phase of more rigid macromolecules. As a starting point, a thermotropic, semi-rigid polymer was selected. Such liquid-crystalline material can be processed from the melt - a major advantage over more rigid macromolecules like poly(*p*-phenylene terephthalamide) (PPTA), which requires processing from lyotropic solutions in sulfuric acid (see Chapter IV).<sup>1</sup> Already in 1975, de Gennes suggested control of the melting temperature - and therewith processability - of thermotropic polymers by combining rigid and kinked or flexible segments in the macromolecular chains.<sup>2</sup> This scheme was demonstrated to be highly effective by, among others, Jackson and Kuhfuss, who synthesized a large portfolio of thermotropic liquid-crystalline polymers.<sup>3,4</sup>

Among the numerous materials produced, copolyesters based on *p*-hydroxybenzoic acid (HBA) and 2-hydroxy-6-naphthoic acid (HNA), commercially produced by Ticona (Germany) under the trade name Vectra<sup>®</sup> were found to be particularly useful. This family of polymers provides an adequate compromise between convenient processability and - inevitably more modest - mechanical properties due to the semi-rigid nature of the macromolecules. It has been demonstrated that high-performance fibers can be directly spun from their thermotropic melt at convenient temperatures of 250-350 °C by applying relatively high wind-up/extrusion speed (draw down) ratios that induce elongational flow fields causing the polymer molecules to orient in the direction of flow.<sup>5</sup> Advantageously, relaxation times of such an oriented melt are relatively long and, therefore, macromolecular orientation can largely be retained during solidification, yielding the desired high-performance fibers.<sup>6</sup> The data in Figure 1 - collected from the literature<sup>5</sup> and generated in this work<sup>7</sup> - show the development of mechanical properties with draw-down ratio (here defined as the ratio of the cross-section areas of the die and the drawn filament). Also illustrated in this figure is the well-established fact that the mechanical properties of as-spun, oriented fibers of this material can be enhanced by heat treatment, i.e. post-condensation at elevated temperatures.<sup>8,9</sup>

Remarkably, - to our knowledge - relatively few efforts have been made to produce films and foils of these thermotropic materials.<sup>10-14</sup> Until now, such product forms typically have been produced by extrusion through slit-shaped dies [also referred to as “slot”-dies]. Table 1 collects selected mechanical properties reported for different tapes or films, which reveal that they generally are substantially inferior to those of the fibers shown in Figure 1. [N.B. We are aware of two studies that report fabrication of samples of higher values of both stiffness and strength.<sup>10, 14</sup> Unfortunately, no details are presented regarding the nature of the polymer, nor are accurate processing descriptions presented. Moreover, notably the data in ref. 10 appear to relate to narrow tapes, rather than foils.]

One reason for the relatively poor properties of most samples is likely to be found in the fact that extrusion of articles of thermotropic liquid-crystalline polymers often results in structures of an unfavorable skin-core morphology,<sup>15</sup> in which the skin displays an elevated degree of molecular order, while macromolecules in the center region appear virtually unoriented and feature unattractive mechanical properties.



**FIGURE 1** Development of the Young's modulus  $E$  (A) and tensile strength  $\sigma$  (B) with draw-down ratio  $\lambda$  of fibers of thermotropic, liquid-crystalline copolyester (Vectra<sup>®</sup>). (○) Data from ref. 5 for a HBA<sub>0.58</sub>/HNA<sub>0.42</sub> copolymer, and (●) this work for HBA<sub>0.73</sub>/HNA<sub>0.27</sub> (see text).<sup>7</sup> Elongations at break are ~2 %. Also shown are data of filaments heat treated for 30 h at 230 °C from ref. 5 (○).

**TABLE 1** Young's modulus,  $E$ , and tensile strength,  $\sigma$ , of unidirectionally oriented films or tapes described in the literature. Subscripts **ae** and **ht** refer to as-extruded and heat treated, respectively. Where known, indicated are the slit die breadth  $b^*$  and height  $h^*$ , draw-down ratio  $\lambda$  and resulting film/tape width  $w$  and thickness  $d$ , heat-treatment time  $t$  and temperature  $T$ , and take-up speed  $v$ .

material	$E_{ae}$ GPa	$\sigma_{ae}$ GPa	$E_{ht}$ GPa	$\sigma_{ht}$ GPa	$b^*/w$ mm	$h^*/d$ mm	$\lambda$ -	$t$ h	$T$ °C	$v$ m/min	ref.
HBA <sub>0.75</sub> /HNA <sub>0.25</sub>	15.3	0.48	13.6	0.66	102*/82	1.7*/0.15	13.7	1/11	260/310	2.58	12
HBA <sub>0.75</sub> /HNA <sub>0.25</sub>	24.9	0.44	28.2	0.83	6.5*	0.18*	-	24	250	1.5	11
HBA <sub>0.75</sub> /HNA <sub>0.25</sub>	31.1	0.48	-	-	102*	-	13.7	-	-	-	13
Vectra <sup>®</sup>	41.0	0.62	-	-	-	-	-	-	-	-	14
unknown	82.8	1.97	-	-	5.1	0.009	-	-	-	-	10

Another reason, as will be also shown in this work, is that the efficient elongational flow generated in standard fiber-spinning operations, can be compromised by employing unoptimized dies or inadequate solidification conditions.

Similarly, disappointing results have been reported for film- and sheet-extrusion of blends of Vectra<sup>®</sup> and thermoplastic polymers, originally aimed at producing in-situ composites of extended semi-rigid-polymer filaments within a flexible polymer matrix. That process was thought to allow economic production of reinforced products via a melt-processing route employing standard equipment (for instance refs. 16, 17). Although the sheets obtained were found to comprise seemingly endless fibrillar structures of the thermotropic polyester, their mechanical properties were inferior when compared to fibers spun from the same polymer.<sup>17</sup> Based on their extensive studies, the authors concluded that even “*pure elongational flow may not be sufficient to achieve a high degree of molecular orientation and accompanying stiffness, but that convergent flow in all directions (such as present in fiber-spinning through a round die) is necessary*”.<sup>16</sup>

As stated above, the aim of the work described here was to produce ultra-high-performance foils of a thermotropic, liquid-crystalline polymer, i.e. foils that do not feature inhomogeneous architectures and exhibit mechanical properties that approach that of spun filaments. In order to achieve this, a series of novel dies were designed, as well as different extrusion schemes explored.

## 2 Die Designs

Three sets of dies were manufactured, referred to as i) reference slit dies, ii) filament-forming dies and iii) filament-fusing dies, which will be detailed hereafter.

### 2.1 Reference Slit Dies

Reference slit die **s1** is of a simple slot shape, and expected to, at best, cause planar orientation of the macromolecules within the extrudate. Slit die **s2** comprises an entrance of exponentially reduced width down to 100  $\mu\text{m}$ , designed to introduce (1D) contractional flow in the extrusion direction, commonly referred to as “strip-biaxial extension” (Figure 2).

### 2.2 Filament-forming Dies

A second set of dies was designed to first create a multitude of highly oriented liquid filaments under beneficial conditions of axial-symmetric 3D contractional flow (as present in fiber spinning), to be subsequently fused into the form of continuous foils. One obvious approach to achieve this objective is, of course, by means of a linear series of spinnerets. That path was, however, not followed simply for its cumbersome space requirement and the large lateral contraction needed to consolidate the liquid filaments into a coherent foil.

The challenge to construct dies that efficiently orient the filament-shaped stream of the molten polymer and guide those into the shape of a foil was addressed in two different ways:

First, a filament-forming die **f1** was constructed in the form of a half cylinder comprising a multitude (130) of cone-shaped channels (diameter entrance: 1 mm; exit: 100  $\mu\text{m}$ ; length: 5 mm), designed to provide confined 3D-contraction flow within the die, guiding the melt directly to the orifice exit (Figures 2 and 3A).

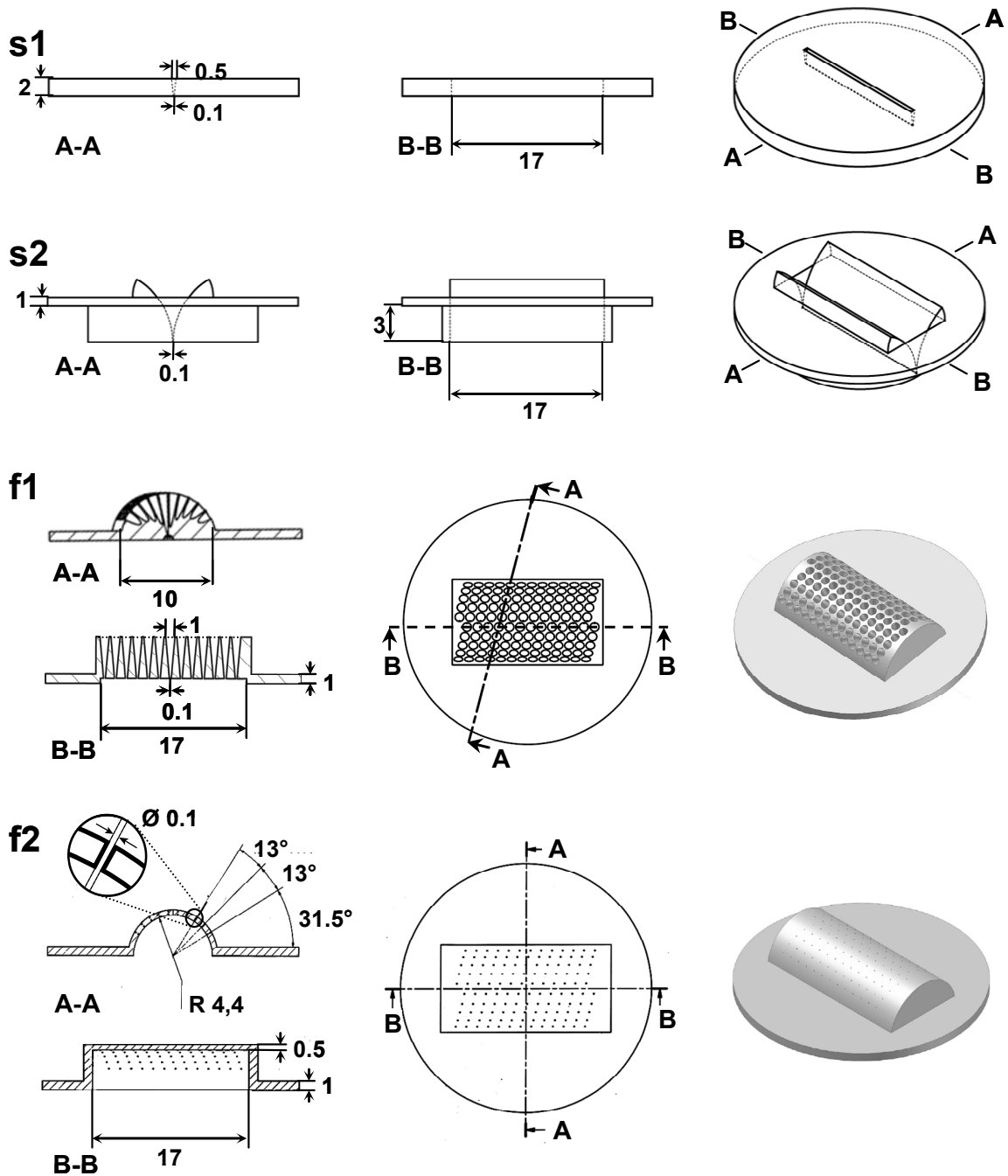
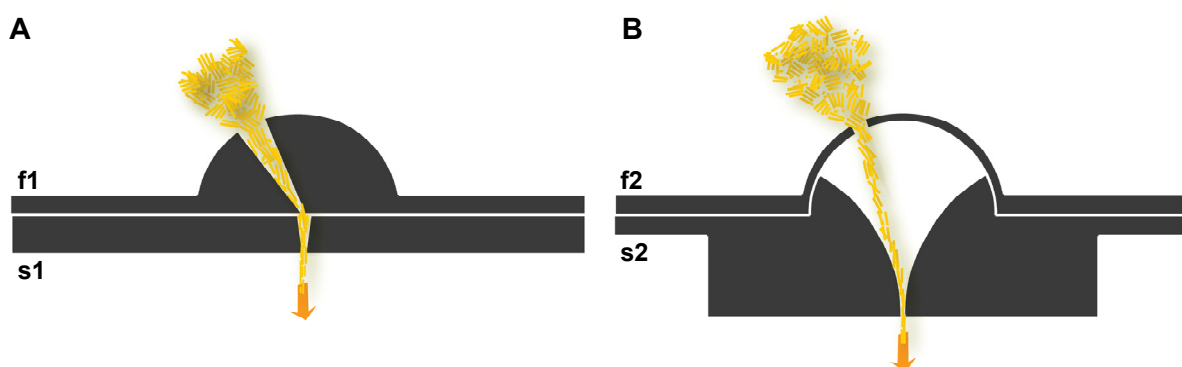


FIGURE 2 Simple slot-type die **s1** (breadth 17 mm; width 100  $\mu\text{m}$ ) and similar die **s2** of identical breadth, but exponentially decreasing width. Filament-forming die **f1**, comprising 130 cone-shaped channels and filament forming die **f2**, consisting of 130 cylindrical-orifices (diameter 100  $\mu\text{m}$ ). The dies **s1** and **s2** can be combined in sets with, respectively, filament-forming dies **f1** and **f2** (see Figure 3). Dimensions are in mm.

In addition, die **f2** was manufactured so that it consisted essentially of a half-cylindrical plate comprising staggered arrays of 130 cylindrical-orifices with a diameter of 100  $\mu\text{m}$  and a land length of 0.5 mm. 3D-contraction flow is anticipated to occur “up-stream” of the die. Furthermore, this die was designed so that in the hollow space below the orifices draw-down could be applied, as in conventional fiber spinning (cf. schematic drawings in Figures 2 and 3B).

### 2.3 Filament-fusing Dies

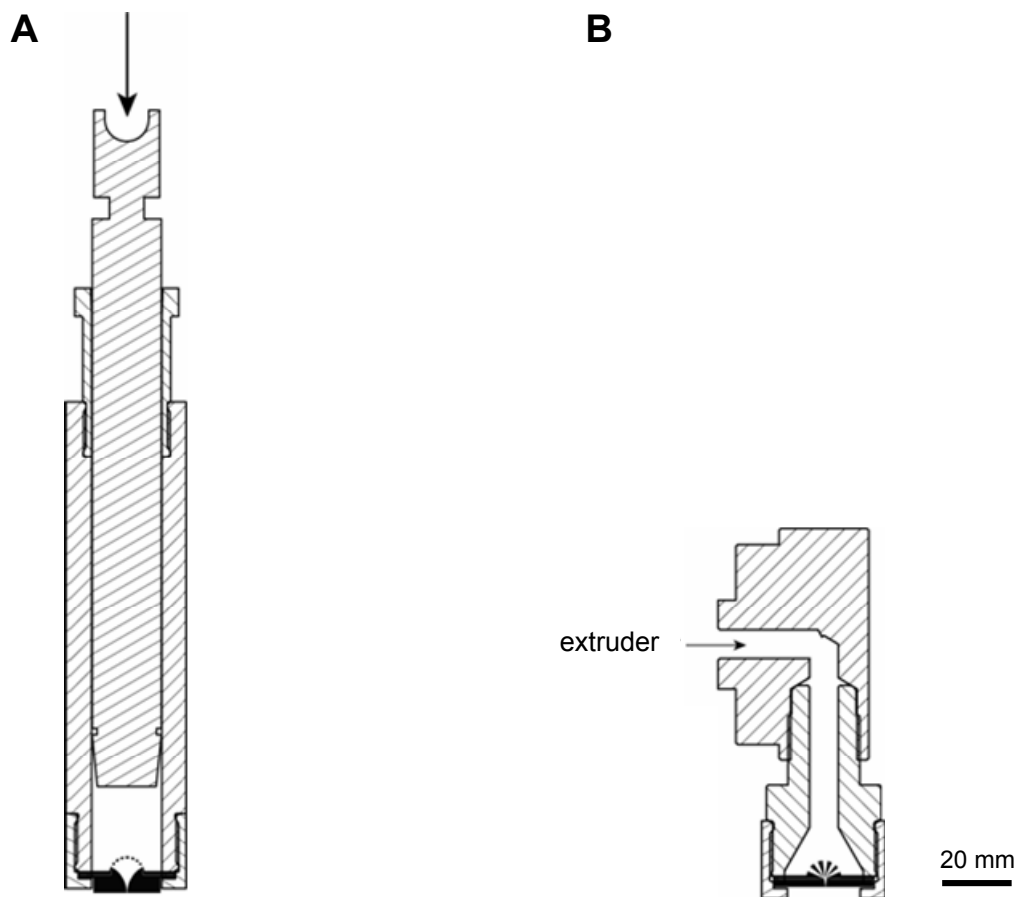
Finally, the above filament-forming dies **f1** and **f2** were combined in sets with, respectively, slit dies **s1** and **s2** (denoted dies **f1-s1** and **f2-s2**) to promote fusion prior to solidification of the liquid filaments generated in the filament-forming dies.



**FIGURE 3** Schematic paths (not to scale) of a melt trough one of 130 channels of dies **f1** and **f2**. **A. f1**: contraction takes place in the conical-shaped channel guiding the molten polymer to an exit of diameter 100  $\mu\text{m}$ . **B. f2**: the liquid-crystalline material passes directly through orifices of 100  $\mu\text{m}$  diameter. The main flow contraction occurs “up-stream”.

The above described dies were mounted onto a simple laboratory-scale, piston-driven device (SpinLine<sup>®</sup>, DACA Instruments, Santa Barbara, USA) with which batches of 25 g were processed, or onto an adapter connected to the head of the Teach-Line<sup>®</sup> single-screw extruder (Collin, Germany) for continuous extrusion (Figure 4).



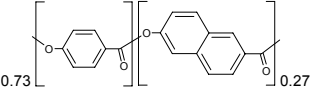


**FIGURE 4** A. Schematic of the laboratory-scale, piston-driven-batch extrusion set-up, here shown equipped with die set **f2-s2**. B. Adapter to Teach-Line<sup>®</sup> single-screw extruder used in continuous processes, mounted with die set **f1-s1**.

### 3 Experimental

**Materials.** The material used was the thermotropic liquid-crystalline polymer Vectra<sup>®</sup> A950 (Ticona, Germany), a random copolymer of 73 mol % *p*-hydroxybenzoic acid (HBA) and 27 mol % 2-hydroxy-6-naphthoic acid (HNA). Selected properties are listed in Table 2. Prior to use, the polymer was dried over night at 80 °C in a vacuum oven.

**TABLE 2** Structure and properties of the thermotropic polymer used in this work. Young's modulus,  $E$ , tensile strength,  $\sigma$ , elongation at break,  $\epsilon$ , melting temperature,  $T_m$ , and density,  $\rho$ . (data received from the supplier)

polymer	chemical structure	$E$ GPa	$\sigma$ GPa	$\epsilon$ %	$T_m$ °C	$\rho$ g/cm <sup>3</sup>	ref.
Poly( <i>p</i> -hydroxybenzoic acid-co-2-hydroxy-6-naphthoic acid) copolyester Vectra <sup>®</sup> A950.		10.6	0.18	3.4	280	1.40	18

**Processing.** Extrusion was performed at 300 °C, initially with the small-scale, batch piston-driven, SpinLine from DACA Instruments (Santa Barbara, USA). Unless otherwise indicated, the extrusion speed was 10 mm/min, corresponding to a throughput of 4.4 g/min, while the take-up speed was varied up to 50 m/min. The extrudate was cooled by the surrounding air and the distance from the die to the first roll was 10 cm.

In subsequent experiments, continuous extrusion was conducted with the Teach-Line<sup>®</sup> single-screw extruder E20T SCD15 (Collin, Germany), also at temperature of 300 °C, with die sets **f1-s1** and **f2-s2**. The same winder as above was used and take-up speeds were varied up to 150 m/min (the maximum of the winder at hand). In this series of experiments the extruded polymer was quenched in a water bath at room temperature; different air-gap distances (i.e. the distance between the die exit and the water surface) were applied.

**Mechanical analysis.** Tensile properties were measured employing an Instron tensile tester 5864 (Norwood, USA). The gauge length was 50 mm and the crosshead speed 5 mm/min. The cross-sectional areas of the specimen were calculated from the weight of each sample using a density of 1.40 g/cm<sup>3</sup> (supplier; and also determined with Ultrapycnometer 1000 (Quantachrome, USA)). In addition, unidirectionally oriented

and planar foils were tested in tension at different loading angles. The specimen width was 4 mm and gauge length at least 8 mm. Clamps were mounted in a rigid fashion to avoid perpendicular shifting along the draw direction during testing.

***X-ray analysis.*** Wide-angle X-ray diffraction (WAXD) patterns were recorded with an Onyx CCD detector at a distance of 65 mm, mounted on an Oxford Diffraction Xcalibur XP instrument using a Mo-K $\alpha$  source (wavelength was 0.7093 Å) operated at -50 kV / 40 mA. Hermans' orientation factors,  $f_h$ , and average orientation angles were derived from the half-width at half-maximum intensity of the third meridian reflection.

***Thermal analysis.*** Melting temperatures and enthalpies of fusion were determined with a Mettler Toledo DSC 822<sup>e</sup> (Greifensee, Switzerland) differential scanning calorimeter. Amounts of about 5 mg sealed in aluminum crucibles were heated at a rate of 10 °C/min under nitrogen.

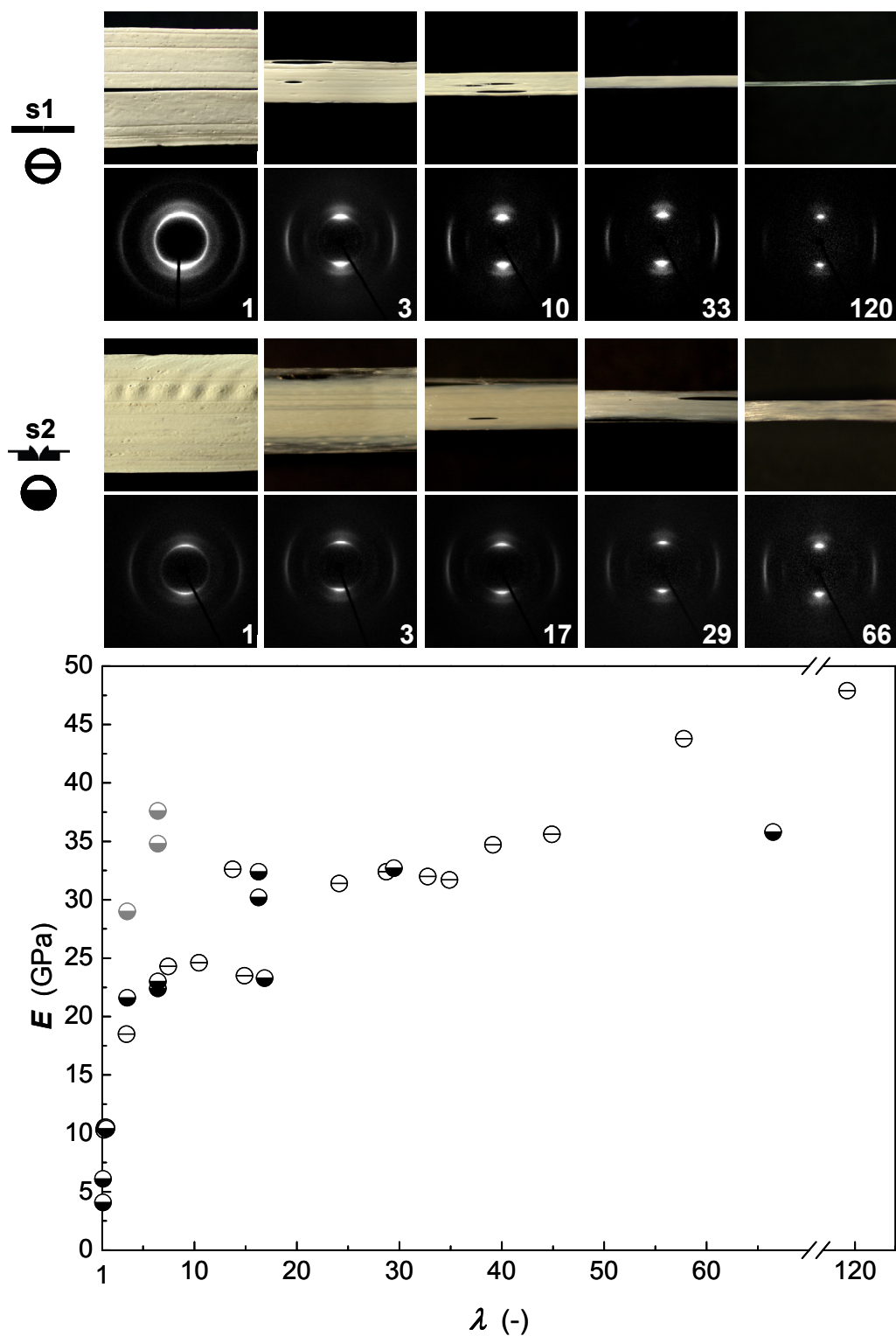
## 4 Results and Discussion

### 4.1 Reference Slit Dies

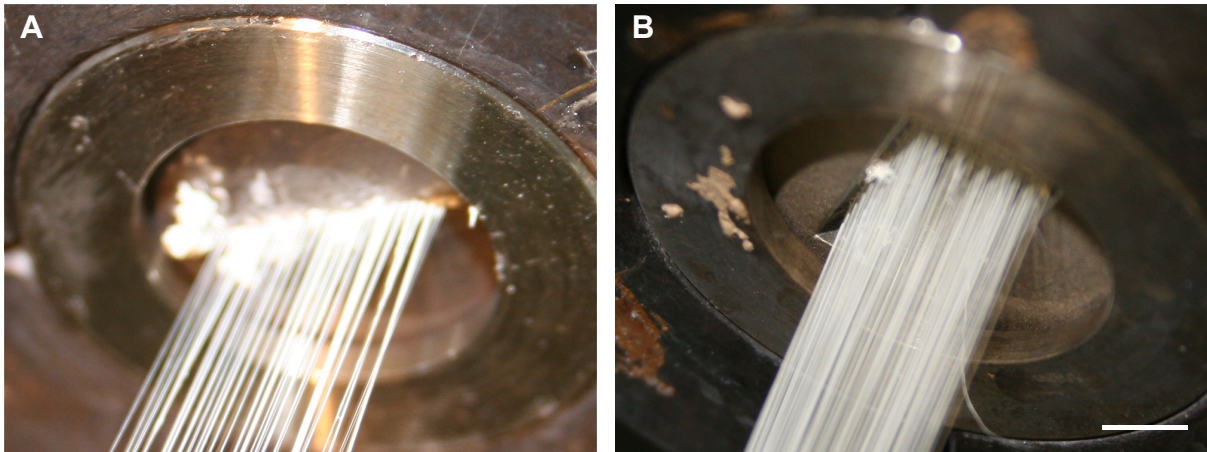
For reference purposes, first, a series of experiments was conducted with the slit dies **s1** and **s2**. Notable difficulties were encountered in the form of severe fibrillation and splitting during extrusion and collection of the foils, especially with die **s1** (Figure 5, top). Moreover, in concert with previously reported observations,<sup>19</sup> the extruded specimens - most notably with die **s2** - featured inhomogeneous structures characterized by a higher stiffness at the outer parts than in the centre of the foil (cf. Figure 5, data in gray). Typical skin-core effects were observed as the more oriented skin could readily be peeled off. Most concerning, though, was that to achieve adequate mechanical properties, a high draw-down ratio  $\lambda$  needed to be applied, which in extrusion with the present reference dies resulted in naturally formed multifilaments, lacking foil-like features; see the optical photographs in Figure 5 of products produced at different draw-down ratios. Corresponding wide-angle X-ray diffraction (WAXD) patterns are also shown in this figure, as well as the values of the Young's modulus vs. draw-down ratio of all samples produced. Not surprisingly, the latter data fell short of those presented in Figure 1 for fibers of this polymer.

### 4.2 Filament-forming Dies

In a second set of experiments, “filament-forming” dies **f1** and **f2** were used in the extrusion process. The photographs in Figure 6 illustrate their capacity to form dense bundles of filaments. However, no foils could be collected, although, due the geometrical guidance in die **f1**, several individual filaments were seen to fuse together. Gratifyingly, though, due to the particular design of the dies, excellent mechanical properties were achieved for filaments produced already at very low draw-down ratios (*nota bene*  $< 3$ ; see Table 3).







**FIGURE 5** Top: Reflected-light optical photographs and corresponding wide-angle X-ray diffraction (WAXD) patterns of extrudates produced with dies **s1** ( $\ominus$  upper series) and **s2** ( $\bullet$  lower series). The width of the photographs represents 15 mm; draw-down ratios  $\lambda$  are indicated in lower right corners of the X-ray patterns. Extrusion direction and product axis are horizontal. Bottom: Young's modulus  $E$  vs. draw-down ratio  $\lambda$  of samples extruded with slit dies **s1** ( $\ominus$ ) and **s2** ( $\bullet$ ); data of outer parts of samples produced with die **s2** ( $\bullet$ ).



**FIGURE 6** Extrusion with filament-forming dies **f1** (A) and **f2** (B). Scale bar corresponds to 5 mm.

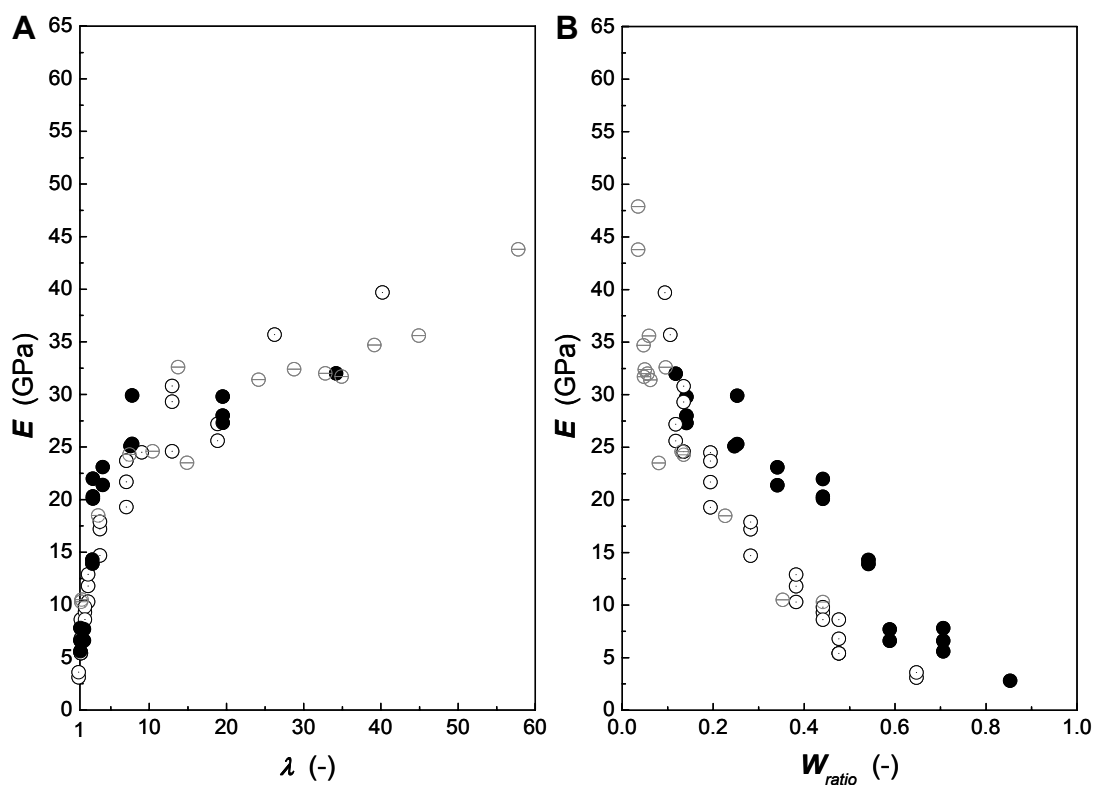
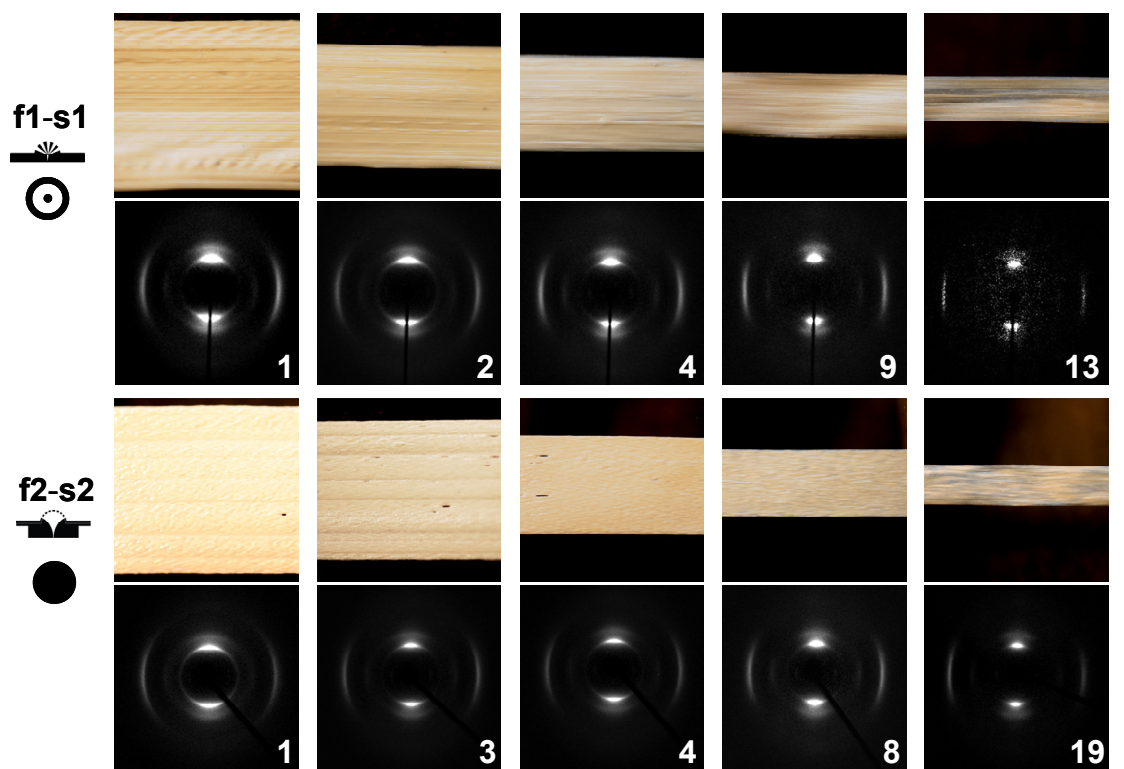
The data presented further reveal that die **f1** was the more efficient one in orienting the liquid-crystalline polymer, as it consistently yielded material of superior stiffness and strength.

**TABLE 3** Mechanical properties of as-spun filaments produced with filament-forming dies **f1** and **f2**.  $\lambda$  refers to the draw-down ratio applied.

die		$\lambda$	diameter $\mu\text{m}$	$E$ GPa	$\sigma$ GPa	$\epsilon$ %
	<b>f1</b>	1.7	76	50	0.8	1.7
		2.5	63	56	0.7	1.3
	<b>f2</b>	1.7	77	26	0.5	3.1
		2.6	62	43	0.6	2.1

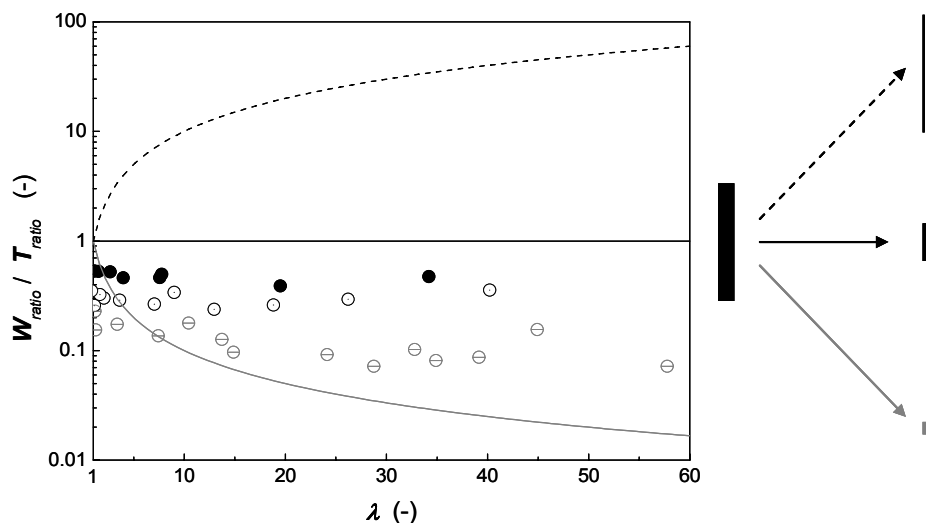
### 4.3 Filament-fusing Dies

Next, results are presented in Figure 7 of experiments in which the above filament-forming dies **f1** and **f2** were employed in combination with slit dies **s1** and **s2**, respectively (referred to as “filament-fusing” dies **f1-s1** and **f2-s2**) in attempts to guide and at least partially fuse the filaments formed with them into liquid foils prior to solidification. While it was pleasing to note that the foils produced were of excellent appearance and no fibrillation or splitting occurred, it was disappointing to find that the development of the Young’s modulus with draw-down ratio - which was highly efficient when employing the filament-forming dies alone - was significantly less pronounced, and essentially as observed when using the simple reference slit dies alone.



**FIGURE 7** Top: Reflected-light optical photographs and corresponding WAXD patterns of extrudates produced with die sets **f1-s1** ( $\odot$  upper series) and **f2-s2** ( $\bullet$  lower series). The width of the photographs represents 15 mm; draw-down ratios,  $\lambda$ , are indicated in lower right corners of the X-ray patterns. Extrusion direction and product axis are horizontal. Bottom: Development of the Young's modulus,  $E$ , with  $\lambda$  (**A**) and width ratio,  $W_{ratio}$ , (**B**; see text) of foils extruded using die sets **f1-s1** ( $\odot$ ) and **f2-s2** ( $\bullet$ ). For comparison, data obtained for products formed with reference slit-die **s1** are plotted in gray ( $\ominus$ ).

Nonetheless, part of the objective was achieved in that the width retention ratio,  $W_{ratio}$  (width of foil  $W$  divided by the breadth of the die  $W_0$ ), of products of a particular stiffness, significantly surpassed those obtained with the reference dies and more so with the set up with die **f2-s2** (cf. Figures 7, 8), especially at low draw-down ratios. This conclusion is quantitatively demonstrated in Figure 8, which visualizes the above results together with the idealized dependence on the draw-down ratio of the dimensions of a rectangular extrudate, expressed as the ratio between  $W_{ratio}$  and  $T_{ratio}$  (= thickness of foil  $T$  divided by the die gap  $T_0$ ). In the preferred case of foil formation, elongation of the molten polymer extrudate would occur uniquely through reduction of the *thickness* and the width of the final product would be the same as that of the die (upper bound). The lower bound condition is that the material preserves its initial thickness and draw down is at the expense of the *width* only, varying the quotient  $W_{ratio} / T_{ratio}$  with  $1/\lambda$ , eventually yielding a fiber-like product, as observed in extrusion with slit die **s1**. Of course, when the initial aspect ratio of the extrudate is maintained in the drawing process, the  $W_{ratio} / T_{ratio}$  equals unity, independent of  $\lambda$ . We can conclude from the data in Figure 8 that the filament-fusing dies are, indeed, more effective than standard slit dies in preserving the shape of the initial extrudate, approaching a constant value for  $W_{ratio} / T_{ratio}$ .



**FIGURE 8** Idealized development of dimensions of product extruded from a rectangular die with draw-down ratio  $\lambda$  (see text). Upper bound (dotted): reduction in *thickness* only, yielding foil. Horizontal: constant width/thickness ratio. Lower bound: (gray) reduction in *width* only, culminating in the form of a filament. Schematic cross-sectional areas on the right illustrate these three cases. Foil form was preserved more effectively with die **f2-s2** (●) than **f1-s1** (○). For comparison, data for extrudates obtained with the reference slit-die **s1** are also plotted (⊖).



## 4.4 Air-gap Extrusion

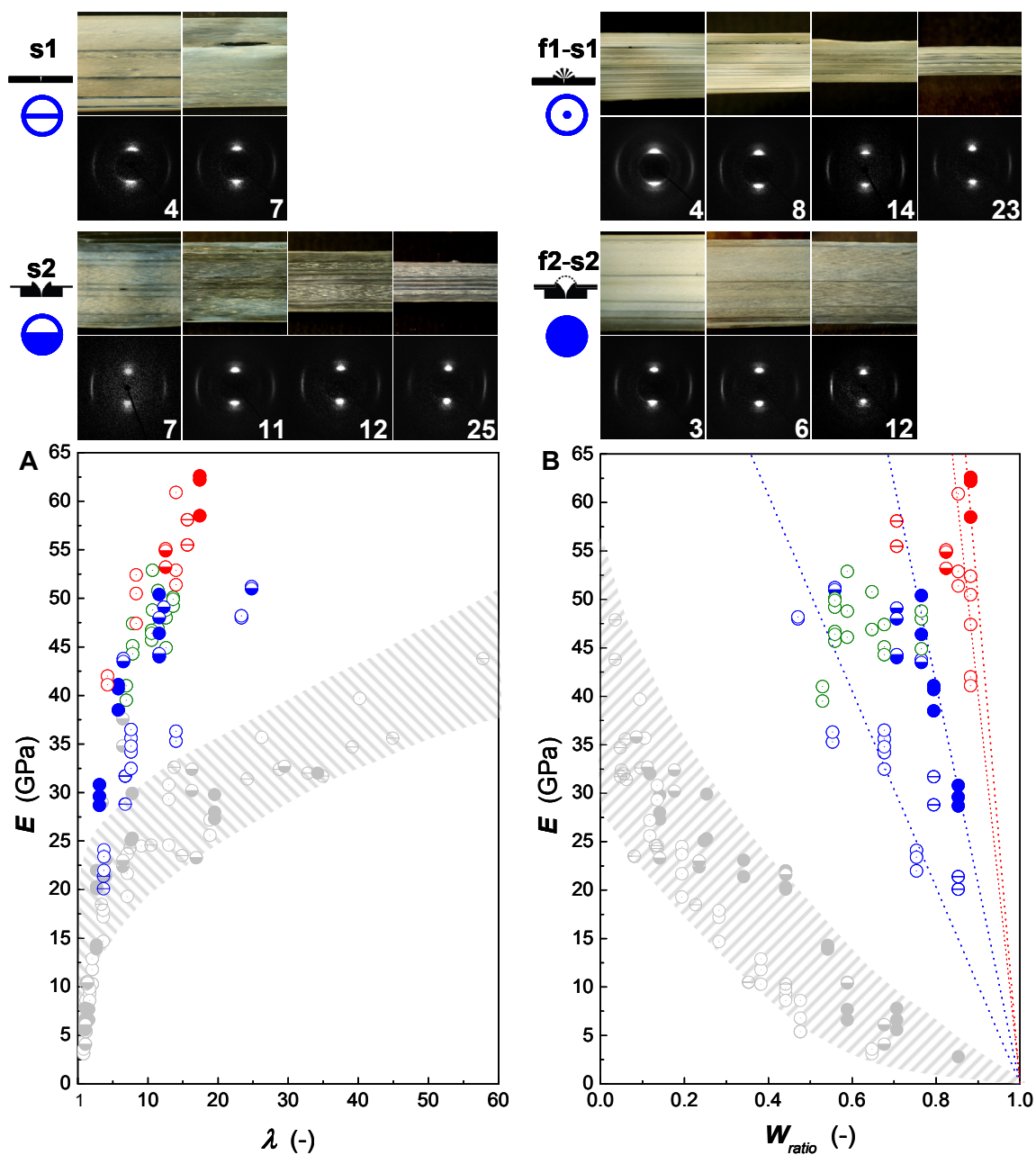
In view of the modest results presented in the previous section, subsequent efforts were directed to consolidation of the extrudate width by air-gap extrusion into a water bath at room temperature. Optimization of this process was initially carried out with the same discontinuous extrusion set-up as above and, subsequently, with the Teach-Line<sup>®</sup> continuous extrusion equipment.

Preliminary experiments were performed with die set **f1-s1**, aiming to obtain ultra-high-performance foils using high throughputs and maximum wind-up speeds. The extruder screw speed in the Teach-Line<sup>®</sup> was varied from 30 to 60 rpm, yielding a maximum throughput of 34 g/min; the winder take-up speed was varied between 50-150 m/min; and the air gap was 5 mm. Even at the higher throughput, foils of adequate mechanical properties were obtained with Young's moduli of ~50 GPa and tensile strengths of ~1 GPa (Table 4). The thickest foils produced in these experiments were 25  $\mu\text{m}$  thick and featured a modulus of 41 GPa and a tensile strength of 0.9 GPa.

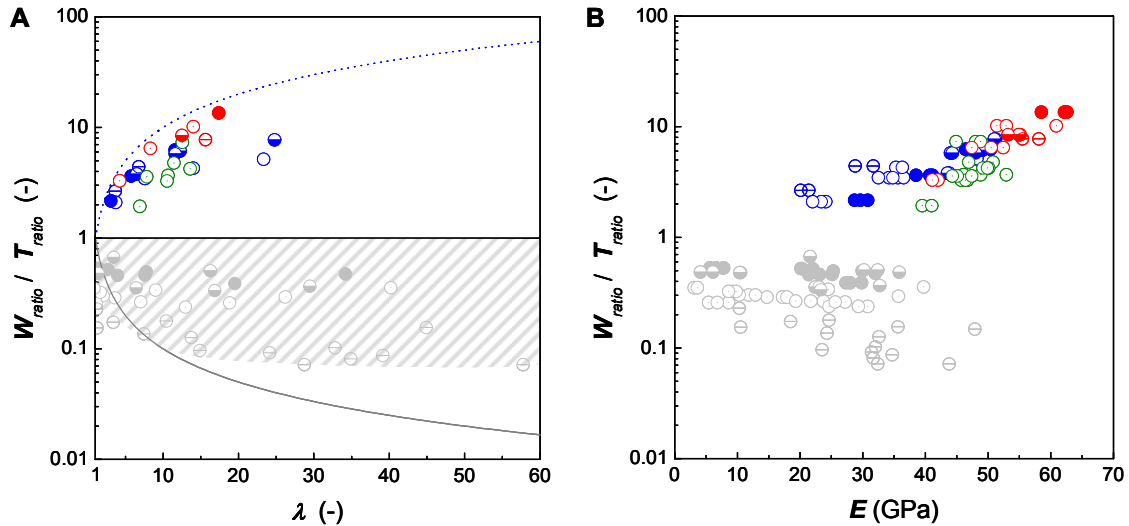
**TABLE 4** Mechanical properties of foils extruded with die set **f1-s1** and an air-gap of 5 mm. Also listed are the extruder  $v_{\text{extruder}}$  and winder  $v_{\text{winder}}$  speed, extruder throughput, resulting foil width,  $w$ , and thickness,  $d$ .

$v_{\text{extruder}}$ rpm	throughput g/min	$v_{\text{winder}}$ m/min	$w$ mm	$d$ $\mu\text{m}$	$\lambda$ -	$E$ GPa	$\sigma$ GPa	$\epsilon$ %
30	15	50	11.5	19	7.8	47	1.0	2.8
50	23	100	9.5	17	10.5	46	1.0	2.5
60	28	150	13	10	12.6	49	0.9	2.5
30	18	100	9.5	13	13.6	50	0.8	2.1
50	31	150	11	14	11.4	51	0.9	2.1
60	34	150	10	16	10.7	53	0.9	2.1

Employing die set **f2-s2**, screw rotation of 10 rpm, throughput of 8 g/min and an air gap of 2 mm yielded optimal results and permitted production of continuous, ultra-high-performance foils with thicknesses as little as 3  $\mu\text{m}$  and of excellent mechanical properties, achieved already at relatively low draw-down ratios (Figure 9), while largely preserving the product width (~90 %; Figure 10).



**FIGURE 9** Appearance and properties of foils produced by the *air-gap/water-quench-extrusion* process. Top: Reflected-light optical photographs and corresponding WAXD patterns of extrudates produced with reference slit-die **s1** ( $\ominus$  left, upper series); die set **f1-s1** ( $\odot$  right, upper series); slit die **s2** ( $\ominus$  left, lower series); and die set **f2-s2** ( $\bullet$  right, lower series). The width of the photographs represents 15 mm; draw-down ratios  $\lambda$  are indicated in lower right corners of the X-ray patterns. Extrusion direction and product axis are horizontal. Bottom: Enhanced development of the Young's modulus,  $E$ , with draw-down ratio  $\lambda$  (A) and width ratio,  $W_{ratio}$ , (B) of foils extruded using die set **f2-s2** ( $\bullet$ ) and slit die **s2** ( $\ominus$ ). Also plotted are data of foils formed with fusion die **f1-s1** ( $\odot$ ) and slit die **s1** ( $\ominus$ ). Young's moduli of extruded foils produced *without* water cooling are all within the gray-shaded area. Further are included characteristics of foils extruded using the Teach-Line<sup>®</sup> extruder with die **f1-s1** and air-gap 5 mm produced under different processing conditions, including the high throughputs that finally yielded line speeds in the order of 150 m/min ( $\odot$ ); with die **s2** ( $\ominus$ ) alone; and die set **f2-s2** ( $\bullet$ ) both at air-gap 2 mm. The modified extended slit die **s1e** ( $\ominus$ ) yielded foils of inferior properties, while in combination as **f1-s1e** ( $\odot$ ) reached nearly the values of **f2-s2**.



**FIGURE 10** A. Development of  $W_{ratio}/T_{ratio}$  with draw-down ratio,  $\lambda$ , in *air-gap/water-quench* extrusion illustrating close-to-ideal preservation of the product width in high-performance foil production. B. Plot of  $W_{ratio}/T_{ratio}$  vs. the Young's modulus  $E$ . Reference data of Figure 8 for samples produced by cooling in air are represented in the gray shaded area. For the meaning of symbols see Figure 9.

As a matter of fact, the data in Figure 9 reveal that the development of the Young's modulus with  $\lambda$  *nota bene* significantly surpassed that observed in fiber spinning (cf. Figure 1). The conspicuous *increase* in  $W_{ratio}/T_{ratio}$  with increasing draw-down ratio is consistent with a highly beneficial predominant reduction in extrudate thickness and little in width - not observed in the previous experiments without water quenching - allowing for large-scale production of ultra-high-performance foils indeed.

In terms of mechanical properties, slit die **s2** alone performed nearly as well as in combination with the upper part **f2**, but yielded foils of inferior homogeneity in thickness throughout their width.

From the above set of results one would be inclined to conclude that foils with better mechanical properties were obtained with die set **f2-s2**, but it has to be noted that - due to geometrical reasons - the smallest air gap possible for die **f1-s1** was 5 mm as opposed to 2 mm used with the former (see Figure 4). That difference is the likely cause of the more modest stiffness of foils produced with set-up **f1-s1**. Hence, a modified version of die **s1** was constructed that featured a slit depth extended by 3 mm (denoted **s1e**), which permitted to reduce the air gap to 2 mm. The data plotted in Figures 9 and 10 reveal that at the same air gap of 2 mm, the modified die set **f1-s1e**

yielded foils of nearly the same characteristics as those produced with the superior die set **f2-s2**. Extrusion with die **s1e** used alone resulted in inhomogeneous foils of inferior mechanical properties and increased splitting behavior.

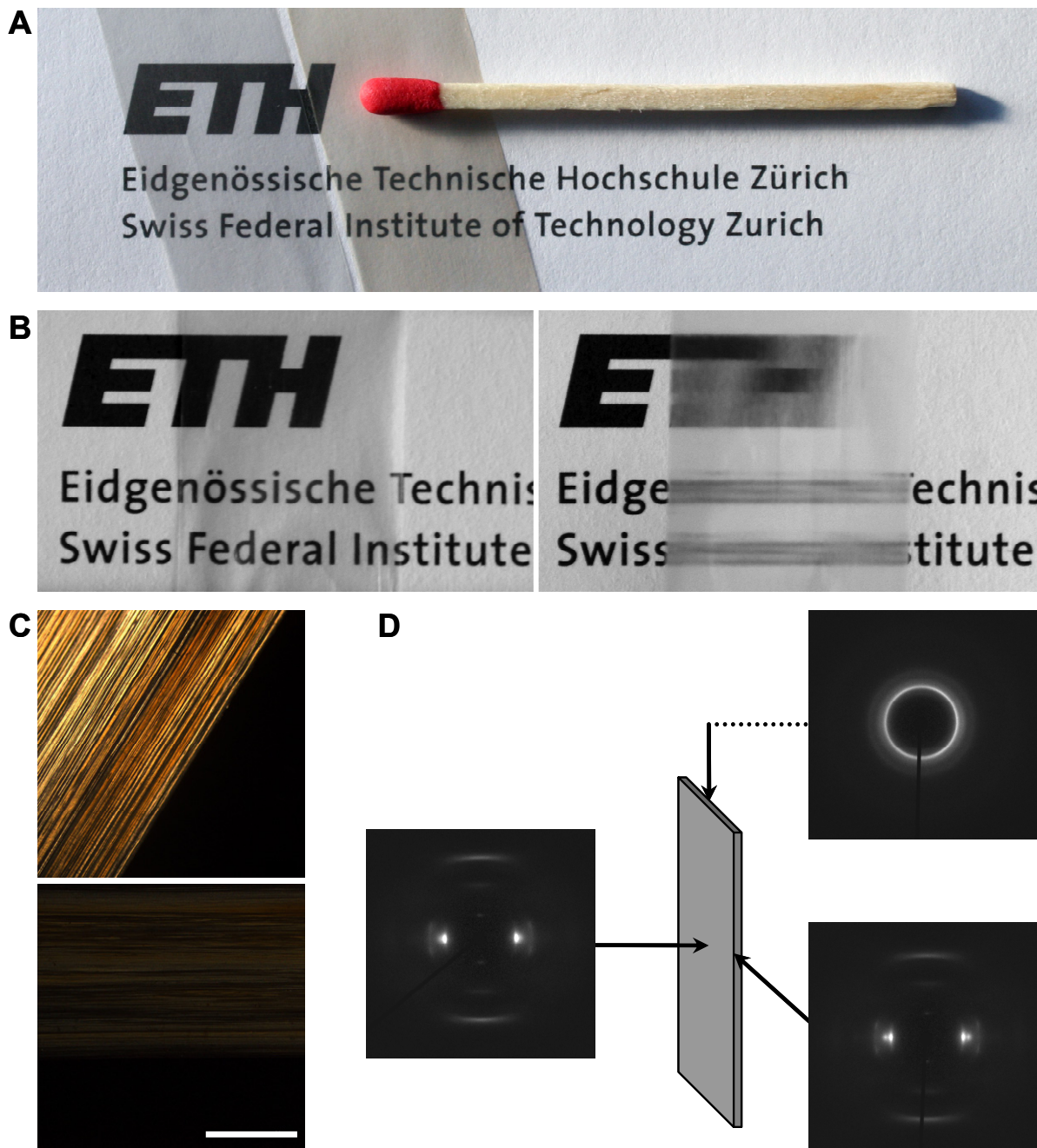
## 4.5 Heat Treatment

As already noted in the introduction, it is well known that treatment at elevated temperatures may enhance properties of as-spun, oriented fibers of the present aromatic polyester, due to post-condensation of the polymer.<sup>20,21</sup> Thus, also in this work, selected foils were post-processed in this fashion. More specifically, foils produced with the air-gap-extrusion process using the filament-fusion set up with die **f2-s2** were annealed for 17 h at a temperature of 260 °C, while subjected to a tensile stress of 3 MPa. The initially essentially transparent, colorless foil turned slightly golden and was of a glossy appearance (Figure 11A).

Table 5 lists selected mechanical and thermal properties, as well as the Hermans' orientation factor,  $f_h$ , of these samples, and those of the untreated foils, as well as data supplied by the producer. The data - not unexpectedly - show that the Young's modulus and tensile strength of the heat-treated foils improved considerably, approaching those of heat-treated filaments. In agreement with earlier reports, also the thermal properties of the samples were found to be markedly affected by the post-processing procedure applied. For instance, the peak melting temperature increased by no less than 20 °C and the enthalpy of fusion and, concomitantly, the degree of crystallinity by more than 300 %.

**TABLE 5** Effect of heat treatment on the Young's modulus  $E$ , tensile strength  $\sigma$ , melting temperature  $T_m$ , enthalpy of fusion  $\Delta H$ , degree of crystallinity  $\Phi_C$  and Hermans' orientation factor  $f_h$  of foils of a draw-down  $\lambda$ , stressed at 3 MPa at a temperature of 260 °C for 17 h. Foils I and II were produced with DACA<sup>®</sup> and Teach-Line<sup>®</sup> equipment, resp. , with die set **f2-s2**. For several samples two melting peaks were detected.  $\Phi_C$  was calculated with the heat of transition at equilibrium of 18.4 J/g according to reference 21.

sample	time h	$\lambda$ -	$E$ GPa	$\sigma$ GPa	$\varepsilon$ %	$T_m$ °C	$\Delta H$ J/g	$\Phi_C$ %	$f_h$ -
Vectra <sup>®</sup> A950	0	1	11	0.2	3.4	273	1.04	5.7	-
foil I	0	12	51	0.8	2.0	278 / 294	1.65	9.0	0.896
foil I heat treated	17	12	63	1.0	1.6	298	5.33	29.0	0.893
foil II	0	17	59	1.0	1.9	278 / 292	0.96	5.2	0.880
foil II heat treated	17	17	71	1.3	1.7	291 / 306	6.51	35.4	0.893



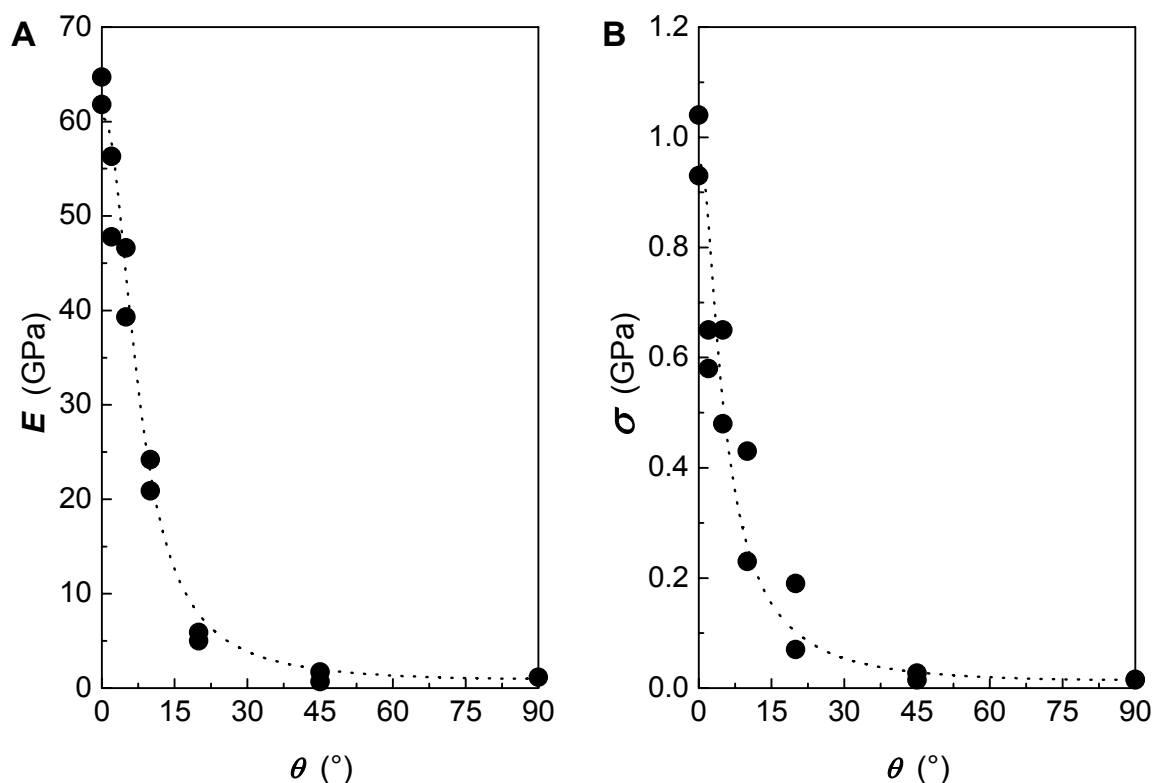
**FIGURE 11** A. Photographs of as-extruded foil II, Table 5 (left), and after heat-treatment (right) placed on letter head revealing their excellent transparency. The width of the foils is 15 mm. B. Foil II directly in contact with letterhead (left) and at a distance of 15 mm above it (right), displaying the highly anisotropic haze of the highly oriented foils. C. Optical micrographs taken between crossed polarizers at  $45^\circ$  (top) and  $90^\circ$  (bottom) with respect to the draw-down direction of foil II; scale bar is 0.5 mm. D. Typical WAXD patterns of a heat-treated foil II taken along the directions indicated, indicative of their fiber orientation; extrusion direction is vertical. To increase the scattering intensity, a sample of ten foils pressed together at  $200^\circ\text{C}$  during 5 min was exposed.

Interestingly, it was found that heat treatment of samples without loading showed an increase in enthalpy of fusion, but resulted in a lower melting temperature.

Photographs of the foils before and after the heat treatment are shown in Figure 11A, both revealing their excellent transparency. Interestingly, the highly-oriented foils also featured a most unusual, directional haze, see Figure 11B: upon increasing the distance between the foil and the text behind it, the latter remained well-defined along the orientation direction of the foil, while perpendicular to it the image became blurred.

Optical microscopy images of a heat-treated foil, taken between crossed polarizers, are presented in Figure 11C and, finally, wide-angle X-ray diffraction patterns of the sample taken from all the three directions are shown in Figure 11D. The latter show the excellent orientation of the macromolecular chains in the extrusion direction, but no evidence of orientation perpendicular to the plane was detected, contrary to that seen in ultra-drawn polyethylene foils (Chapter II). Also, it was found that heat treatment did not improve the degree of macromolecular orientation, consistent with the view that the enhanced mechanical properties are principally due to increased molecular weight and degree of crystallinity.

As already discussed in Chapter I, one well-known, major draw back of unidirectionally oriented polymer fibers - as well as foils - is the extreme dependence of their mechanical properties on the angle, with respect to the orientation direction, at which they are tested. This, of course, is also true for the present oriented foils of the thermotropic liquid-crystalline aromatic polyester investigated, as quantitatively illustrated in Figure 12.



**FIGURE 12** Test-angle,  $\theta$ , dependence of the Young's modulus,  $E$ , (A) and tensile strength,  $\sigma$ , (B) of an as-extruded foil II (Table 5). The dotted curves were calculated using the Tsai-Hill equations (see Chapter I).

## 4.6 Laminates

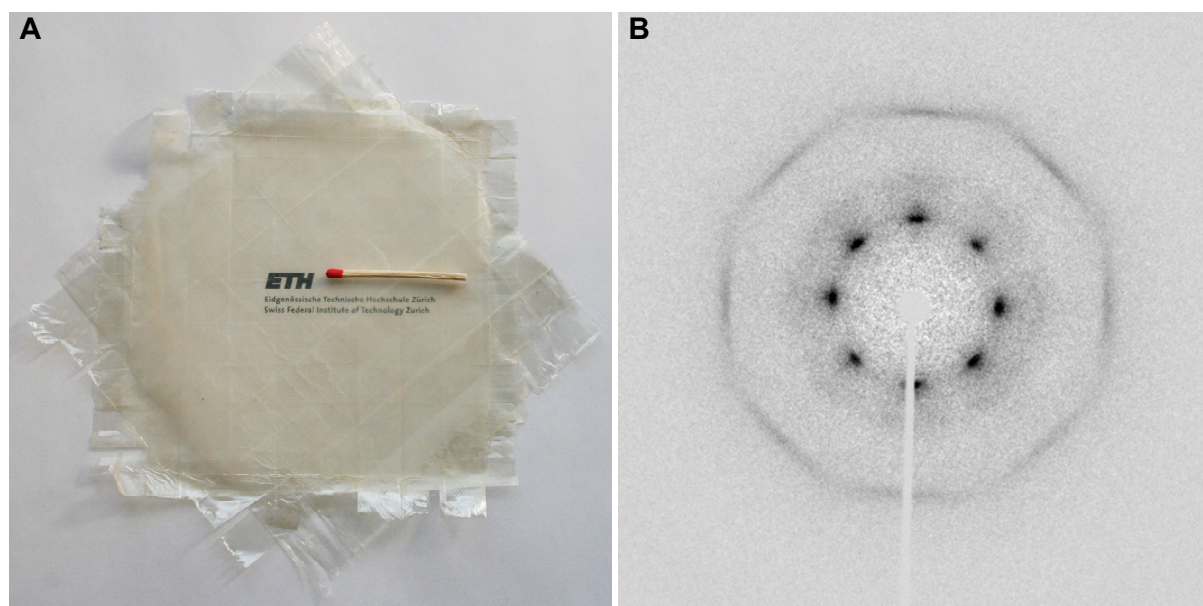
Subsequent efforts were directed towards development of foils of isotropic mechanical properties in their plane. As in the previous chapter concerning polyethylene, (quasi-) isotropic samples were produced by laminating uniaxially oriented foils according to similar protocols.

Thus, in first attempts, four layers of as-extruded foils were pressed without any additive at 200 °C and 450 Pa. Remarkably, it was not possible to press the unidirectionally oriented foils at angles of 45 ° into laminates as, invariably, fracture occurred. The foils adhered well together only at small angles, up to 5 °, between them. The origin of this phenomenon may be found in the surface texture or the rigidity of the constituent macromolecules. Nonetheless, multiple foils could be pressed by hot compaction at 0 ° or at small off-angles, resulting in relatively thick (0.2 mm) unidirectionally oriented sheets.

In view of the above results, the commonly applied route was followed, i.e. using hot-melt adhesives to bond the foils together. In a first step, 5 and 10 wt. % solutions of Bostik (USA) polyester HM7228 in dichloromethane were prepared. Next, the solutions were doctor-bladed on transfer paper and finally pressed onto the foils at 200 °C. Subsequently, the transfer paper was removed and the thus coated foils were pressed together at 200 °C and 450 Pa. Peeling of the “glued” foils resulted in pronounced pulling of fibrils out of them, which reveals that bonding to the adhesive was stronger than the intermolecular or interfibrillar forces in the extruded materials. Therefore, it was deemed to be unnecessary to improve their surface adhesion properties.

Four-ply [0/ 45/ 90/ 135] laminates were produced with a final thickness as thin as 18 µm, which still featured the remarkable transparency of the individual foils (Figure 13A). Wide angle X-ray diffraction patterns indicated that the highly oriented structure of the foils was well retained during the lamination process (Figure 13B).

The Vectra® A950 content in the laminates was determined by thermo-gravimetric analysis (TGA) to be, respectively, 95 wt. % and 78 wt. %, when solutions containing 5 wt. % and 10 wt. % of Bostik HM7228 were used to apply the adhesive coating.

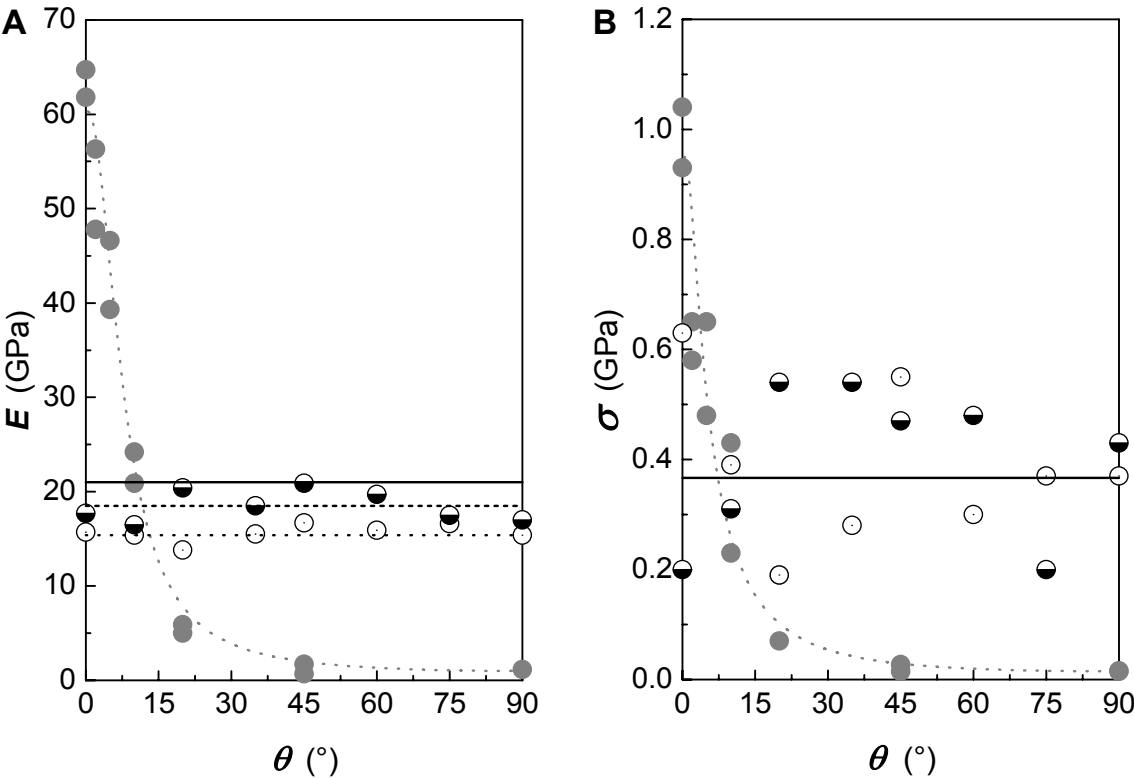


**FIGURE 13** **A.** Four-ply laminate on letter head illustrating its remarkable transparent appearance. The length of the match placed on top of the laminate is 50 mm. **B.** Wide angle X-ray diffraction pattern of the same sample, revealing that the highly oriented structure of the individual foils was retained during the lamination process.



Finally, the mechanical characteristics of the laminates were determined at room temperature in the standard tensile tests, and are shown in Figure 14. As expected, the stiffness and strength of the laminates obtained were well below the corresponding values of the uniaxially oriented foils, but surpassed those at test angles 45 ° and 90 ° by a factor of no less than 15. The “isotropic” Young’s modulus in the plane of the samples was found to be somewhat lower than the theoretically expected one of 23.7 GPa (1/3 of 63 GPa of the uniaxially oriented foil used in producing the laminates). However, it should be taken into account that the latter comprised 5 and 22 wt. % adhesive, leading to maximum expected values of, respectively, 22.5 GPa and 18.5 GPa, which are essentially the values that were recorded.

Surprisingly, most experimentally determined tensile strengths - despite the relatively large scatter - surpassed the expected values based on that of the unidirectionally oriented foil (Figure 14, right). This may be attributed to the clamping effects, which are, of course, more pronounced in “off-angle” testing a single foil than for a four-ply laminate.



**FIGURE 14** Young’s modulus,  $E$ , (A) and tensile strength,  $\sigma$ , (B) of balanced, four-ply laminated foils vs. test angle,  $\theta$ , comprising 95 wt. % (●) and 78 wt. % (○) Vectra® A950. For comparison, data of unidirectionally oriented foils are displayed in gray. Theoretical maxima calculated according to the Tsai-Hill equations (see Chapter I) are shown as a solid line.

## 5 Conclusions

In this work it was demonstrated that continuous, high-performance (uniaxially) oriented foils that are free of a skin-core structure and feature adequate resistance against fibrillation, can be produced of the thermotropic liquid-crystalline copolyester Vectra<sup>®</sup> A950 in a simple air-gap-extrusion process with the use of filament-forming/fusing dies. Further, it was shown that the rate of the development of the Young's modulus,  $E$ , with draw-down ratio,  $\lambda$ , of foils significantly surpassed that observed in *nota bene* fiber spinning. Most remarkably, foils as thin as 3  $\mu\text{m}$  were obtained with mechanical properties that approached those of commercially produced fibers, while preserving as much as 90 % of the width of the die, through which they were extruded.

Finally, it was demonstrated that the uniaxially oriented foils could be laminated with as little as 5 wt. % of an adhesive, yielding planar foils as thin as 18  $\mu\text{m}$  which were characterized by excellent, isotropic, in-plane specific mechanical properties, i.e. a Young's modulus  $E = 20 \text{ GPa}$  and a tensile strength  $\sigma = 0.5 \text{ GPa}$ ; true high-performance foils, indeed.

## 6 References and Notes

1. Kwolek, S. L. *FR Patent* 1,526,745 **1968**; *US Patent* 3,600,350 **1971**.
2. de Gennes, P. G. ; *C. R. Acad. Sci. (Paris) Ser. B* **1975**, 281, 101.
3. Jackson, W. J. ; Kuhfuss, H. F. *US Patent* 3,778,410 **1973**.
4. Jackson, W. J. ; Kuhfuss, H. F. *J. Polym. Sci. Polym. Chem.* **1976**, 14, 2043.
5. Muramatsu, H. ; Krigbaum, W. R. *Macromolecules* **1986**, 19, 2850.
6. Wissbrun, K. F. ; Griffin, A. C. *J. Polym. Sci. Polym. Phys.* **1982**, 20, 1835.
7. Monofilaments of Vectra A950 were produced at 300°C, followed by cooling in air with the SpinLine from DACA (Santa Barbara, USA). The spinneret had a diameter of 0.3 mm. Mechanical tests were performed at constant cross-head speed of 30 mm/min using an Instron tensile tester 4411. Gauge length was 300 mm. Cross-sectional area of the monofilaments was calculated from the weight using a density of 1.40 g/cm<sup>3</sup>.
8. Luise, R. R. *US Patent* 4,247,514 **1981**.
9. Warner, S. B. ; Lee, J. *J. Polym. Sci. Polym. Phys.* **1994**, 32, 1759.
10. Calundann, G. W. ; Jaffe, M. Proceedings of the Robert A. Welch Conference on Chemical Research, *XXVI. Synthetic Polymers* **1982**, 280.
11. Ide, Y. *US patent* 4,332,759 **1982**.
12. Ide, Y. ; Buckley, A. *US patent* 4,384,016 **1983**.
13. Ide, Y. ; Chung, T. S. *J. Macromol. Sci. Phys.* **1985**, B23, 497.
14. Lusignea, R. W. *Polym. Eng. Sci.* **1999**, 39, 2326.
15. Sawyer, L. C. ; Jaffe, M. *J. Mater. Sci.* **1986**, 21, 1897.
16. Crevecoeur, G. ; Groeninckx, G. *Polym. Eng. Sci.* **1993**, 33, 937.
17. Crevecoeur, G. ; Groeninckx, G. *Polym. Eng. Sci.* **1990**, 30, 532.
18. Product information; [www.ticona.com](http://www.ticona.com) **2006**.
19. Meier, M. *SPE ANTEC* **1989**, 200.
20. Cheng, S. Z. D. *Macromolecules* **1988**, 21, 2475.
21. Chung, T. S. ; Cheng, M. ; Goh, S. H. ; Jaffe, M. ; Calundann, G. W. *J. Appl. Polym. Sci.* **1999**, 72, 1139.



# IV

*Lyotropic Liquid-Crystalline Aramid*



# 1 Introduction

It was already discussed in Chapter III that remarkably few successful efforts to produce foils of thermotropic liquid-crystalline polymers have been reported; this is also true for lyotropic species. An overview of selected mechanical properties known for different foils of such materials is listed in Table 1, which demonstrates that they are considerably inferior to their corresponding fibers indeed (cf. Chapter I).

In attempts to form foils of poly(*p*-phenylene terephthalamide) (PPTA), lyotropic solutions were extruded through annular and slit-dies by Fellers *et al.*, resulting in ribbons of poor mechanical properties.<sup>1-3</sup> Disappointing results have been reported also for extruded tapes of poly(*p*-phenylene benzobisoxazole) (PBO) and poly(*p*-phenylene benzobisthiazole) (PBT), which featured only about 10 % or less of the mechanical properties of filaments of the same material.<sup>4-7</sup>

Nonetheless, a few authors described some successful developments. For instance, PBT was extruded into uniaxially oriented, but narrow and readily fibrillating tapes with properties approaching those of fibers.<sup>8,9</sup> Additionally, Lusignea describes PBT films with a Young's modulus of up to 270 GPa, however, most regrettably without providing information about the processing parameters employed and the dimensions of the resulting films.<sup>10</sup> Finally, a 10-year research program at Celanese devoted to processing PBT, unfortunately, resulted in the production of wrinkled foils of a maximum width of 15 mm only.<sup>11</sup>

Among the causes for the relatively few successful efforts are the lack of efficient orientation-inducing foil-forming dies and difficulties encountered in coagulation of lyotropic liquid-crystalline polymers, which are processed from solutions in strong acids, typically comprising only 20 % or less of the polymer, often resulting in the formation of creased and porous structures.

Attempts have been made to circumvent the above issues by forming biaxially oriented foils instead of uniaxially ordered products. Presently, such foils from *p*-aramids are commercially produced by DuPont Teijin Films (Aramica<sup>®</sup>) for use by the electronics industry as insulating foils and in printed circuit boards.<sup>12</sup> These films feature a Young's modulus of 15 GPa and a tensile strength of about 0.4 GPa (cf. Chapter I). Also, production of biaxially oriented foils of PBT using counter-rotating dies is

described.<sup>13</sup> However, obviously and as already noted in the introduction to this thesis, their mechanical characteristics are but a fraction of those of their fiber counterparts.

**TABLE 1** Young's modulus,  $E$ , tensile strength,  $\sigma$ , and elongation at break,  $\epsilon$ , of selected unidirectional foils/tapes of lyotropic polymers described in the literature. Subscripts  $ae$  and  $ht$  refer to as-extruded and heat-treated, respectively. Where known, indicated are the die breadth  $b^*$  and height  $h^*$  and film/tape width  $w$  and thickness  $d$ . ABPBI refers to poly(2,5(6<sup>2</sup>)-benzimidazole).

material	method	$E_{ae}$ GPa	$E_{ht}$ GPa	$\sigma_{ae}$ GPa	$\sigma_{ht}$ GPa	$\epsilon_{ae}$ %	$\epsilon_{ht}$ %	$b^*$ mm	$w$ mm	$h^*$ mm	$d$ $\mu\text{m}$	ref.
PPTA	uniaxial annular	0.6	1.6	0.03	0.05	12.0	8.0	0.8-6.0	-	0.2	-	1
PPTA	uniaxial annular	4.5	-	0.23	-	7	7.0	-	-	-	-	3
PPTA	uniaxial annular	8.3	-	0.25	-	-	-	-	-	0.03-0.2	-	2
PPTA	biaxial	-	15	-	0.40	-	20.0	-	-	-	4-16	12
PBO	slit die	7.6	-	0.10	-	0.8	-	6	3	0.25	50	4
PBT <sub>0.3</sub> / ABPBI <sub>0.7</sub>	coat- hanger die	30	88	0.69	0.92	5.5	2.4	-	-	-	-	7
PBT	slit roll	96	135	1.30	2.29	3.3	1.8	12.7	4.5	0.2	70	14
PBT	mandrel	96	-	1.10	-	1.1	-	160	4.5	0.2	3-9	15
PBT	slit extrusion	132	238	1.23	1.51	2.5	1.0	-	4-9	-	5-10	8
PBT	unknown	207	270	2.00	-	0.9	-	-	-	-	-	10

Clearly, the data presented in Table 1 display - as found for thermotropic liquid-crystalline polyesters - that heat treatment of processed foils and tapes of these lyotropic polymers increases their Young's modulus as well as tensile strength.<sup>16</sup>

In the present chapter, in an initial proof-of-principle attempt, the route of foil formation described in the Chapter III for the thermotropic, semi-rigid copolyester Vectra<sup>®</sup>, will be adapted to process the lyotropic, rigid-chain PPTA. As indicated in Chapter I, a major challenge resides here in the fact that this polymer decomposes prior to melting, and, hence, is spun into fibers from solutions containing ~80 % sulphuric acid into a water coagulation bath, requiring, among other things, equipment that is resistant to corrosion.<sup>17</sup>



## 2 Experimental

**Materials.** The polymer used was a relatively high-molecular weight poly(*p*-phenylene terephthalamide) (PPTA) (courtesy Dr. V. Gabara, E. I. du Pont de Nemours & Co., USA, inherent viscosity 7.8 dl/g). The solvent was 98 % sulfuric acid (Aldrich).

Prior to use, the polymer was dried overnight at 100 °C in a vacuum oven. A quantity of 5 g of polymer was dissolved in 15 ml sulfuric acid at 80 °C resulting in a 16 wt. % solution. Dissolution was carried out using a glass-walled, stainless steel double-helix mixing device (courtesy Dr. D. J. Sikkema, then of AKZO Nobel) under argon atmosphere during 6 h. The resulting “dope” thus obtained was quenched in liquid nitrogen and stored in the frozen state.

**Processing.** Extrusion was executed at 90 °C with a laboratory-scale, piston-driven device (SpinLine<sup>®</sup>, DACA Instruments, Santa Barbara, USA). Schematics of the extrusion apparatus are shown in the previous chapter. The “filament-fusing” die set, there denoted **f2-s2**, was used. Unless otherwise indicated, the extrusion speed was 25 mm/min, corresponding to a throughput of 11 g/min. The extrudate was coagulated in a water bath at room temperature. Naturally, the all-important air-gap distance was varied. The take-up speed was approximately 20 m/min, and was performed manually (see below, Figure 1).

**Mechanical analysis.** Tensile properties were determined employing an Instron tensile tester 5864 (Norwood, USA). The gauge length was 30 mm and the crosshead speed 3 mm/min. The cross-sectional areas of the test specimens were calculated from the weight of each sample using a density of 1.44 g/cm<sup>3</sup> (determined with Ultracycrometer 1000 (Quantachrome, USA)). In addition to tests along the extrusion direction, the properties of the foils produced were examined in tension also at angles different from the axis of extrusion. In the latter tests, the specimen width was about 2 mm and the gauge length at least 8 mm. Clamps were mounted in a rigid fashion to avoid perpendicular shifting along the draw direction during testing. Values presented here are the average of at least three tensile tests, or the maximum where indicated.

Dynamical mechanical thermal analysis (DMTA) was performed with a Mettler DMA861e (Greifensee, Switzerland) instrument. Isothermal scans of unidirectionally oriented foils were measured at 10 Hz in the temperature range from 100 to 370 °C, as

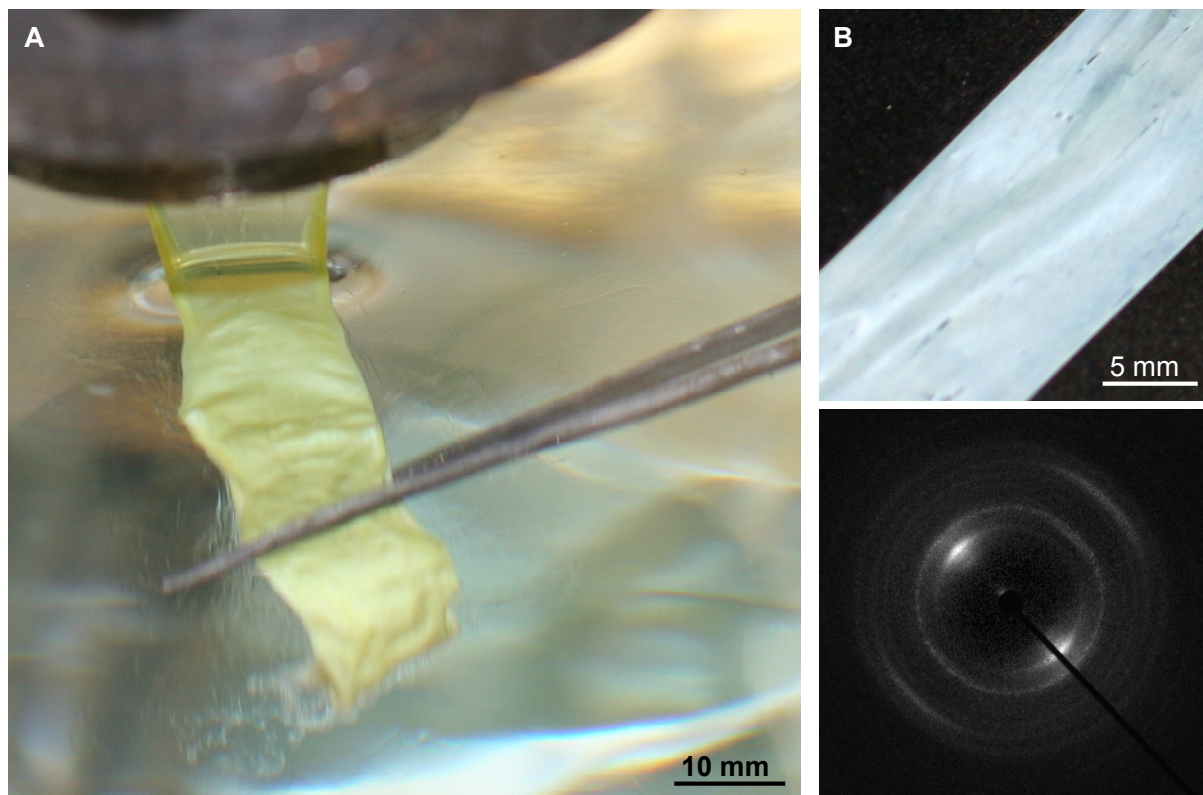
well as at room temperature.

***X-ray analysis.*** Wide-angle X-ray diffraction (WAXD) patterns were recorded with an Onyx CCD detector at a distance of 65 mm, mounted on a Oxford Diffraction Xcalibur XP instrument (Abingdon, UK) using a Mo-K $\alpha$  source ( $\lambda = 0.7093 \text{ \AA}$ ) operated at -50 kV / 40 mA. Hermans' orientation factors,  $f_h$ , and average orientation angles were derived from the half-width at half-maximum intensity of the third equatorial reflection.

## 3 Results and Discussion

### 3.1 Foil Extrusion

Due to the limited amount of polymer available and the required relatively high throughput of the PPTA solution, it was not feasible with the equipment available to take up the foil continuously with a winder, and, hence, the extrudate was withdrawn manually with tweezers into the coagulation bath (Figure 1A). With this highly-improvised technique, light-yellow foils with an opaque appearance of a typical width of 12 mm were readily obtained (Figure 1B). It was found that the optical appearance (as well as other properties) of the foils improved as the air gap was reduced; the smallest gap employed was  $\sim 1$  mm. WAXD patterns of the as-produced *wet* samples indicated already a pronounced degree of orientation of the PPTA macromolecules along the extrusion direction. It has to be noted that the foils featured imperfections, such as voids from residual solvent. Remarkably, the as-produced samples were not prone to fibrillation or splitting.



**FIGURE 1** A. Commencing air-gap extrusion into a water coagulation bath of a 16 wt. % PPTA solution; draw down was applied manually. B. Photograph of the resulting wet, as-extruded foil of a width of 12 mm (top) and corresponding WAXD pattern of the wet product (bottom).

The as-produced foils were, subsequently, washed with water for a period of at least 4 h, until that waste water contained no more acid. Following that washing step, the foils were dried at 120 °C over night whilst being kept at constant length, which caused their color to turn to a brighter yellow and, most interestingly, to become highly transparent (Figure 2, top). During the drying procedure the width of the foils decreased by approximately 30 % of that of the initial, as-extruded samples. Typically, dried specimens had a thickness of 10  $\mu\text{m}$  and a width of 8 mm.

A scanning electron micrograph of an as-extruded, dried foil that was deliberately partly spliced at room temperature is presented in Figure 2, bottom. A multitude of fibrillar connections can be discerned in this image, indicative of the ability of the foils to sustain loads perpendicular to the extrusion direction.

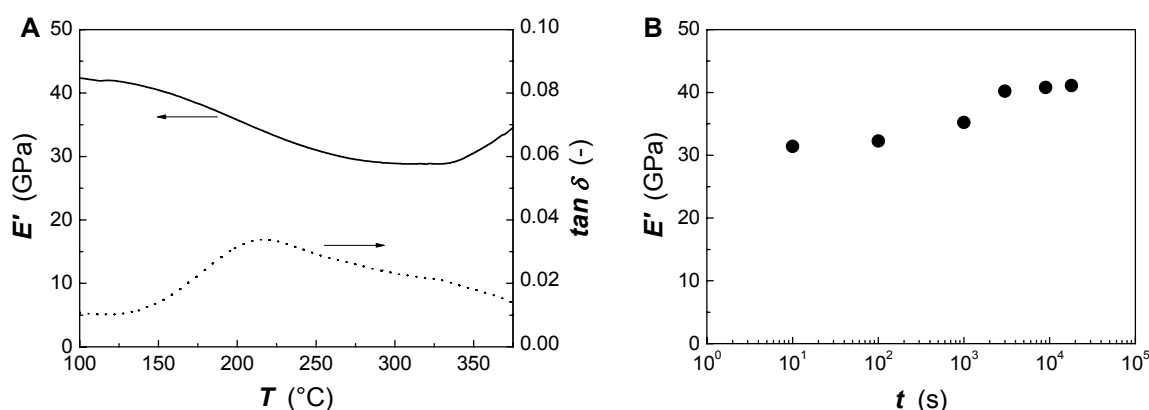


**FIGURE 2** A. Optical photograph of a dried PPTA foil placed on top of letter head, illustrating its transparency. The width of the foil is 8 mm. B. Scanning electron micrograph of an as-extruded, dried foil that was spliced longitudinally.

## 3.2 Heat Treatment

As already demonstrated by the data in Table 1, it is a well-established fact that treatment at elevated temperatures enhances the mechanical properties of freshly-coagulated PPTA,<sup>16, 18</sup> and was, hence, also applied to the present air-gap-extruded foils.

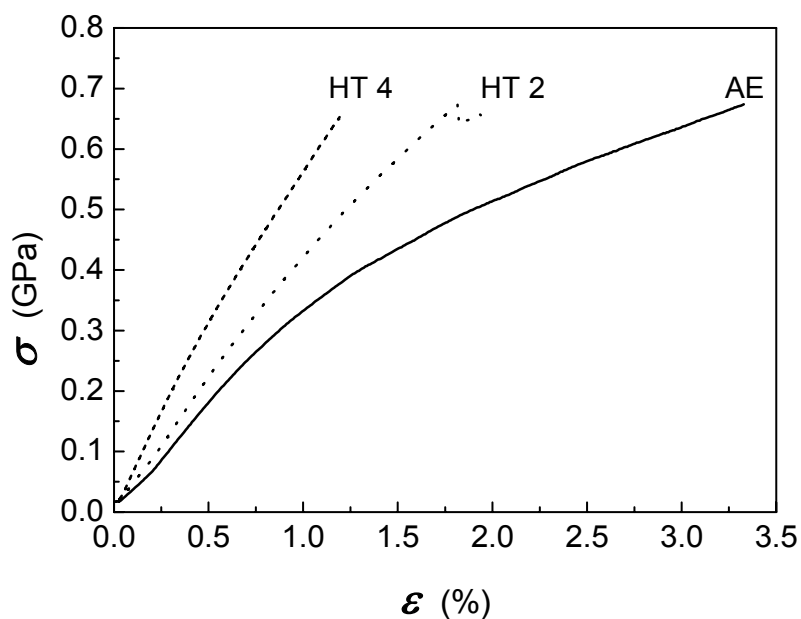
Preliminary tests were conducted to determine the optimal heat-treatment temperature regime. For this purpose, dynamical mechanical thermal analysis (DMTA) was performed with dried PPTA foils. A typical result is shown in Figure 3A, which features a scan that reveals a transition around 200 °C, where the damping - expressed as the loss factor,  $\tan \delta$  - displayed a maximum. Furthermore, an increase in the storage modulus,  $E'$ , was noted above 330 °C. This observation indicates that above that temperature improvement of mechanical properties occurred, and, therefore, heat treatment was conducted in that region.



**FIGURE 3** A. Dynamical mechanical thermal analysis of an as-extruded, dried PPTA foil at a frequency of 10 Hz. Storage modulus,  $E'$ , and loss factor,  $\tan \delta$ , are plotted vs. temperature. B. Storage modulus,  $E'$ , (also determined at 10 Hz at room temperature) vs. heat-treatment time at 350 °C of PPTA foils produced *without* applied strain.

Thus, a set of samples was heat treated, initially *without* applying strain, for different periods of time at 350 °C, and subsequently subjected to DMTA in isothermal mode at room temperature. The data in Figure 3B reveal that treatment during 50 min resulted in an increase of 30 % of the storage modulus, but that longer periods of time did not lead to significant further enhancement.

Finally, the as-extruded, dried foils were heat treated under constant load of 35 MPa at 350 °C under argon flow for two different time periods, i.e. 2 and 4 h (denoted, respectively, HT 2 and HT 4) and their mechanical properties analyzed in tensile tests. Typical stress-strain curves of the foils produced are presented in Figure 4, and representative values of the Young's modulus, tensile strength and elongation at break in Table 2.



**FIGURE 4** Stress-strain curves of selected as-extruded, dried, AE (—) PPTA foils, and of samples heat treated at 350 °C under a load of 35 MPa for 2 h, HT 2 (···), and 4 h, HT 4 (---).

**TABLE 2** Heat-treatment time,  $t$ , averaged values of the Young's modulus,  $E$ , tensile strength,  $\sigma$ , and elongation at break,  $\epsilon$ , of as-extruded (AE) and heat-treated (HT) PPTA foils under a load of 35 MPa, average orientation angles,  $\delta$  and Hermans' orientation factors,  $f_h$ , calculated from the (006) reflections in the corresponding WAXD patterns.

sample	$t$ h	$E$ GPa	$\sigma$ GPa	$\epsilon$ %	$\delta$ °	$f_h$ -
AE	0	$44 \pm 4$	$0.7 \pm 0.1$	$3.3 \pm 0.7$	9.0	0.86
HT 2	2	$51 \pm 8$	$0.7 \pm 0.1$	$1.9 \pm 0.1$	8.4	0.88
HT 4	4	$63 \pm 5$	$0.6 \pm 0.1$	$1.1 \pm 0.1$	8.0	0.89

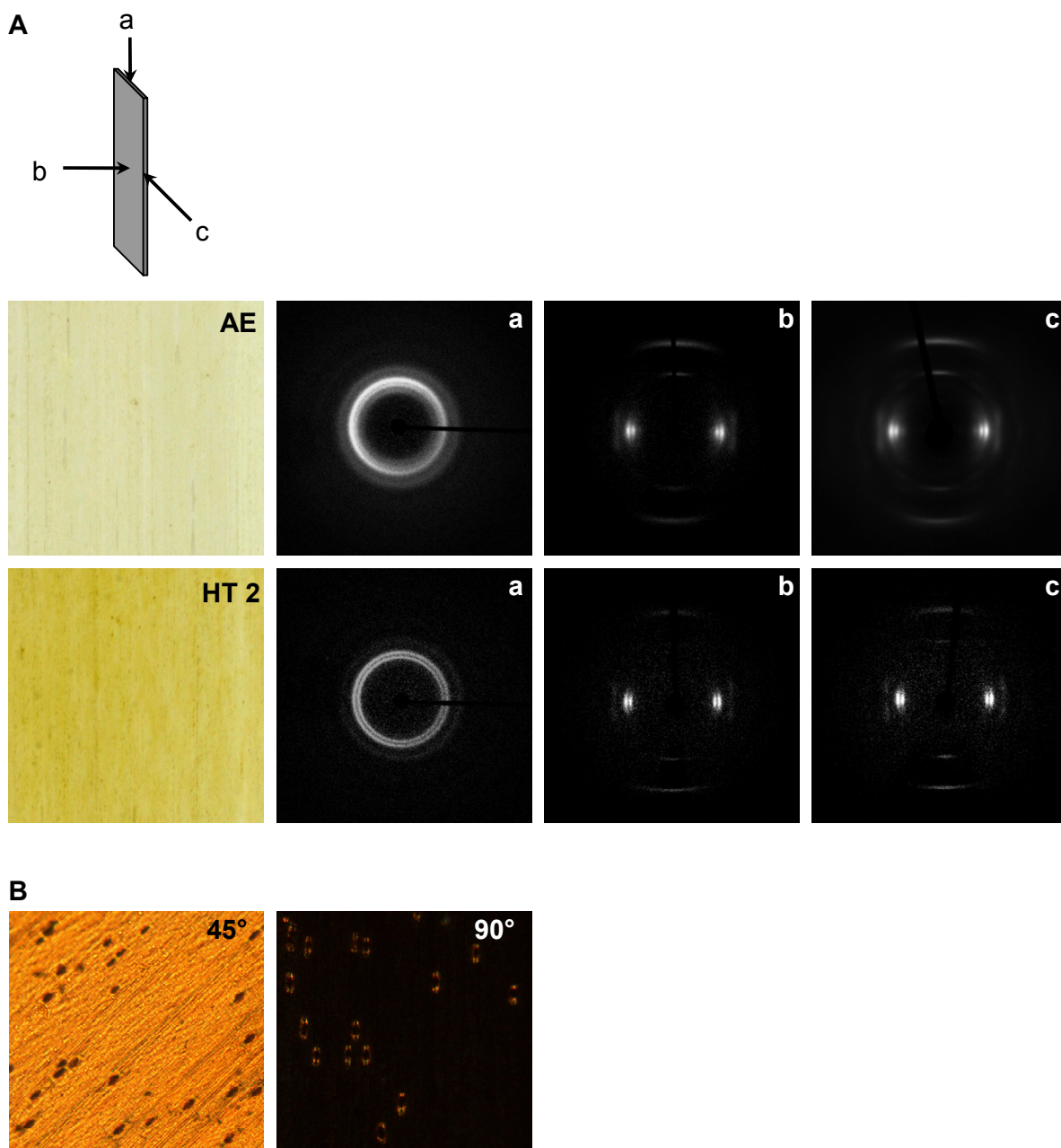
Expectedly, the Young's modulus of the samples increased, from about 44 GPa found for the as-extruded foils, to values exceeding 60 GPa. Unfortunately, a slight reduction was observed in values of the tensile strength, which is attributed to the excessively long heat-treatment time (which was conducted in a simple oven flushed with argon). The latter is likely to result in thermal degradation, as indicated by the color change. This, perhaps, could be overcome by shorter heat-treatment times, together with increased applied strain.

The increase of the stiffness of the PPTA foils, resulting from the heat treatment, naturally, was due to improved ordering of the constituting macromolecules, as indeed detected by wide-angle X-ray diffraction (cf. Figure 5). As commonly observed, the equatorial  $\langle 006 \rangle$  reflection sharpened and the calculated Hermans' orientation factor increased, as the half-width at half-maximum intensities of the radial intensity scans decreased. Clearly, the WAXD patterns in Figure 5 indicate that there is no in-plane alignment of the macromolecules in the foils, as also failed to occur for the thermotropic polyester in the previous chapter. More likely, the foils feature a radially arranged (fiber-orientation) structure, as advanced by Dobb *et al.* .<sup>19</sup>

Figure 5 further reveals the highly uniaxially oriented character of the PPTA foils in optical micrographs, taken between crossed polarizer, but also shows the presence of remaining pores, likely due to the removal of the sulfuric acid during coagulation.

### 3.3 Test-angle Dependence

It appears that in this work the first uniaxially oriented PPTA foils of sufficient width were produced that enable determination of the test-angle dependence of their mechanical properties and, therewith, permit a comparison with the theoretical trends presented in Chapter I.

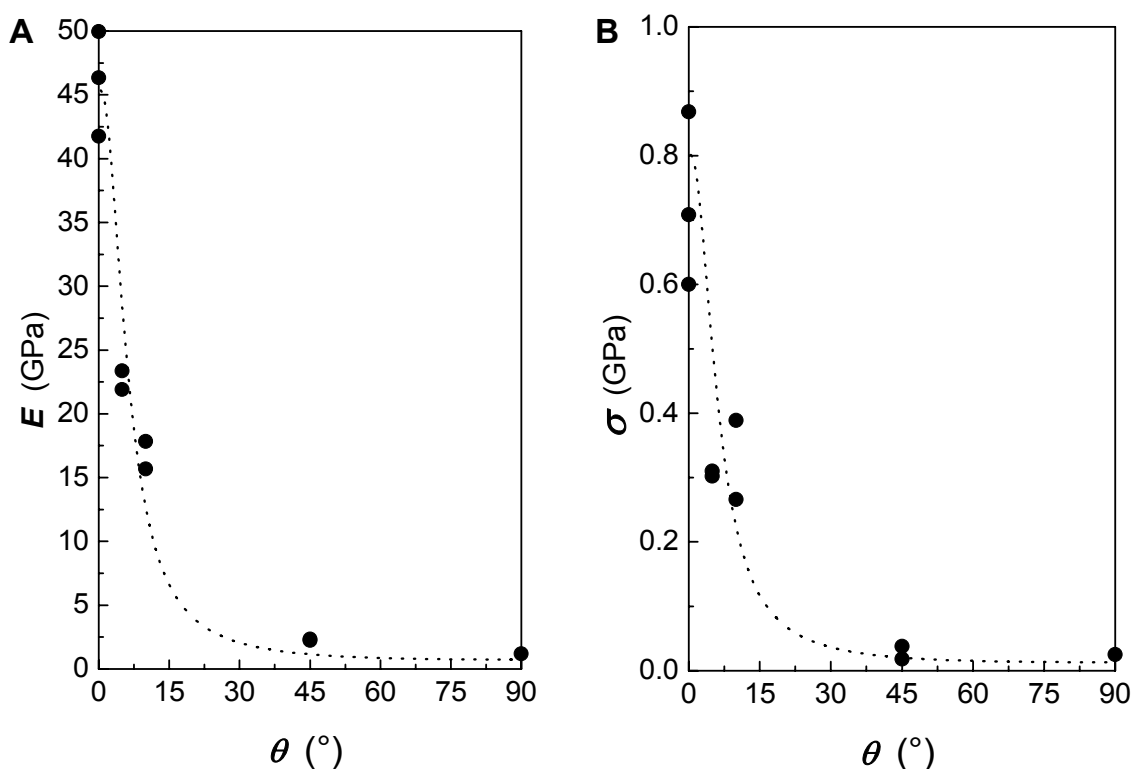


**FIGURE 5** A. Optical appearance (photograph width 1.5 mm) and wide-angle X-ray diffraction (WAXD) patterns of as-extruded (AE) and 2 h heat-treated (HT 2) PPTA foils. WAXD patterns were recorded along the three directions indicated in the top-left panel: extrusion direction, a; and perpendicular, b; and parallel to the foil plane, c. B. Polarized-light micrographs of a heat-treated PPTA foil HT 2 at angles indicated at the upper right corner, demonstrating their pronounced birefringence. The width of these images corresponds to 0.5 mm.

The results of tensile tests, conducted at various angles with respect to the extrusion direction, of as-extruded, dried PPTA foils are shown in Figure 6. Values of the Young's modulus were found to decrease from 44 GPa and a tensile strength of 0.7 GPa parallel to the air-gap-extrusion direction to as low as, resp. , 2.3 GPa and 0.038 GPa, and 1.2 GPa and 0.025 GPa at 45 ° and 90 ° to it. Gratifyingly, however,



the experimentally observed angular dependence of the Young's modulus is of the same nature as that of the theoretical curve presented in Chapter I. The present dependence can be fitted to that of a transversely isotropic material with a longitudinal modulus  $E_l = 44$  GPa, a transverse modulus  $E_t = 1.2$  GPa, a shear modulus  $G_{lt} = 1.1$  GPa and a Poisson's ratio,  $\nu_{lt}$ , of 0.4. Analogously, the angular dependence of the tensile strength of the PPTA foil fits well to that of a transversely isotropic material as discussed in Section I. 2.1. Comparison of these modulus values with the maximum attainable moduli mentioned in Chapter I shows, of course, that the present foils were yet not fully oriented, which could be further optimized. Finally, it should be noted, that due to the limited amount of polymer available, no attempts could be made to produce meaningful, balanced, planar laminates as presented in the previous Chapters II and III.



**FIGURE 6** Test-angle dependence of the Young's modulus,  $E$ , (A) and tensile strength,  $\sigma$ , (B) of as-extruded, dried PPTA foils. Dotted curves calculated according to Eq. 1 and 3 in Chapter I, assuming a Poisson's ratio of 0.4.

## 4 Conclusions

Non-fibrillating, transparent PPTA foils possessing a relatively high maximum modulus (50 GPa) and tensile strength ( $\sim 0.9$  GPa) were produced with a simple air-gap-extrusion process employing a novel filament-fusing die. Reduction of the air gap was found to be a most effective way to promote the formation of oriented, thin foils. In contrast to results reported by Aoki *et al.*,<sup>1</sup> little difficulties were encountered in maintaining the rectangular cross-section of the extrudate, i.e. it readily retained the intended foil shape, by executing air-gap extrusion with the present die set. Upon heat treatment, an increase of macromolecular orientation in the extrusion direction was detected by X-ray analysis, resulting in an increase of the maximum Young's modulus to 67 GPa, however, accompanied by a slight reduction of the tensile strength due to thermal decomposition.

Clearly, there is ample room for optimization of the presented air-gap-extrusion process and improvement of the properties of the foils produced therewith, such as developing a continuous process, enhancing heat treatment, etc. . Nonetheless, part of the objective of this work was achieved in that the concept of coherent foil extrusion was adapted and also found to be useful for lyotropic liquid-crystalline polymers. And, for the first time, the full test-angle dependence of the mechanical properties of oriented PPTA is reported.

## 5 References

1. Aoki, H. ; Onogi, Y. ; White, J. L. ; Fellers, J. F. *Polym. Eng. Sci.* **1980**, 20, 221.
2. Flood, J. E. ; White, J. L. ; Fellers, J. F. *J. Appl. Polym. Sci.* **1982**, 27, 2965.
3. Bodaghi, H. ; Kitao, T. ; Flood, J. E. ; Fellers, J. F. ; White, J. L. *Polym. Eng. Sci.* **1984**, 24, 242.
4. Choe, E. W. ; Kim, S. N. *Macromolecules* **1981**, 14, 920.
5. Minter, J. R. ; Shimamura, K. ; Thomas, E. L. *J. Mater. Sci.* **1981**, 16, 3303.
6. Hwang, W. F. ; Wiff, D. R. ; Benner, C. L. ; Helminiak, T. E. *J. Macromol. Sci.-Phys.* **1983**, B22, 231.
7. Hwang, W. F. ; Wiff, D. R. ; Verschoore, C. ; Price, G. E. ; Helminiak, T. E. ; Adams, W. W. *Polym. Eng. Sci.* **1983**, 23, 784.
8. Feldman, L. ; Farris, R. J. ; Thomas, E. L. *J. Mater. Sci.* **1985**, 20, 2719.
9. Feldman, L. ; Zihlif, A. M. ; Farris, R. J. ; Thomas, E. L. *J. Mater. Sci.* **1987**, 22, 1199.
10. Lusignea, R. W. *Mat. Res. Soc. Symp. Proc.* **1989**, 134, 265.
11. Chenevey, E. C. ; Timmons, W. D. *Mat. Res. Soc. Symp. Proc.* **1989**, 134, 245.
12. Product information; Aramica<sup>®</sup> PPTA Film, [www.teijin.co.jp](http://www.teijin.co.jp) **2006**.
13. Baars, D. M. ; Bretches, D. D. ; Davis, R. B. ; Harvey, A. C. ; Lusignea, R. W. *US Patent* 6,132,668 **2000**.
14. Chenevey, E. C. ; Kafchinski, R. *US patents* 4,487,735 **1984**; 4,606,875 **1986**.
15. Chenevey, E. C. ; Kafchinski, R. *US patent* 4,898,924 **1990**.
16. Lee, K. G. ; Barton, R. ; Schultz, J. M. *J. Polym. Sci. Polym. Phys.* **1995**, 33, 1.
17. Blades, H. *US Patents* 3,767,756 **1973**; 3,869,429 **1975**.
18. Pottick, L. A. ; Farris, R. J. *Polym. Eng. Sci.* **1985**, 25, 284.
19. Dobb, M. G. ; Johnson, D. J. ; Saville, B. P. J. *Polym. Sci. Polym. Phys.* **1977**, 15, 2201.



V

*Bacterial Cellulose*



# 1 Introduction

Cellulose is the main cell component of plants and trees and provides them their structural integrity. Its theoretical uniaxial Young's modulus is calculated to be 120 GPa.<sup>1</sup> However, when incorporating intramolecular hydrogen bonds into the calculations, a value as high as 170 GPa along the chain direction has been advanced.<sup>2</sup> For certain natural fibers a maximum stiffness of 90 GPa has been reported.<sup>1</sup>

Interestingly, highly oriented structures of cellulose are produced by bacteria in the form of fibrillar ribbons of diameters less than about 0.1  $\mu\text{m}$ , which appear as a coherent gel at the surface of a sugar-based nutrient medium in a static culture.<sup>3</sup> Such bacterial cultures were used in Europe for home-making of vinegar, and still today, for example, for the production of *nata de coco* dessert in the Philippines and Indonesia, and *teekevass* in Russia. There also have been numerous investigations directed to application of bacterial cellulose (BC) in the medical industry. For instance, products of BC in its wet state include wound dressing pads, temporary skin and connective-tissue replacement.<sup>4</sup>

Bacterial cellulose (BC) from *Acetobacter xylinum* has been extensively studied by Iguchi *et al.*, who produced dried films of the above referred gels and reported these to exhibit a planar structure with exceptional mechanical properties, i. e. a Young's modulus exceeding 15 GPa.<sup>5-7</sup> For comparison, blown films of regenerated cellulose feature a stiffness of only 8 GPa.<sup>8</sup> Surprisingly, the damping values (i.e.  $\tan \delta$ ) of the BC films were found to be high in comparison to other high-modulus materials. The latter characteristic lead to application as transducer diaphragms in loudspeakers.<sup>9</sup> Another example of the practical use of BC is in the manufacturing of optically transparent composites with phenol-formaldehyde, which exhibit a Young's modulus of 19 GPa and a bending strength of 370 MPa.<sup>10, 11</sup>

A major problem, which hampers large-scale production of bacterial cellulose, is the fact that it is growing slowly and statically at the surface of its nutrition media.<sup>12</sup> Efforts in optimization include use of agitated cultures: pellets, rotating disks and wind-up rollers.<sup>13, 14</sup>

Considering, however, the theoretically estimated values of the stiffness of uniaxially oriented cellulose referred to above, - depending on the model selected - a Young's

modulus of 40 to 57 GPa would be the theoretical maximum value for planar films; a most attractive prospect, indeed (see Chapter I).

The aim of the work presented in this chapter was, thus, to produce bacterial cellulose foils with enhanced stiffness. The approach chosen was to continuously apply stress to a BC gel sheet during its formation.



## 2 Experimental

**Materials.** The nutrient medium employed was that described by Hestrin and Schramm,<sup>15</sup> which contained 50 g sucrose, 5 g (NH<sub>4</sub>)<sub>2</sub>SO<sub>4</sub>, 3 g KH<sub>2</sub>PO<sub>4</sub>, 0.05 g MgSO<sub>4</sub>·2H<sub>2</sub>O in 1 l distilled water. The medium was adjusted to pH 4.5 by adding ascorbic acid. *Acetobacter xylinum* strain was obtained from a Russian Teekevass medium (courtesy Dr. Kirill Feldman, ETH Zürich) to which a precultivated solution was added. After 4 days of incubation at room temperature, the samples obtained were treated for 1 h in an aqueous solution of 0.5 % NaOCl, rinsed overnight and, sandwiched between polyamide meshes and finally dried at 120 °C for 10 min in a hot press. Selected specimens were treated in 5 % aqueous NaOH during 10 h, followed by hot-pressing as above.

In addition, two specimen of 50 x 30 mm were grown for 7 days while kept constraint between a set of clamps. The strain was then increased daily up to a value of 30 %. Furthermore, one sample was additionally stretched in a 10 % NaOH aqueous solution to an ultimate value of 43 %.

**Mechanical analysis.** Tensile properties were determined employing an Instron tensile tester 5864 (Norwood, USA). The specimen width was 2-4 mm and gauge length at least 8 mm, and the crosshead speed was 10 %/min. The cross-sectional areas of the samples were calculated from the weight of each sample using a density of 1.40 g/cm<sup>3</sup>, determined with Ultrapycnometer 1000 (Quantachrome, USA). Planar- and unidirectionally oriented foils were tested in tension at different loading angles.

**X-ray analysis.** Wide-angle X-ray diffraction was conducted with an Oxford Diffraction Xcalibur XP instrument (Abingdon, UK) equipped with a Mo-K $\alpha$  source (wavelength 0.7093 Å) operated at -50 kV / 40 mA. X-ray diffraction patterns were recorded with an Onyx CCD Detector at a distance of 65 mm.

**Microscopy.** Samples for scanning electron microscopy (SEM) were coated with platinum. SEM photographs were taken with a Zeiss/LEO 1530 Gemini camera (Oberkochen, Germany) and polarized-light microscopy images with a Leica DMRX instrument (Wetzlar, Germany).

### 3 Results and Discussion

Bacterial cellulose gel layers of thicknesses in the wet state of up to 20 mm were grown with and without applying stress and with and without subsequent treatments.

In one series of experiments, in addition to freely growing a BC gel layer, a sample was produced while applying a strain of 30 % *during its growth*, and post-stretched in aqueous NaOH to 43 % as detailed in the experimental section above.

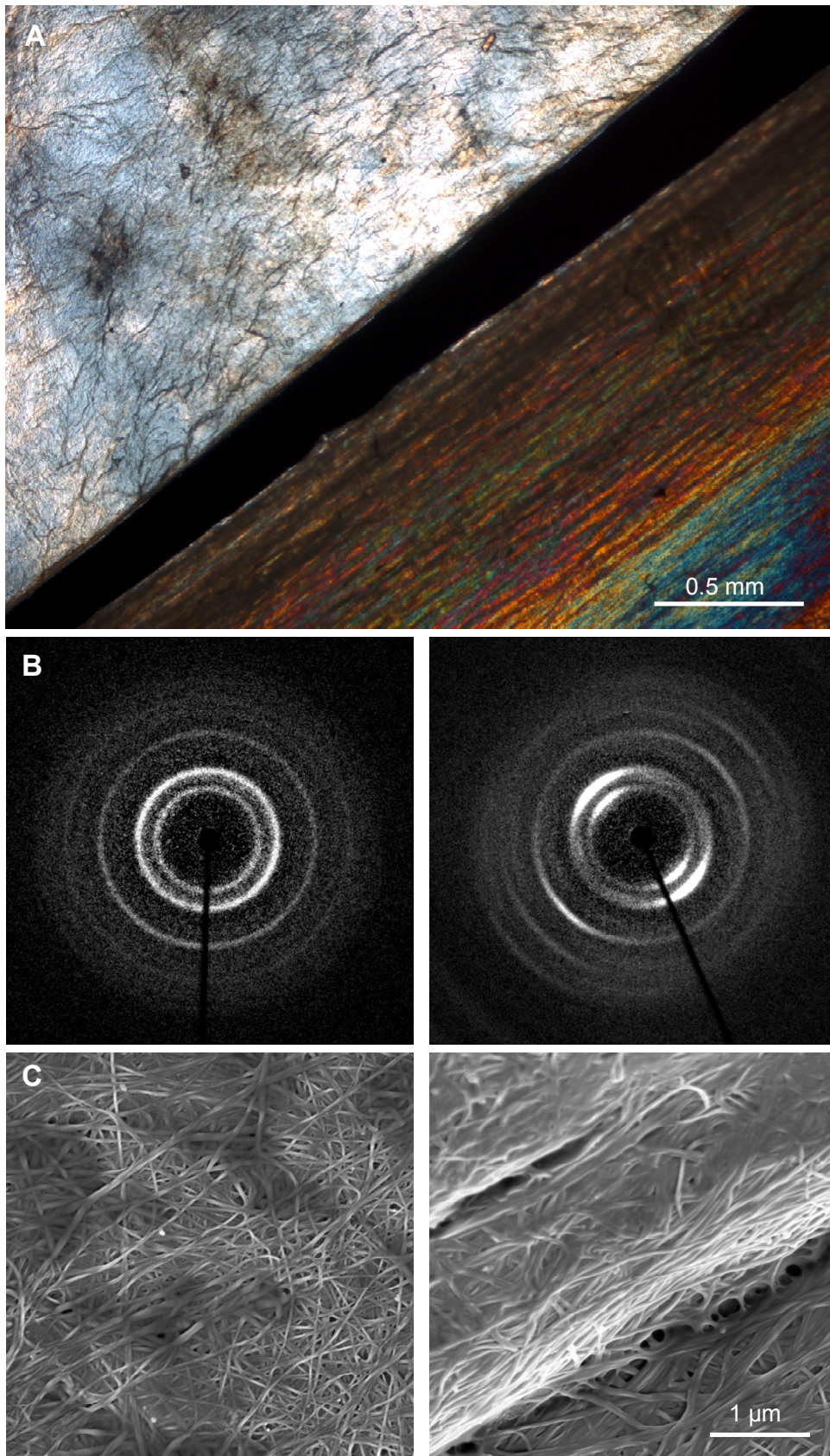
In Figure 1, optical micrographs, wide-angle X-ray diffraction (WAXD) patterns and scanning electron micrographs (SEM) are presented of the oriented BC foils, as well as of the reference, freely grown, dried film, revealing a (modest) degree of orientation of the former. The WAXD patterns are consistent with those reported in the literature and indicate the presence of the cellulose I polymorph.<sup>16, 17</sup>

In another series, strain was applied to initially planar (i.e. grown *without application of strain*), wet BC foils that were treated with aqueous NaOCl. It was observed that these wet gels could be stretched up to about 20 %. However, by adding sodium dodecyl sulfate detergent, extensions of up to 30 % were achieved. By contrast, treatment with octadecyltrimethylammonium chloride resulted in films that could be stretched by only 15 %. From these results, it would appear that the deformation behaviour of BC, not surprisingly, significantly depends on the strength of the hydrogen bonds between the cellulose entities.

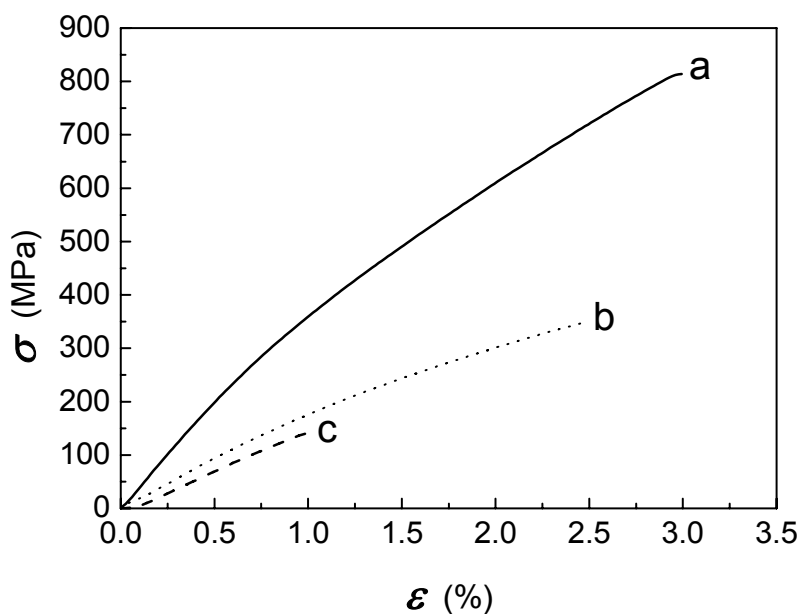
Typical stress-strain curves of selected (dried) foils are displayed in Figure 2; the corresponding mechanical characteristics are listed in Table 1.

**TABLE 1** Mechanical properties of differently treated, dried bacterial cellulose foils.  $\lambda$  denotes the degree of elongation applied. **a-c** correspond to denotation in Figure 2.

#	treatments	$\lambda$ %	$E$ GPa	$\sigma$ MPa	$\epsilon$ %
<b>a</b>	planar, as grown	0	16	136	1.0
<b>b</b>	planar, NaOH	0	19	350	2.5
<b>c</b>	unidirectionally <i>in-situ</i> stretched, NaOH	43	43	814	3.0
	unidirectionally <i>in-situ</i> stretched	30	25	510	2.6
	stretched with sodium dodecyl sulfate	14	28	367	1.6
	stretched with octadecyltrimethylammonium chloride	9	27	435	1.9
	pulp	0	10	140	2.2



**FIGURE 1** Bacterial cellulose foils grown freely and while applying 30 % strain. **A.** Optical micrographs, taken with crossed polarizers, of reference, freely grown foil (top left) and oriented BC sample (bottom right) featuring birefringence. **B.** Corresponding WAXD patterns and **C** scanning electron micrographs of the samples in **A**; left: planar foils, right oriented BC.

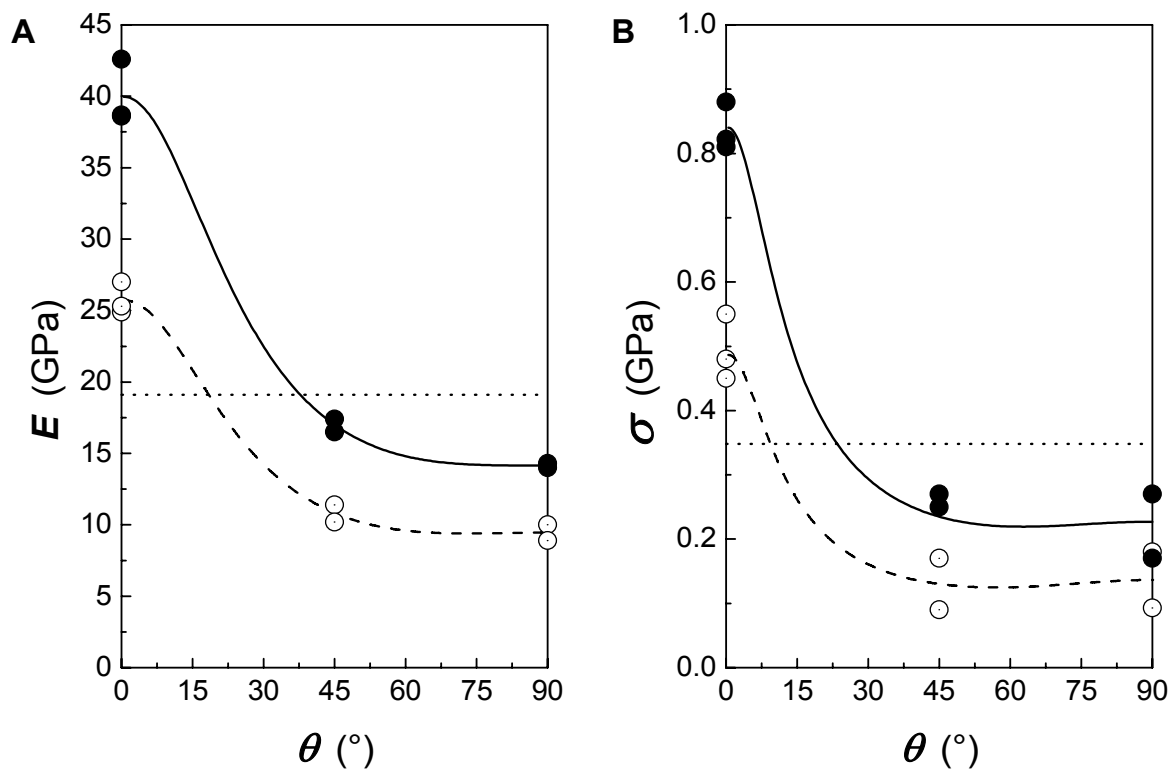


**FIGURE 2** Stress-strain curves of selected, dried bacterial cellulose foils: (a) reference planar, as-grown, dried foil without NaOH treatment; (b) planar grown, NaOH-treated; (c) unidirectionally, *in-situ* stretched foil, NaOH-treated.

In agreement with earlier reports, an increase of mechanical properties was observed for treatment with aqueous NaOH, in comparison with the untreated, dried BC foils, most notably in the tensile strength and elongation at break (cf. Table 1). Gratifyingly, a significantly more important improvement was found, however, for foils grown while being stretched and post-treated with aqueous NaOH: *nota bene* a three-fold increase in elongation at break, an almost tripling of the Young's modulus and 600 % increase in tensile strength resulted when compared to planar, freely grown and dried BC.

In addition, for comparison purposes, the characteristics of a cellulose foil produced from pulp (i. e. "paper") are listed Table 1. For this purpose, an as-grown BC gel was cut into pieces and blended with water in an ordinary kitchen blender. The resulting pulp was pressed and dried at 120 °C into a paper-like foil. The data reflect the inferior properties of the "paper", which, of course, lack the continuous structure of the BC foils.

Finally, the test-angle dependence of the mechanical properties of unidirectionally stretched, 50 mm-wide BC foil, as well as of planar NaOH-treated foil are shown in Figure 3. Most interestingly, applying strain during growth resulted in foils of significantly enhanced stiffness, strength *and* elongation at break at only a very modest expense of these properties in the traverse direction.



**FIGURE 3** A. Young's modulus,  $E$ , vs. test angle of NaOH-treated BC foils drawn *after* growth by 30 % (○) and drawn 30 % *during* growth and post-stretched in NaOH to 43 % (●). Curves calculated according to Tsai-Hill (cf. Chapter I), assuming a Poisson's ratio of 0.4. For comparison, the horizontal dotted lines are the mechanical properties of a planar NaOH-treated *unstretched* specimen (Table 1 b). B. Corresponding tensile strength data.

## 4 Conclusions

This chapter was concerned with the formation of high-performance, oriented bacterial cellulose foils. Major improvements in the stiffness and tenacity were achieved by *in-situ* orienting the growing films through application of up to 30 % strain, followed by post-drawing in aqueous NaOH to a total strain of 43 %. Maximum tensile moduli and strengths of, respectively, 43 GPa and 0.9 GPa were observed, which, respectively, exceed or are equal to that of the high-performance Cordenka<sup>®</sup> EHM rayon fiber (cf. Chapter I) and which represent more than a doubling of the values of these characteristics in the stretch direction while losing only one-fourth perpendicular to it, when compared to the corresponding values for planar grown, NaOH-treated foils. Finally, it should be noted that Bohn *et al.* in drawing during growth of BC in an aqueous NaOH solution reached a strain of 45 %, but their foils featured a Young's modulus of only 19 GPa and tensile strength of 0.6 GPa for reasons unknown to the author.<sup>18</sup>

## 5 References

1. Meyer, K. H. ; Lotmar, W. *Helv. Chim. Acta* **1936**, 19, 68.
2. Tashiro, K. ; Kobayashi, M. *Polym. Bull.* **1985**, 14, 213.
3. Haigler, C. H. ; Chanzy, H. *J. Ultrastruct. Mol. Struct. Res.* **1988**, 98, 299.
4. Czaja, W. ; Krystynowicz, A. ; Bielecki, S. ; Brown, R. M. *Biomaterials* **2006**, 27, 145.
5. Iguchi, M. ; Mitsuhashi, S. ; Ichimura, K. ; Nishi, M. ; Uryu, M. ; Yamanaka, S. ; Watanabe, K. *US Patent* 4,742,164 **1988**.
6. Yamanaka, S. ; Watanabe, K. ; Kitamura, N. ; Iguchi, M. ; Mitsuhashi, S. ; Nishi, Y. ; Uryu, M. *J. Mater. Sci.* **1989**, 24, 3141.
7. Iguchi, M. ; Yamanaka, S. ; Budhiono, A. *J. Mater. Sci.* **2000**, 35, 261.
8. Nishi, Y. ; Uryu, M. ; Yamanaka, S. ; Watanabe, K. ; Kitamura, N. ; Iguchi, M. ; Mitsuhashi, S. *J. Mater. Sci.* **1990**, 25, 2997.
9. Fink, H. P. ; Weigel, P. ; Bohn, A. *J. Macromol. Sci., Phys.* **1999**, B38, 603.
10. Nakagaito, A. N. ; Iwamoto, S. ; Yano, H. *Appl. Phys. A: Mater. Sci. Process.* **2005**, 80, 93.
11. Yano, H. ; Sugiyama, J. ; Nakagaito, A. N. ; Nogi, M. ; Matsuura, T. ; Hikita, M. ; Handa, K. *Adv. Mater.* **2005**, 17, 153.
12. Yoshinaga, F. ; Tonouchi, N. ; Watanabe, K. *Biosci., Biotechnol., Biochem.* **1997**, 61, 219.
13. Sakairi, N. ; Asano, H. ; Ogawa, M. ; Nishi, N. ; Tokura, S. *Carbohydr. Polym.* **1998**, 35, 233.
14. Gostomski, P. ; Bungay, H. ; Mormino, R. *Biol. Syst. Eng.* **2002**, 830, 69.
15. Hestrin, S. ; Schramm, M. *Biochem. J.* **1954**, 58, 345.
16. Takai, M. ; Tsuta, Y. ; Hayashi, J. ; Watanabe, S. *Polym. J.* **1975**, 7, 157.
17. Haigler, C. H. ; Brown, R. M. ; Benziman, M. *Science* **1980**, 210, 309.
18. Bohn, A. ; Fink, H. P. ; Ganster, J. ; Pinnow, M. *Macromol. Chem. Phys.* **2000**, 201, 1913.





# VI

## *Conclusions and Outlook*



# 1 Conclusions

The results presented in this thesis can be divided into two parts: i) the formation of high-performance, unidirectionally oriented foils, ii) and the production of planar, laminated foils therewith.

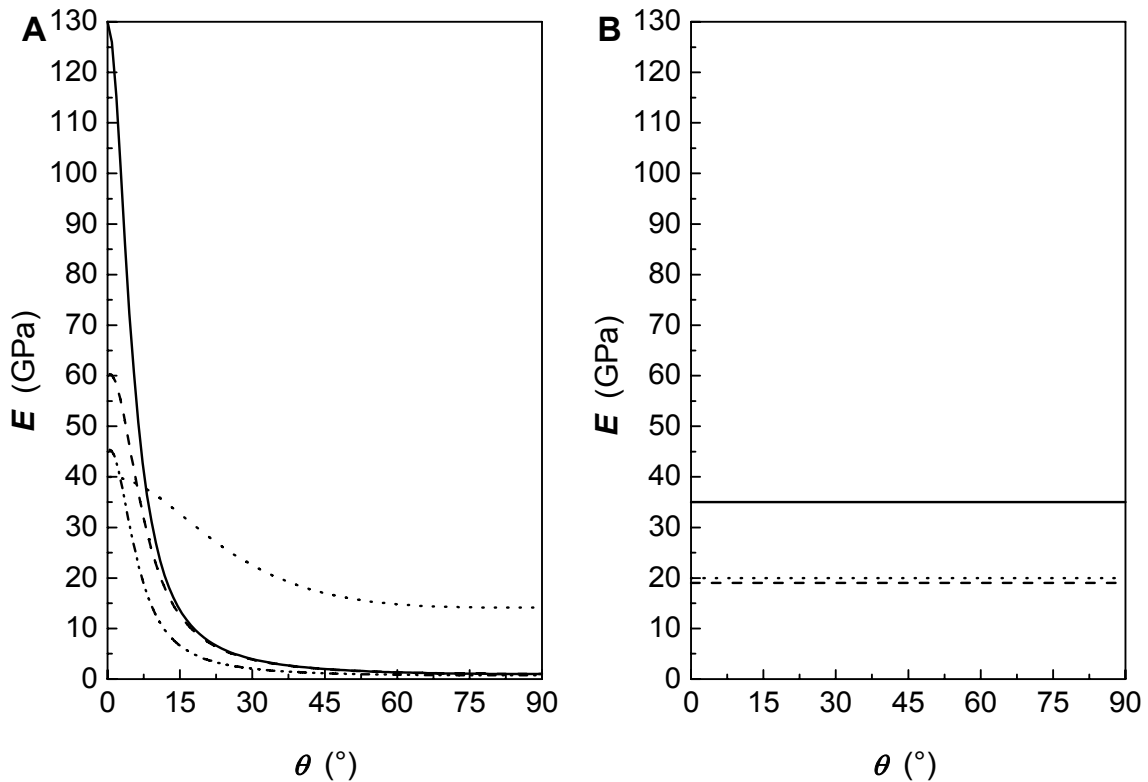
## 1.1 High-performance Unidirectional Foils

Uniaxially oriented high-performance foils of different classes of polymeric materials were produced. First, ultra-drawing of highly disentangled ultra-high molecular weight polyethylene - a flexible macromolecule - yielded transparent foils of outstanding mechanical characteristics (Chapter II). Second, a semi-rigid, thermotropic liquid-crystalline polyester was processed into foils using specially designed dies and employing air-gap extrusion (Chapter III). The same concept was adopted to form oriented structures from the lyotropic aramid poly(*p*-phenylene terephthalamide) with dry-jet-wet extrusion (Chapter IV). Finally, oriented foils of bacterial cellulose were grown *in-situ* while applying uniaxial stress, which featured improved mechanical properties in the direction of stretch (Chapter V). Gratifyingly, in three of the four cases the mechanical properties of the foils produced approached, or at times exceeded, those of their fiber counterparts (cf. Table 1).

**TABLE 1** Maximum Young's modulus,  $E$ , and tensile strength,  $\sigma$ , of foils produced in this work and corresponding values of the commercially available fibers listed in Chapter I.

	Foil $E$ GPa	Fiber $E$ GPa	Foil $\sigma$ GPa	Fiber $\sigma$ GPa
UHMW PE	148	116	3.3	3.6
HBA/HNA	71	72	1.3	3.2
PPTA	67	113	0.7	3.0
(Bacterial) Cellulose	43	38	0.8	0.9

The highly anisotropic character of the foils was revealed - in many cases for the first time - by angle-dependent tensile tests, which are summarized in Figure 1A. It has to be mentioned, though, that, although the foils were anisotropic indeed and featured poor properties in the transverse direction, they displayed sufficient resistance against fibrillation to further process them, for instance, in laminates.

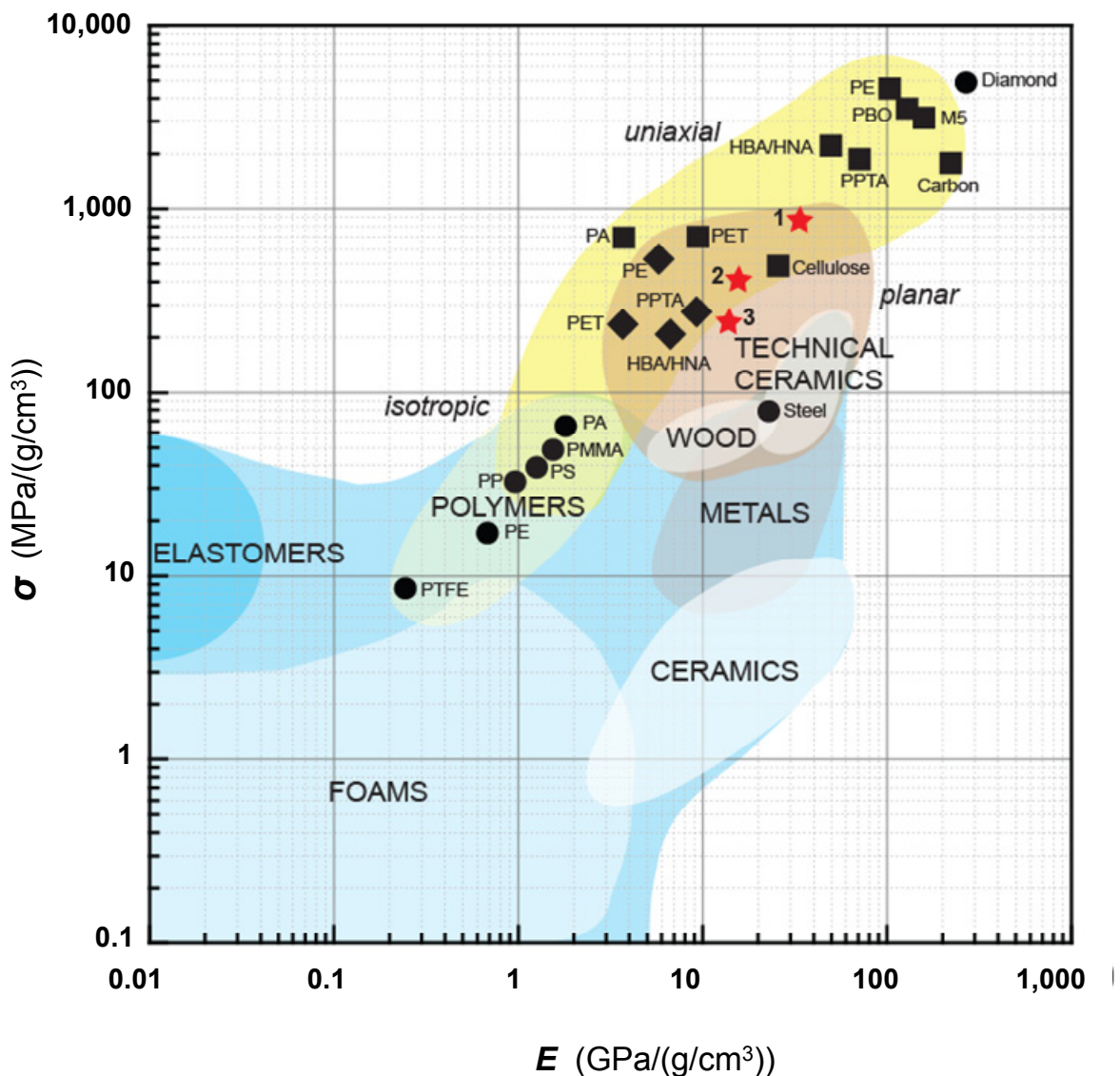


**FIGURE 1** Young's modulus,  $E$ , vs. test angle,  $\theta$ , of unidirectionally oriented foils (A) and planar, balanced 4-ply foils (B). (—) UHMW PE, (---) HBA/HNA, (---) PPTA and (.....) Bacterial Cellulose (curves fitted to experimental data, see Chapters II-V).

## 1.2 High-performance Laminates

The highly anisotropic character of the unidirectionally oriented foils, in which the macromolecular chains are arranged predominantly in a parallel fashion, was reduced, and in certain cases eliminated, by laminating layers at different angles, yielding foils of improved stiffness and strength in the direction perpendicular to the orientation direction of the constituent layers; but, of course, at the expense of properties parallel to that.<sup>1</sup> Nonetheless, foils of outstanding planar mechanical properties were produced (cf. Figure 1B), rivalling those - on equal weight basis - of glass and aluminium.

The latter statement is, perhaps, best illustrated by Figure 2, in which an Ashby-type plot is presented of the specific strength vs. stiffness of a broad spectrum of materials and material forms.<sup>2</sup> This graph shows that the foils produced in the present work significantly expand the envelope of high-performance materials of use in demanding mechanical applications.



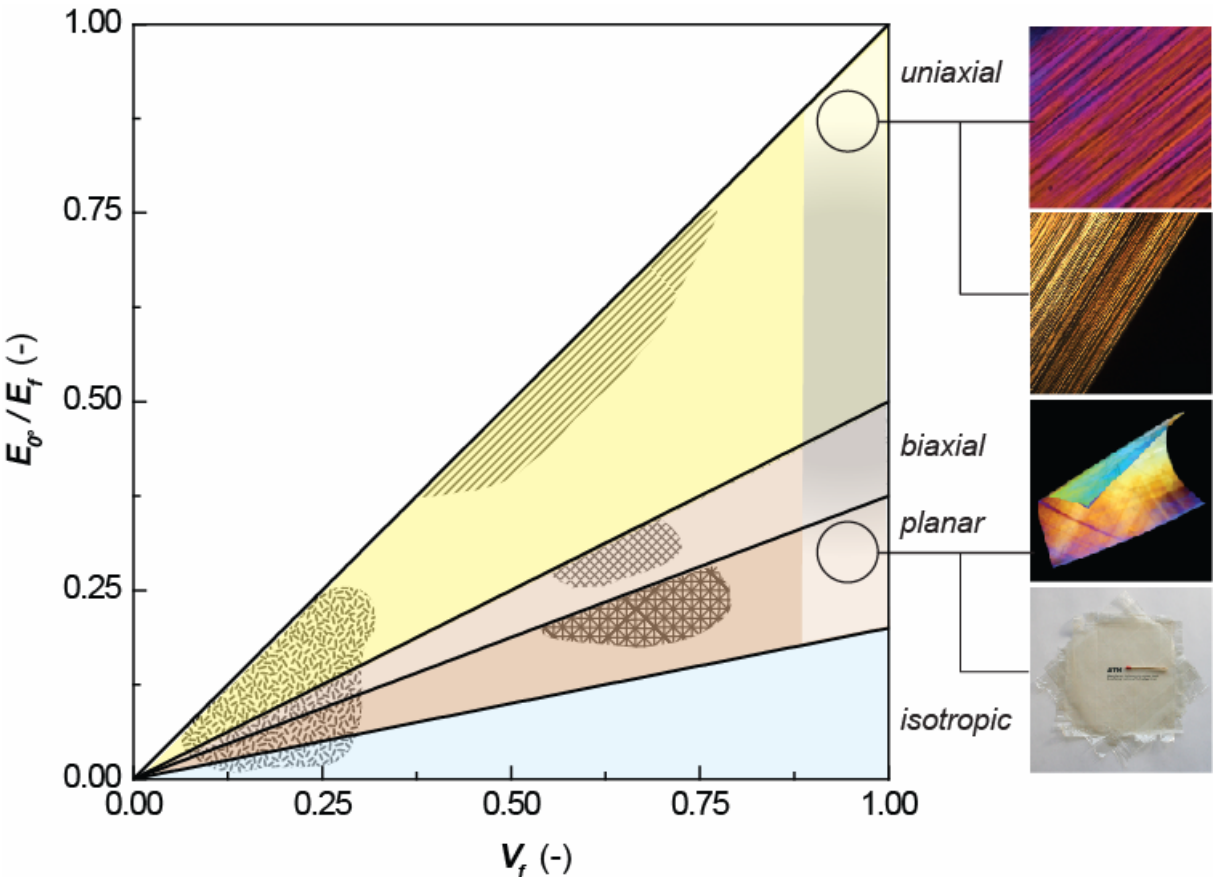
**FIGURE 2** Specific strength vs. Young's modulus of a spectrum of materials and material forms. As representative isotropic bulk polymers, poly(tetrafluoroethylene) (PTFE), isotactic polypropylene (PP), polyamide 6 (PA), poly(methyl methacrylate) (PMMA), atactic polystyrene (PS), are included, as well as planar poly(ethylene terephthalate) (PET) foil, ■ unidirectionally oriented polymer fibers, or ◆ foils and planar laminates produced in this work, marked as ★, where **1** is UHMW PE, **2** HBA/HNA laminate and **3** bacterial cellulose foil. For other abbreviations see Chapter I.

### 1.3 Composites

The unidirectionally oriented foils produced in this work offer advantages as reinforcing material for composites - traditionally consisting of high-performance fibers embedded in a (low stiffness) matrix - in that they are of a significantly smaller surface area than a multitude of filaments. That feature, of course, greatly reduces the

amount of matrix material needed, as shown in this work, to quantities as low as a few percent, culminating in a “brick-like structure”. Furthermore, the likelihood of incorporating detrimental voids is greatly reduced when employing high-performance foils.

Indeed, one major goal attained in this study is to produce “composites” of excellent mechanical properties employing little or no matrix material. For illustrative purposes, Figure 3 displays the ranges of properties reached with the foils produced, in comparison with those of traditional composites.



**FIGURE 3** Plot of the ratio of the Young’s modulus of a composite,  $E_{\theta^e}$ , and that of the reinforcing fiber/foil,  $E_f$  vs. the volume fraction,  $V_f$ , of the latter. The circles represent the limits of the range of materials produced in this work, while the textured areas indicated, where standard composites, ranging from random, short-fiber injection-molded thermoplastics to unidirectional reinforced materials, are found (the latter data were taken from ref. 3).

## 1.4 Final Conclusion

In the literature, only relatively few attempts are described of successful production of high-performance unidirectional and planar balanced foils or tapes. The work presented in this thesis provides general routes to manufacturing such product forms with properties approaching those of their commercially available, high-strength/high-modulus fiber counterparts. Availability of such high-performance foils may open a new era in composite design, as, clearly, construction with foils in many cases is more convenient and cost-effective than the cumbersome spreading of yarns and aligning of filaments, as practiced by, for instance, *Van Wees* (The Netherlands),<sup>4</sup> *Oxeon BA* (Sweden)<sup>5,6</sup> and *NSA Technologies SA* (Switzerland) (now *North Sails Research SA*).

## 2 Outlook

The present thesis describes methods for processing members of three major groups of polymeric materials, i.e. flexible, semi-rigid and rigid chain polymers, into high-performance, unidirectionally oriented foils, as well as planar laminates made therewith. In this last section, a number of issues will be discussed that can be improved or remained unaddressed in this work.

### 2.1 High-performance Foils

Clearly, for industrial applications, the developed foil-production processes need to be scaled up with the principal aim to form foils of increased width (e.g. > 1 m), for which a number of parameters already have been presented here.

Furthermore, it would be of interest to investigate the formation of sheets of increased thickness, which would require careful consideration of the possible development of skin-core structures. The latter might be avoided by multi-hole designs of the extrusion dies.

The influences of heat-treatment processes were explored only little in this work. But the well-known advantages, also reported here, encourage further investigations and should be evaluated in more detail.

Other opportunities that were not addressed in the present study were properties different from mechanical characteristics. It is well known that molecular orientation may enhance other characteristics as well, such as barrier-, electronic- or optical properties. Investigations in these areas might prove to yield most interesting and useful products, such as, for instance, robust polarizers for lasers.

Finally, the concepts presented in this thesis may very well be applicable to and of use for a class of materials that plays a major role in demanding mechanical applications, i.e. carbon (fibers), which today are formed in sheet-like products by spreading filaments followed by consolidation.<sup>7,8</sup> As noted in the Chapter I, carbon fibers typically are formed from pitch or polymeric precursors. Certain mesophase pitches can be processed directly into fibers by melt spinning using multi-hole spinnerets and applying a draw-down.<sup>9</sup> The alternative is to employ polyacrylonitrile (PAN)



precursor fibers, which, however, are difficult to fully graphitize.<sup>10</sup> The resulting fibers typically exhibit a structure wherein graphite planes are oriented radially from the centre towards the outer surface or are randomly arranged.

Extruding mesophase pitch employing the fusion-dies developed in this work may yield foils of an in-plane graphitic layer structure, such as those observed by, for instance, Lu *et al.*.<sup>11,12</sup> Additionally, the observation that processing rectangular carbon ribbons through a slit nozzle results in better mechanical properties than for circular fibers due to secondary alignment with respect to the plane edges, indicates the potential of the fusion-dies developed in this thesis.<sup>13,14</sup> In this context, it should be noted that Shinohara *et al.* already mentioned the promising possibility to extrude mesophase pitch to a film of width/thickness ratio of 10/1.<sup>15</sup>

Alternatively, oriented foils of PAN, produced according to the method presented in Chapter II for UHMW PE, may be converted into carbon foils by appropriate thermal treatment.

## 2.2 High-performance Laminates

As shown in this work, laminates of high-performance, unidirectional foils may exhibit outstanding mechanical properties provided that adequate adhesion between the individual layers exists. In the case of the thermotropic polyester, this was achieved by applying a hot melt-adhesive onto the foils, followed by lamination (Chapter IV), which is a relatively cumbersome, but nonetheless useful approach (see Figure 4). Clearly, it would be desirable to generate an alternative to this method.

One option would be to co-extrude hot-melt adhesives on the top and bottom of the foils, as in the production of all-polypropylene composites (PURE®).<sup>16,17</sup> Alternatively, the concept of adding a lower melting polymer, as in Chapter II for UHMW PE foils, could be adopted.



**FIGURE 4** Remote-controlled 2 m tall model boat featuring a front sail constructed with laminated Vectra® foils produced in this work (Chapter IV), illustrating a possible application, which could be up-scaled in the future. The weight saving of the sail was determined to be 30 %, while its performance is highly improved in terms of strength and stiffness.

### 3 References

1. Gordon, J. E. *Proc. R. Soc. London, Ser. A* **1970**, 319, 137.
2. Ashby, M. F. *Materials and Process Selection in Mechanical Design*; Butterworth Heinemann, Oxford (UK), **1999**.
3. Gutowski, T. G. *Advanced Composites Manufacturing*; p. 18; John Wiley & Sons, Inc. **1997**.
4. [www.vanwees.nl](http://www.vanwees.nl); [www.crossply.com](http://www.crossply.com) **2007**.
5. [www.oxeon.se](http://www.oxeon.se) **2007**.
6. Khokar, N. *US patent* 6,539,983 **2003**.
7. Benstead, B. C. ; Seith, R. T. *US Patent* 4,183,993 **1980**.
8. Nojiri, T. ; Yakushiji, K. ; Yoshinaga, M. ; Terasaka, H. *US Patent* 5,487,512 **1996**.
9. Singer, L. S. *US Patent* 4,005,183 **1977**.
10. Ram, M. J. ; Riggs, J. P. *US patent* 3,657,409 **1972**.
11. Appleyard, S. ; Lu, S. ; Rand, B. *WO Patent Application* 01/02632 **2001**.
12. Lu, S. ; Blanco, C. ; Appleyard, S. ; Hammond, C. ; Rand, B. *J. Mater. Sci.* **2002**, 37, 5283.
13. Mochida, I. ; Yoon, S. H. ; Korai, Y. *J. Mater. Sci.* **1993**, 28, 2135.
14. Fortin, F. ; Yoon, S. H. ; Korai, Y. ; Mochida, I. *Carbon* **1994**, 32, 1119.
15. Shinohara, K. ; Mondori, J. ; Miyanaoshita, H. ; Kurimoto, T. *US Patent* 5,326,510 **1994**.
16. Commercial available products: [www.pure-composites.com](http://www.pure-composites.com); [www.curvonline.com](http://www.curvonline.com) **2006**.
17. Jacobs, J. A. J. ; Peijs, A. A. J. M. ; Schimanski, T. *Patent Application* EP 127573 A1 **2003**.



# Acknowledgements

I would like to emphasize that little in this thesis results from the work of one individual only. For that reason, I want to pay a tribute to all who contributed in one way or another during that extraordinary and unforgettable period of my doctoral studies.

Very first of all, I would like to thank Paul Smith for having me in his research family and to enjoy the most fantastic and challenging time of my life, during which I have learned more than only science, being to me a doctor father that let me realize that science breathes from inspiration and art.

I am highly grateful to Han Meijer of the Eindhoven University of Technology (TU/e), The Netherlands, who contributed enormously with his knowledge in processing technology and intense assistance, and co-refereed this thesis.

Further, I would like to thank Ton Peijs for being co-examiner of this dissertation and for giving me the opportunity to stay at Queen Mary University London.

I wish to acknowledge Theo Tervoort for his contributions to the mechanical theoretical sections and also being co-examiner of this thesis, Walter Caseri for, among many other things, remembering lunch time and Wolfgang Kaiser for helpful discussions.

Special thanks go to Kirill “Schneck” Feldman for having him always around, helping me out in all kind of situations. Thanks for the continuous enthusiasm during the realization of this work and critical but helpful comments.

As stated, many people were involved in the experimental part of this work. First, I would like to thank Matthias ”Shakespeare” Gössi for the introduction in Igor-evaluations of X-ray experiments, Lorenz “Kawa” Brunner and later Karin “Sweety” Bernland for sharing a office with me and helping me out many times. Further, I thank Fabien “HC-griller” Choffat and Christian “Namisats” Müller for their assistance in foreign eastern countries. I would also like to thank Jan Giesbrecht helping me out during foil extrusion and model-boat sailing. Marc Simonet is recognized for his support with the SEM imaging and Lars Kocher of the Crystallography Group of the Department of Materials, ETH Zurich, for assistance with the WAXD experiments. Furthermore, I would like to thank all the other folks of the Polymer Technology

Group for great unforgettable teamwork, for assistance in the lab and for the good times outside the lab.

Special thanks go to the team of the mechanical workshop for their help with designing and manufacturing essential experimental equipment, in particular to Werner Blattmann and Fredy Mettler. Further, Erwin Dekkers, Patrick de Laat and Mariëlle Dirks-Smit of TU/e are acknowledged for precise manufacturing of the special extrusion dies.

I also wish to acknowledge our industrial partner, Createx SA, Morges, Switzerland, for the interesting collaboration. Gérard Gautier and Eduard Kessi, first of Createx SA, then NSA, SA, and now with North Sails Research, who are deeply recognized for many helpful comments and use of their unique equipment.

Further, I wish to extend my gratitude to Chris Reynolds providing me with great help at my stay in London.

Jeroen “Fishy” Visjager, Paul Nazarro and Oliver Jünger from Ticona are acknowledged for providing generous supplies of thermotropic liquid-crystalline polymer.

And, of course, Geordies’ for the stimulating hosts and guests and providing a platform where discussions and ideas got space to grow.

To Anja, the warmth of my heart, I owe everything since none of this would have happened without you on my side.

Last but not least, I want to thank, my family for their love, patience and support and simply for always being there for me.

## Curriculum Vitae

The author of this thesis was born on the 6<sup>th</sup> of September 1977 in Zurich, Switzerland. He grew up in Dübendorf, completed there secondary school in 1992, and graduated from high school in Wetzikon in 1997. In 1998 he started his studies in Material Science at the Swiss Federal Institute of Technology (ETH) Zurich, which he successfully completed with a Diploma thesis in 2003 in the Polymer Technology Group of the Department of Materials, headed by Paul Smith. In the scope of an industrial practical program during his studies he worked in 2001 at Nortel Networks, Zurich and in 2002 at Phonak Hearing Systems, Stäfa. In 2003 he started the study described in this PhD thesis, also in the Polymer Technology Group of the Department of Materials of ETH Zurich.

*«Tout peut arriver dans la vie, et surtout rien.»*

*Michel Houellebecq, Plateforme; Editions Flammarion 2001.*